Assessment of Two Sets Intensity Measures of Ground Motion with Seismic Damage Indices of Masonry-infilled Steel Frames

Mohsen Shahaki Kenari

Submitted to the
Institute of Graduate Studies and Research
in partial fulfillment of the requirements for the degree of

Doctor of Philosophy
in
Civil Engineering

Eastern Mediterranean University
May 2019
Gazimağusa, North Cyprus

Approval of the Institute of Graduate Studies and Research

Prof. Dr. Ali Hakan Ulusoy
Acting Director

I certify that this thesis satisfies all the requirements as a thesis for the degree of Doctor of Philosophy in Civil Engineering.

Assoc. Prof. Dr. Serhan Şensoy
Chair, Department of Civil Engineering

We certify that we have read this thesis and that in our opinion it is fully adequate in scope and quality as a thesis for the degree of Doctor of Philosophy in Civil Engineering.

Assoc. Prof. Dr. Mürüde Çelikağ
Supervisor

Examining Committee

1. Prof. Dr. Mizan Doğan
2. Prof. Dr. Cem Topkaya
3. Assoc. Prof. Dr. Mürüde Çelikağ
4. Assoc. Prof. Dr. Giray Özay
5. Asst. Prof. Dr. Umut Yıldırım

ABSTRACT

The objective of this study is to investigate the nonlinear behavior of two dimensional 3, 5, 8 and 12 story steel frames with and without masonry infill considering the intensity measure (IMs) parameters of near-fault ground motions and dynamic Soil-Structure Interaction (SSI).A single story and single bay steel frame numerical model was validated by using two software, SAP2000 and OpenSees and comparing the structural periods obtained. Then the validation of OpenSees numerical model against the experimental results from literature was done. This was followed by using the validated models to create the rest of the numerical models. Aspect ratio of the superstructure and non-dimensional frequency are selected as the main parameters for the soil-structure system. Two sets of earthquake ground motions, ordinary seismic records (OSR) and pulse-like seismic records (PLSR) were used for the nonlinear dynamic analysis. Seismic performance was evaluated using the general indicators of damage (modified Park-Ang index), maximum inter-story drift ratio (MIDR) and roof drift ratio (RDR). The correlation between the multiple IMs with and without pulse-like seismic excitation and the damage indices of 3 forms of steel moment frames; bare, partially and fully infilled was determined using the Spearman correlation coefficient. Also, a significant part of correlation between the damage criteria and IMs was assessed. It was concluded that the spectral acceleration (S_a) and velocity (S_v) of the structures period strongly correlated with MIDR and RDR and that velocity correlated with the seismic parameters. The correlations for PLSR and OSR differed for each case and IMs with ground motion can help predict the parameters for building failure in various systems. In most ground motion parameters, the presence of masonry-infilled walls decreased the correlation coefficient for a fully infilled frame

when compared to a bare frame. It should be noted that GSDI has high correlation with MIDR than with RDR. The correlation coefficients with the effect of the SSI were reduced by a range of about 10-20% for a model frame with flexible base when compared with the same model with a fixed base. Therefore, the use of PLSR is important when SSI is considered, since it generally negatively effects the correlation of damage indexes and causes considerable change in the behavior of partially infilled and fully infilled frames with respect to bare frames and high rise with respect to low rise frames.

Keywords: Intensity measures, Ordinary records, Pulse-like records, Damage index, Steel frame with masonry infill, Soil-structure interaction

ÖZ

Bu çalışmanın amacı dinamik toprak-yapı etkileşiminin (SSI), yakın fay hattı zemini hareketlerine maruz kalan ve yanal dirençli sistemleri olan, iki boyutlu çelik çerçevelerin, doğrusal olmayan davranışına olan etkisini incelemektir. Üst yapının en-boy oranı ve boyutsuz frekans toprak-yapı sisteminin ana parametreleri olarak seçilmiştir. Bu çalışma, çelik çerçeve içerisinde dolgu duvar olan yapıların yoğunluk ölçümlerini (IM) temsil eden parametrelere verdiği tepkiyi incelemiştir. İki set deprem yer hareketi, sıradan sismik kayıtlar (OSR) ve nabız-benzeri sismik kayıtlar (PLSR), dolgu duvarı olan çok katlı çelik yapıların doğrusal olmayan dinamik analizinde kullanılmıştır. Sismik performans, genel hasar göstergeleri (modifiye Park-Ang indeksi), maksimum katlar arası öteleme oranı (MIDR) ve çatı öteleme oranı (RDR) kullanılarak değerlendirildi.Nabız-benzeri sismik uyarımı olan ve olmayan çoklu IM parametreleri ile dolgu duvarları olan ve olmayan çelik moment çerçevelerin hasar endeksleri arasındaki ilişki Spearman korelasyon katsayısı kullanılarak belirlenmiştir. Ayrıca, hasar kriteri ve yoğunluk ölçümleri arasındaki korelasyonun önemli bir kısmı değerlendirilmiştir. Sonuç, yapı periyodunun spektral ivmesinin (S_a) ve hızının (S_v) maksimum katlar arası öteleme oranı (MIDR) ve çatı öteleme oranı (RDR) ile kuvvetle ilişkili olduğunu ve hızın sismik parametrelerle korelasyon gösterdiğini ortaya koymuştur. sıradan sismik kayıtlar (OSR) ve nabız-benzeri sismik kayıtlar (PLSR) için korelasyon farklıydı. Sonuçlar, yer hareketi ile yoğunluk ölçümlerinin (IM) analizinin, çeşitli sistemlerde bina göçme parametrelerini tahmin etmesine yardımcı olabileceğini ortaya koymuştur. Dolgu duvarların varlığı, çıplak bir çerçeve ile karşılaştırıldığında tamamen dolu bir çerçeve için korelasyon katsayısını değiştirdi. GSDI'nın, MIDR ve RDR ile yüksek korelasyona sahip olduğunun not edilmesi gerekir. Toprak-yapı

etkileşiminin etkisi ile pin tabanlı çerçeve modelinin korelasyon katsayıları sabit tabanlı bir model çerçeveye göre yaklaşık % 10-20 oranında azalmıştır.

Anahtar Kelimeler: Yoğunluk ölçümleri, Sıradan kayıtlar, Nabız-benzeri sismik kayıtlar, Hasar indeksi, Duvar dolgulu çelik çerçeve, Toprak-yapı etkileşimi

I could not forget to state the invaluable support of my wife (ALEMEH JOON) who his friendship and exchange of opinions helped in this research.

"Thank you for being my voice of reason, my heart of the matter, and my sounding board. Thank you for always helping me think clearly, for helping me find the answers to my questions, and for giving me the courage to try. You have always believed in me and my capabilities, and you never doubted just what I can do. Thank you for the love that you keep giving me, even when I am in my most unlovable state. I love you forever"

ACKNOWLEDGMENT

I am so appreciative of my supervisor Assoc. Prof. Dr. Mürüde Çelikağ for her patience, guidance and encouragement throughout this study. Her experience and knowledge have played a main role in my research.

TABLE OF CONTENTS

LIST OF TABLES

LIST OF FIGURES

LIST OF SYMBOLS

Ω	Bandwidth
λ_1	Coefficient Used to Determine Equivalent Width of Infill Strut
θ	Angle of the Infill Height-to-length Aspect Ratio in Radians
ϑ	Poisson's Ratio
u_0	Displacement System
$\dot{u}_0$	Velocity of System
A	Design Base Acceleration (g)
A_0	Foundation Cross Section
a_{rms}	Acceleration Root-mean-square
B	Response Coefficient of the Building
C	Specific Mass
C_φ	Sway Damping
C_h	Rocking Damping
d_{rms}	Displacement Root-mean-square
E_{fe}	Expected Modulus of Elasticity of Frame Material
E_i	Hysteretic Energy of the Member
E_{me}	Expected Modulus of Elasticity of Infill Material
h_{col}	Column Height between Centerlines of Beams in cm
h_{inf}	Height of the Infill Panel in cm
I	Importance Factor of the Building
I_f	Compound Velocity-related Intensity Measure
I_a	Compound Acceleration-related Intensity Measure
I_d	Compound Displacement-related Intensity Measure

I_v	Compound Velocity-related Intensity Measure
I_{col}	Moment of Inertia of Column
k_φ	Sway Stiffness
k_h	Rocking Stiffness
P_d	Destructiveness Potential
r_{inf}	Diagonal Length of Infill Panel in cm
t_{inf}	Thickness of Infill Panel and Equivalent Strut in cm
V_s	Shear Wave Velocities of Soil
V_p	Dilatational Velocities of Soil
v	Velocity
P_0	Force
R	Behavior Coefficient of the Building
r_0	Radius of the Equivalent Circular Foundation
v_{rms}	Velocity Root-mean-square
V	Base Shear Force
T_m	Mean Period
$S_a\ (T_1)$	Spectral Acceleration
$S_v\ (T_1)$	Spectral Velocity
$S_d\ (T_1)$	Spectral Displacement
W	Total Weight of the Building

LIST OF ABBREVIATIONS

AI	Arias Intensity
ASI	Acceleration Spectrum Intensity
B-Frame	Bare Frame
CAV	Cumulative Absolute Velocity
CI	Characteristic Intensity
DI	Damage Index
EDA	Effective Design Acceleration
EPA	Effective Peak Acceleration
EPV	Effective Peak Velocity
F-Frame	Fully-infilled Frame
GSDI	Global Structure Damage Index
HI	Housner Intensity
IMs	Intensity Measures
IP_R	Impulsivity Index
LDP	Linear Dynamic Procedure
LSP	Linear Static Procedure
MIDR	Maximum Inter-story Drift Ratio
OSRs	Ordinary Seismic Records
P-Frame	Partially-infilled Frame
PGA	Peak Ground Acceleration
PGD	Peak Ground Displacement
PGV	Peak Ground Velocity
PLSRs	Pulse-like Seismic Records

RDR	Roof Drift Ratio
SED	Specific Energy Density
SMA	Sustained Maximum Acceleration
SMV	Sustained Maximum Velocity
SSI	Soil-structure Interaction
VSI	Velocity Spectrum Intensity

Chapter 1

INTRODUCTION

1.1 Introduction

During the last few decades there has been increased attention on the behavior of steel and concrete structures with infill walls (Personeni et al. 2008). Over the years structural standards based on analysis by using bare frame. However, real structure always have infills in different forms and locations and the consideration of infill walls for the analysis of structures are important, since this may lead to an increase in the stiffness and lateral load resisting capacity of structures (Korkmaz et al 2008). The presence of the infill in the structure causes changes in the interaction of the structural members (Ko et al 2008). Nonlinear dynamical analysis were used to investigate selected parameters of the five-story steel frame by Jafari, 2018. According to the results, at least 20% reduction of the fundamental period of infilled steel frame can be considered instead of bare frame.

Furthermore, research results showed that the increase in the structural height (high-rise) has effect on reduction of the fundamental period of the structure. The above research indicates that the presence of infill has a significant influence on the structure's response when compared to the bare frame one.

The relationship between structural failure and earthquake record was investigated by Yakut and Yilmaz 2008. In their analysis, it was assumed that the structure was located

on a rigid ground, but in general, this assumption cannot be correct unless the structure was located on a very strong material, such as rock. Also, there was no mention of the effect of soil-structure interaction. On the other hand, consideration of soil-structure interaction helps to identify whether the structural response is elastic or non-elastic.

Among the hazardous phenomena, devastating earthquakes are responsible for some of the largest number of casualties and financial loss. Unfortunately, the number of casualties in urban areas of developing countries is considerably higher due to earthquakes. Furthermore, the numbers of earthquake survivors that are left homeless in developing countries are more than 40 times higher than those in the developed countries (Moghadam 2006). Hence, the negative impact of earthquakes on the economies of developing countries is significant. Studies show that in the years 1987 and 1988, the direct and indirect impact of earthquakes on the economies of developing countries has been between 3% and 4% of annual gross domestic product (Akkar and Galkan, 2003). Damages to structures caused by the 1994 Northridge-USA , 1995 Kobe-Japan, 1999 Izmir-Turkey, Chi Chi-Taiwan and 2003 Bam earthquakes showed that there is huge difference between the response of structures to earthquakes in the near and far field. In addition, the impact of structural failure depends on many parameters of the earthquake in near-field (Decanini and Saragoni, 2000). Investigations about earthquakes carried out after near field showed that the displacement of fault effective earthquakes is very high. Due to a significant change of ground motion (near-fault earthquakes), structures cannot withstand the base shear forces resulting from near-fault earthquakes. Therefore, the necessity of examining and recognizing near-fault records and incorporating the effects of these records into seismic regulations and improving the capacity of structures for the high demand of the displacement caused by near-fault earthquakes has been the subject of research in

recent decade. In line with this necessity, the UBC97 regulations consider the effects of near faults by providing a series of magnification factors. This series of magnitude coefficients in the near-fault areas is applied in relation to the equivalent static method and within the recommendations of the regulations (Li and Xie 2007).

According to the third edition of Iran's code (2800 Standard, 2003), no provision is made for earthquakes near the fault, and it is stated that "In general, avoid the construction of a building near active faults where there is a probability of a rupture at the earth's surface during a seismic ground motion, and in cases where construction of the building is inevitable in the fault zone, in addition to complying with the rules of the Code, special technical measures should be taken". The fourth edition of Iran's code (2800 standard, 2014), in addition to repeating the above sentence, has also used the refinement coefficient of the spectrum *N*, which will result in design for a larger design spectrum (2800 standard, 2014). Today, there are several methods available for modeling soil under structure and its directional effects on the structures response. One of the most efficient of these methods is the Cone model. The type of soil underlying the structure may have significant influence on the structures response, particularly if the structure is constructed on soft soils. In conventional designs, it is assumed that the structure is placed on a rigid substrate; this assumption may be acceptable for structures on a bed rock, but when the structure is built on soft soils, this would considerably reduce the accuracy of the calculations. The following are among the effects that soil-structure interaction can have on the structural response:

a) Damage Index of structure in near-fault zone
b) Elastic and non-elastic displacement in an equivalent system degree of freedom
c) Seismic base shear force of the structure's foundation
d) The distribution of lateral forces throughout the height of the story etc.

The pulse-like ground motion propagates in a direction perpendicular to the fault towards the structure, which is very destructive. In these earthquakes, a major part of earthquake energy is placed in one or more primary pulses (Tothong and Cornell 2008).

1.2 Research Necessity

Considering the research carried out so far and available in literature, it is clear that there has been considerably more investigation on the behavior of reinforced concrete frames with and without infill walls when compared to steel frames. Hence there is need for further investigation of steel frame behaviour with and without infill walls.

On the other hand, the soil type underlying the foundation of the steel structure is also important and contribute to the overall behavior of the building, particularly when subjected to seismic motions. Therefore, the structure's response was also studied with consideration of the effect of soil flexibility on the steel framed structures located on two soil types (soft soil and hard soil). In this regard, a cone model was used for the modeling of underlying soil (Wolf and Deeks 2004). In cone method, soil dynamic system is modeled in homogenous half-space according to material resistance method by using a rod vertical axis where cross sectional characteristics can be changed along the axis.

On the other hand this investigation needs to be done more realistically for earthquake regions considering real earthquake data. Hence, the present study considered the effects of pulses caused by near-field earthquakes on the response of steel structures with, without and partial infill walls. According to the statistics presented in connection with the fault profile and seismic record of the cities of Iran, the following

results can be extracted (Moghadam, H 2006): 70 percent of Iran's cities are less than 20 kilometers away from the faults, and some of these faults are more than 300 kilometers long. 40 percent have seismic record with magnitude higher than six Richter which is justifiable in the context of earthquakes near the faults in Iran.

According to data recorded on near-faults (Northridge, Kobe, Turkey and Bam) during the last two decades, there is indication of severe financial losses when compared to the effect of those similar and even larger earthquakes. Furthermore, the near fault earthquakes cause various behavior of structures under the influence of such earthquakes compared to the records of far-fault earthquakes. Comparison of the responses of the structures under the effect of earthquakes in the near-fault with and without earthquake-induced pulses indicates that the response value of the structure with pulse-like seismic records is higher in the case of without pulse-like (Malhotra, 1999). Pulse-like seismic records with high-velocity can make intensive inelastic demands on multi-story building (Hall et al. 1995).

Therefore, the study of the above cases revealed the importance of research and study on near-fault records and the study of the effect of soil-structure interaction on the structural response. Hence, the effects of nonlinear behavior of the soil on the nonlinear response of structures subjected to two sets records is evaluated by using nonlinear dynamic time history analysis.

1.3 Problem Statement

The response of the structure under strong ground motion depends on the soil conditions of the substructure. Generally, soil modeling is not considered or neglected, and in dynamic analysis of structures, the soil often assumed rigid under the foundation

and its flexibility is not taken into account. Before the study of the effect of soft soil on the structure one needs to know which damage index is more important. In order to investigate the behavior of structures with and without SSI, three types of steel frames, bare, partially and fully-infilled, were considered. First, the comparison of two set earthquakes pulse-like seismic records in near-field and ordinary seismic records is investigated and then the importance of soil-structure interaction in the near-fault zone is discussed. These movements include a pulse-like in time history of the ground motion velocity, which are often in the direction perpendicular to the fault rupture in places close to the fault in which the earthquake rupture propagates towards the site. Accordingly, two-dimensional structural models with different building heights on hard soil (fix-base), designed with the standard 2800 Iran classification. Then, in two sets of earthquakes near - fault and ordinary seismic records on the failure index are examined.

1.4 Research Objectives

In the Hazus-MH classification (2003), heights Steel buildings were categorized as LR: low-rise (1-3 stories), MR: mid-rise (4-7 stories) and also HR: high-rise (8+ stories). The purpose of this study was to investigate the response of moment framed steel structures with 3, 5, 8, and 12 stories and bare, partially infilled and fully infilled walls non-linear dynamic time-history analysis was used. From existing seismic records and literature it is known that pulse-like seismic records may cause severe damage for building. On the other hand, ordinary seismic records frequently represent a long-period pulse in the velocity time histories that cause an unusual shape in the response spectrum (Tothong and Cornell 2007). Hence the response of the structure in pulse-like and ordinary seismic records can be considerably different. Also the study investigated the effects of soil-structure interaction on structural behavior by

considering soft and hard soils underlying the structures. In order to compare the structural behavior as a result of using bare, partially and fully infilled walls the changes in the period of structure, damage index as maximum inter-story drift, roof drift ratio and modified Park-And damage index were studied. Park-Ang damage index is the combination of the parameters of ductility demand and energy absorption capacity (Park and Ang 1985). Also, to study the frequency of near-fault earthquakes, soil-structure interaction on the structural response under each of these frequency were considered. Hence the originality of this study can be listed as follows:

- There are limited number of study in literature regarding steel framed structures with and without infill walls and also considering their behavior with soil-interaction. Furthermore, the methods and the seismic parameters of intensity measures (IMs) listed below that were used to carry out this study are also not widely used in literature for such studies:
    a) Use of 3, 5, 8 and 12 story steel 2D frames with bare, partially and fully masonry infilled.
    b) Categories of records based on the pulse like and ordinary (no pulse like)
    c) Cone method of modelling soft soils underlying the structure
    d) 32 seismic parameters of IMs being used in this study which is more than in other studies from literature.

This study provided results to help engineers understand the effect of infill walls on low, mid- and high-rise structures located on soft and hard soils by using non-linear time-history analysis of structures using near field seismic data.

1.6 Organization of Thesis

The thesis is prepared in seven chapters and is as follows:

- The first chapter includes general knowledge and introduction to the subject, research necessity, problem statement and objective of this research.
- The second chapter is about ways to consider the effect of soil-structure interaction, as well as past research on pulse-like seismic records and so structural damage index is considered.
- The third chapter is methodology where structural 2D frame models without or with partial and full infill, are described and the pulse-like and ordinary seismic records are introduced.
- Verification of Soil-Structure Interaction is detailed in chapter 4.
- The verification of the steel framed models with and without infill wall is given in chapter 5.
- The sixth chapter discusses the results of the analysis by doing comprehensive analysis of correlation coefficients, looking into the correlation between Earthquake intensity criteria, correlation between damage criteria and correlation between Earthquake intensity criteria and structural response.
- Chapter 7 presents the overall conclusions obtained from this study as well as suggestions for future research.

Chapter 2

LITERATURE REVIEW AND BACKGROUND

2.1 Introduction

An integral part of the research process on seismic hazard analysis (SHA) is the assessment of the expected seismic damage and losses of the structure due to the ground motions of specific earthquakes. In case of seismic loads, intensity, energy and frequency of earthquakes play an important role in causing damages. Specific features of near-fault earthquakes from an engineering point of view were first investigated by Bertero et al. (1978).

Results of an analytical study of a severely damaged building during the San Fernando earthquake indicate that the long-term acceleration pulse was the main cause of this structural damage. Generally, near-fault earthquakes have strong dynamic motions with peak ground accelerations (PGA), peak ground velocity (PGV), and peak ground displacements (PGD) (Baker, 2008).

These movements include a pulse-like in time history of the ground motion velocity, which are often in the direction perpendicular to the fault rupture in places close to the fault where the earthquake rupture propagates towards the site. The damage level occurred in buildings due to the early earthquakes depends on two factors; structural performance and generated seismic loads. The performance of non-structural members, such as infills in buildings, has been one of the most important factors in

changing the behavior of structures and causing structural collapse during previous earthquakes (Northridge 1994, Kobe 1995, Chi-Chi 1999, Bam 2003, Christchurch 2011).

Successful correlation among the above-mentioned damages ensures the accurate assessment of seismic performance and prediction of the structural response. Adopting an optimal ground motion intensity measures that correlates with the performance requirements of demand of engineering is also of significance.

Numerous seismic parameters have been proposed to demonstrate the intensity of earthquakes, which have similar degrees of structural damage. The correlation between seismic parameters and structural damage factors has attracted the attention of many researchers.

Arjomandi et al. (2009) have evaluated the dependence between various parameters of seismic acceleration and the damage level due to 1, 2, 3, 4, 5 and 10 story steel buildings. A set of several cumulative and non-cumulative variable damage indexes had been introduced which were cyclic-fatigue-based and modal-parameter-based. They studied the relationship between the performance levels of FEMA-356 and the magnitude of damage index. 20 records selected from FEMA-440 was used for nonlinear dynamic analysis.

Krishnan et al. (2012) have estimated the damage to high-rise buildings located in wide areas by combining the predictions of the ground motion with numerical analysis of structural models.

Most of these studies use numerical methods to calculate the structural responses, and a "building-specific" forecast for a specific scenario can provide a precise estimate of the damage. However, numerical methods may require costly resources that are not appropriate for full scale analyses. In addition, these methods do not always indicate accurate responses of the existing buildings due to the lack of information and structural design details (material quality, boundary conditions, etc.) that eventually demand approximate assumptions. Generally, near-fault earthquakes have strong dynamic movements with PGA, PGV, and PGD. Many seismic parameters have been proposed to express the intensity of earthquakes, which have similar degrees of structural damage. The correlation between seismic parameters and structural damage factors has attracted the attention of many researchers. Kostinakis et al. (2015) examined the seismic responses of symmetric and asymmetric 5-story concrete buildings in 3-dimensions using 64 ground motions caused by bi-directional earthquakes. The performance of the buildings has been evaluated for the maximum and average inter-story drift ratio and the index of global structural damage based on Park-Ang structural damage index. The results showed that the (S_a) in the main period of the structure (T_1) has the significant correlation between the maximum and average inter-story drift ratio, and the velocity related to the seismic parameters comes second. Yakut and Yilmaz (2008) have analyzed 16 concrete frames under a series of 80 records of ground motion using nonlinear time history analysis. These frames are selected to represent low-rise, middle-rise, and high-rise frames and maximum inter-story drift ratio was used as damage index. The results showed that spectral intensity parameters such as PGV, PGA and S_a (T_1) had more effective correlation compared to other parameters.

The relationship between the structural response and ground motion parameters has been investigated using the ground motion data in California and based on vulnerability assessment methods that use inter-story drift ratio as the damage index. 115 seismic ground motions records for 114 types of steel buildings and 76 types of reinforced concrete buildings were used in this study (Perrault and Guéguen 2015). Three categories of height were selected in order to compare with HAZUS-MH classification (2003) for buildings: low-rise, mid-rise, and high-rise buildings, for buildings of 1-3 stories, 4-7 stories and 8 and more stories, respectively. The low-rise category included 70 buildings, the mid-rise consisted of 96 buildings and the high-rise category included 68 buildings. They showed that the classification of buildings by their type could reduce misunderstandings in the structural responses. On the other hand, according to HAZUS method, the building drift can be assumed as the damage index and the first step of obtaining the damage prediction equation of the building (Perrault and Guéguen 2015).

In order to present an acceptable response, 204 near-fault pulse-like seismic records were selected and from these 23 seismic parameters were determined for an acceptable response of a tested three-story concrete frame (Cao and Ronagh 2014). The main objective of this paper was to determine the seismic parameters that are most correlated with building damage by using Park-Ang damage index model and the maximum inter-story drift ratio (MIDR) (Cao and Ronagh 2014).The results showed that the intensity of velocity spectrum is a prominent parameter that has the best correlation with Housner intensity, S_a (T_1), and S_d(T_1). In contrast, the results indicated that the peak acceleration parameter did not correlate well with building damage.

The internal correlation between 10 ground motion intensities from 20 well-known acceleration records, which included maximum inter-story drift ratios as the damage index, and the highest intensity of a reinforced concrete frame, has been studied by Elenas (2000). He studied the relationship between the near-field and the global damage of the structures. He has shown that correlation coefficients of Pearson and Spearman have similar correlations between some seismic parameters and two global structural damage indexes (Modified Park-Ang model and maximum softening of DiPasquale and Cakmak model). He concluded that PGA has a weak correlation with damage indexes, while energy spectral parameters have a strong correlation with damage indexes. Therefore, a large number of seismic records must be evaluated to obtain accurate results.

Elenas and Mesjouris (2001) have suggested that the PGA parameters provide a relatively weak relationship with the Park-Ang global model, the maximum acceleration of ground and the maximum inter-story drift ratio. On the other hand, energy and spectral parameters make good correlations with these three indexes.

Nanos et al. (2008) demonstrated significant relationships between durations of strong ground motions and the global damage indexes of the building that included Park-Ang model, and DiPasquale and Cakmak model. They evaluated the correlation of seismic parameters related to 450 records of artificial strong motions with global damage indexes of a 6-story RC frame. They concluded that Arias Intensity (AI) had a strong correlation with damage indexes. Generally, the correlations between strong motion parameters and damage indexes are different and depend on time definition.

Elenas (2011) examined the relationship between seismic intensity parameters and structural damage indexes, such as, modified Park-Ang index and inter-story drift ratio. Studies have shown that the spectral energy parameter plays an important role in relation to the damage index.

Yang et al. (2009) collected and categorized two sets of pulse-like and ordinary near-fault ground motions of Chi-Chi, Taiwan, and Northridge earthquake records. They evaluated the correlation between 30 parameters of intensity measures and index of maximum non-elastic displacement of a single degree of freedom structure and also improved EPA (effective peak acceleration) and EPV (effective peak velocity).

Investigating the nonlinear dynamic responses of the designed frame showed that the ground motions caused by the same earthquake may cause significant changes in dynamic features of the structure (Gutierres and Chopra 1973).

Anderson (1987) indicated that the nonlinear response of the structure to ground motion is dependent on duration and relative pulse acceleration which is enormously destructive to various structures. Makris and Black (2004) obtained similar results and peak ground velocity was approved as the intensity index for near-fault earthquake.

2.1.1 Nonlinear Analysis

Nonlinear analysis considers the nonlinear behavior of materials and can be carried out by using two methods:

a) Nonlinear Dynamic Analysis

b) Nonlinear Static Analysis

In nonlinear dynamic analysis method, the structural response is calculated by considering the nonlinear behavior of materials and nonlinear geometric behavior of the structure. The basis of nonlinear dynamic modeling and its acceptance criteria is similar to nonlinear static method. The main difference is the use of time history analyses for response calculation.

The target displacement is directly measured and calculated using nonlinear dynamic analysis and time history of the ground motion. The calculated response is very sensitive to the features of the ground motion, so it is better to analyze for more than one record. Since the mathematical model used in this method directly considers the effects of non-elastic response of the materials, the internal forces obtained from this method are approximately equal to the forces created in the structure during earthquakes.

2.2 Seismic Behavior Assessment of Infilled Frame Structures

In FEMA 356 (2000) code, simple and easy methods for design and analysis of infilled frame structures have been used based on the results of experimental and analytical research. Hence, based on the above mentioned results, some methods were proposed for general use as well as recommendations for determining new relationships in seismic regulations.

In addition, some researchers have investigated the bracing of structures with frame infills, due to their role in resisting seismic loads or used them to enhance or rehabilitate the structure (Barkhordary and Tariverdilo 2011). Obviously, the categorization of the studies as stated is only for general familiarity with the works

done in field of infills, and there may be studies in which all three categories are simultaneously investigated.

2.3 Considering the Effects of Masonry-infills in Buildings

In recent decades, many researchers and engineers have studied the effects of masonry-infills in structural frames, and the effects of masonry infill walls on the behavior of the structures has been one of the concerns of engineers.

Since the materials of these walls and their strength and stiffness as a result are highly dependent on the location of construction and available materials, most countries, have rules for considering the effects of masonry infill walls according to their existing climatic conditions and included them in their own design regulations. Iran, has not been an exception to this, and some rules regarding the effect of masonry infill walls on structural behavior have been added to Standard No.2800 (2014) over the past years. One of these rules that considers the effects of walls in the building is rule 1-5-6 of Standard No. 2800(2014), which states that if non-structural members do prevent the displacement of structural members during earthquakes, the interaction effect of these members with structural system should be considered in analysis.

Despite extensive studies in recent decades lack of a design basis in regulations is not surprising, due to the different interaction parameters. There are two methods that can be used to consider the effects of infill walls in the main frame:

a) The infill wall is considered separately from the frame and its contribution to structural behavior is ignored.
b) The infill wall is assumed to be inside the frame and attached to it and the interaction between the main frame and the infill wall is considered.

If the infill wall is attached to the frame, it is possible that the infill wall hits the frame during the earthquake, causing shear forces and bending moments in the columns and forms a short column mechanism. In this case, shear failure, will be inevitable especially in concrete and steel structures.

The stiffness and extra resistance due to the presence of infill walls during dynamic loading, will extensively change the behavior of the structure. During the seismic stimulation, the increase in stiffness reduces the vibrational period, which results in increased forces on the structure. On the other hand, the strength capacity increases and the ductility demand of the structural elements will change (Shinozuka et al 2001).

2.3.1 Masonry Infilled Frame

Infill is defined as a panel that partially or completely covers the opening of a steel or concrete frame and is surrounded by beams and columns. The masonry infill materials that are considered in FEMA-356 (2000) are consist of brick-infills made of cement or pottery and do not include infills made of stone or glass.

The infills that have gaps between the frame and infill at the top and sides of them are considered as separated infills from their surrounding frames in such a way that the occurrence of maximum expected deformations of the frame is freely possible.

Infills must be braced in the out of plain direction so that their stability is guaranteed against the loads in this direction. Panels that are fully in contact with their surrounding frame in all four directions are called shear frame infills. The members and joints of the surrounding frame of an infill should be evaluated for the effects of the frame and infill interaction. These effects include the forces transmitted from the infills to the beams, columns and the frame joints in a part of their length.

2.3.2 Available Masonry-infilled Frame

Existing frame infills are all infills which have been existing in the building before rehabilitation. The existing infills should be examined separately against the lateral in plain and out of plain forces. If it is proven that the existing masonry infill frame are in appropriate condition in accordance with FEMA-356 (2000), it can be assumed that their behavior is the same with the behavior of new masonry-infills.

2.3.3 Stiffness of Masonry- infilled

The elastic in-plane stiffness of a solid unreinforced masonry infill panel prior to cracking shall be represented with an equivalent diagonal compression strut of width, *a*, given by Equation (Eq.1). The equivalent strut shall have the same thickness and modulus of elasticity as the infill panels it represents FEMA-356 (2000). The width of *a* in cm is:

$$a = 0.254[\lambda_1 h_{col}]^{-0.4} r_{inf} \quad \text{(Eq. 1)}$$

In which

$$\lambda_1 = \left[\frac{10 E_{me} t_{inf} \sin 2\theta}{E_{fe} I_{col} h_{inf}}\right]^{0.25} \quad \text{(Eq. 2)}$$

Where h_{col} = Column height between center lines of the beams; h_{inf} = Height of the infill panel; E_{fe} = Expected modulus of elasticity of the frame material; E_{me} = Expected modulus of elasticity of the infill material; I_{col} = Moment of inertia of the column; L_{inf} = Length of the infill panel; r_{inf} = Diagonal length of the infill panel; t_{inf} = Thickness of the infill panel and equivalent strut; θ = Angle whose tangent is the infill height-to length aspect ratio. In the above calculations, only a part of the panel should be in full contact with the frame. Stiffness of cracked unreinforced infilled-masonry shall be represented with equivalent struts; the strut properties shall be determined from

analyses that consider the nonlinear behavior of the infilled-masonry system after the masonry is cracked.

The equivalent compression strut analogy method may also be used to represent the elastic stiffness of a perforated unreinforced masonry infill panel (Figure 2.1). The equivalent strut properties shall be determined from stress analyses of infill walls with representative opening patterns. Elastic stiffness for both existing and new infill walls shall be considered to be the same.

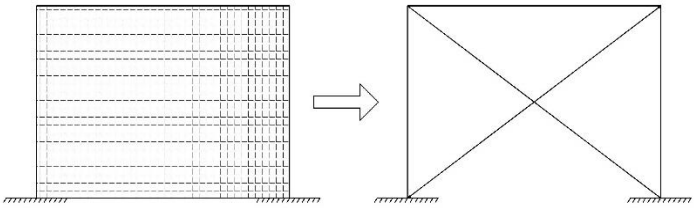

Figure 2.1: Infilled-masonry Equivalent Compression Strut.

2.4 Soil-structure Interaction

In the previous section, the relationship between structural failure and earthquake record was investigated and there was no mention of the effect of soil-structure interaction. In the analysis, it is assumed that the connection of the structure to the ground is rigid, but in general, this assumption is incorrect unless the structure is placed on very strong materials such as rocks. When the structure is placed on hard soil, seismic excitation moves directly to the structure without changing its content. But in real terms, when the structure is constructed on soft soils, there are two fundamental changes in system analysis: First, the seismic excitation will change after the construction of the structure. Secondly, a structure on a soft soil is a different system than a hard soil. So, the structures prefer to interact with the surrounding soils. In some

cases, it can be said that consideration of the effect of soil-structure interaction will make the design of the structure economically or uneconomical feasible according to the type and characteristics of the soil and structure.

Soil-structure interaction causes the change of elastic and non-elastic response of the structure. Constructing on a flexible substrate creates a new system that is more flexible than a rigid substrate. In addition, the transfer of a part of the vibrational energy to the infinite space results in a new source of damping called radiation damping and changes the dynamic behavior of the structure. If such a structure is placed on a flexible substrate then this may cause a change in the nonlinear response of that structure. Therefore the study of the effect of soil-structure interaction and the response of the structures should include the effect of soil structure on the non-elastic behavior of the structure. In principle the effect of soil structure on the nuclear reactors or in general the effect of the soil-structure interaction is very important and it cannot be ignored. In general, the effect of soil-structure interaction is very important and cannot be ignored. In the regulations, the force generated by seismic ground motion excitation on the structure is sometimes low and at sometimes too much. In analyzing structures that are highly sensitive, such as, the nuclear reactor structures, advanced analyzes are required and even some of these analysis are still being re-evaluated. The methods presented in this text are intended to simultaneously study the effects of free field and the effect of self-construct (Wolf and Deeks 2004). In this context familiar methods such as the methods of material resistance or stiffness methods as well as new methods, such as, finite element method are discussed. But the main focus of this research is on a novel approach called the methods of materials or Cone method. In this method unlike more precise numerical methods an analyst can acquaint himself with the characteristics of the effect of soil-structure interaction and given the precision

of engineering considering the effect of soil structure interaction on a wide range of structures. Many ground investigations were carried out by using this approach. A number of these are provided since it is not possible to refer to all (Wolf and Deeks 2004).

The problem of soil-structure interaction occurs when the structure on a rigid earth is neglected. In general, consideration of soil can be considered from two different perspectives: First, the waves released from the fault change due to the passage of different layers of the soil. This phenomenon has the site effects. Secondly, the structure also interacts with the soil and has a different behavior. However there are cases where consideration of this effect increases the forces and deformations and promotes the design in terms of safety especially in structures with high weight and high stiffness of the reactor. Hence, considering the effect of soil-structure interaction can only be scientifically attractive. From economical and security point of view this can justify the formation of soil structure interaction with the effect of kinematic interaction and inertia interaction.

Studies show that the effect of inertia interaction is more important than the kinematic interaction (Veletsos 1993). A qualitative example of the kinematic and inertial interaction is shown in Figure 2.2. Assume that the waves around the boat would provoke the free-field band. So the boat will represent the foundation and the person standing up will represent the structure. The low oscillation will cause average of the waves reaching his body and will fluctuate due to the fluctuation of the personal inside the boat. This oscillation is created and kinematics is similar to induction inferences (KI).

When a person moves in the boat, his vibration will strike, due to his mass and Newton's first law. This vibration causes the oscillation. This oscillation is the same as the inertia effect (II) Mahsuli (2006).

The effect of the soil-structure interaction on the dynamic response of the structure was investigated by various researches over the past three decades. Accordingly, the evaluation of the dynamic response of the structure, taking into account the effect of soil- structure interaction, has two parts. The first part is the earthquake correction recorded in the free field, so that the input stimulation is calculated in advance. The second part is the replacement of the structure with a soil-structure system, which considers the effect of soil in the dynamic analysis. Then this soil-structure system will be analyzed under the by seismic ground motion excitation.

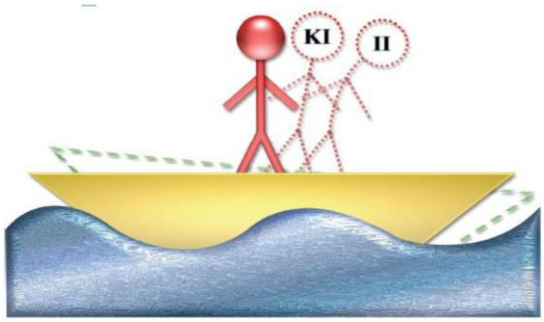

Figure 2.2: An Example for Explaining the Kinetic Interaction and the Interaction of Inertia Mahsuli (2006).

2.5 The Purpose of the Interaction of Soil-structure

In structural dynamics, the aim is to obtain the deformations of a structure under the influence of dynamic loading. Structural element formed finite element with the number of degrees of freedom. After that, the equation of motion for the structured element is obtained and it is solved by the advanced methods available. But the fact is

that the structure deals with the surrounding soil. So it's not true that the analysis will only focus on modeling the structure. Structural deformations subjected to seismic ground motion are affected by three systems of interconnected structures, foundations and geological environments below and around the foundation. Soil-structure interaction analyzes the cumulative response of these systems to the motion of the free field.

Some of the seismic loads first enter the soil around the structure and then transported through the soil to the structure. Soil is an almost infinite surrounding, or an infinite domain. In a static loading, the distance between the seismic loads can be removed at a distance far from the structure inside the soil from the engineering viewpoint. It is considered as a virtual boundary, and hence, soil can be modeled as a structure, and the soil and structure surrounding can be merged. But this cannot be done under dynamic load conditions since the virtual boundaries reflect the waves that come from the vibrating structure in to the soil element and prevent their radiation to the infinity. In fact, in the actual state of earthquake waves, it is reflected after the collision of the substructure, and earthquake waves are reflected in the substructure, away from the structure. In the event that the waves are displaced by these virtual boundaries, they again encounter a new barrier and return back to the structure. Proper modeling is needed for this kind of surrounding and structural dynamics and the soil dynamics are two important parameters to be considered for this purpose.

The purpose of the analysis of the interaction of soil - structure is shown in Fig.2.3, where the structure is located on a layer of soil that can be part of the structure that is left within the soil, and this soil can also be layered. Our goal is to investigate the dynamic behavior of the structure and to reduce the effect of dynamic behavior of soil.

It should be noted that the effect of wave propagation within the soil to infinity should be applied in the model. So the environment of almost infinite soil acts like an energy sink.

Also, in this image, part of the structure and the soil are elemental, which is necessary in some methods of analysis such as the direct method.

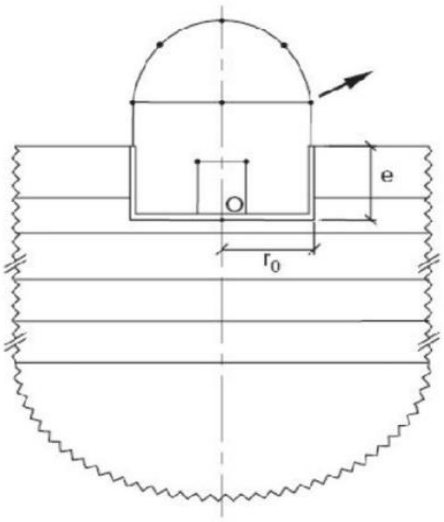

Figure 2.3: System Structure and Soil in a Desired Loading Wolf and Deeks (2004).

2.6 Various Methods for Measuring the Effects of Soil – structure Interaction

During dynamic excitation of a structure, it is common practice to introduce earthquake loads. This is acceptable when the soil stiffness located under the structure is high. Otherwise, the response of the structure under the influence of the soil-structure interaction phenomenon (as described in the previous section) will be different.

The effect of soil flexibility on the dynamic response of the structure has been the subject of research over the last three decades. Considering the effect of soil-structural interaction there are two different methods in assessing the dynamic response of the structure. The first method is to modify the data of the recorded earthquake to match with the free field motion and then analyze the structure by using this modified stimulation. In the second method, replace the structure by a new model that takes into account the effect of the soil and then carry out analysis by using the same modified data of free field motion. These two methods, if applied correctly, lead to an answer.

Different methods have been devised to consider the effect of soil-structure interaction by using free-field motion, each of which has its own disadvantages and advantages. But all these methods can be grouped into two categories: direct and indirect or substructure methods.

Direct methods are methods in which structures and soil are modeled and analyzed simultaneously using a virtual boundary. An indirect method is a method in which a structure by a mechanical equivalent system is connected to a ground.

When indirect methods are considered the soil-structure systems are divided into two parts. The first part consists of the structure on the substrate and the second part includes the soil having a common boundary with the structure.

Since the effect of the cinematic interaction is important and influential on the structures with a shallow foundation, it is necessary to study the parametric performance of the structure in the inelastic domain, with the consideration of both the kinematic interaction and the inertia Ghannad and Ahmadnia. This soil research is

based on conic and structural models, an SDOF was introduced with a bilinear behavior of soil and structural models. The analyses for two dimensional parameters that represent the degree of the effect of the interaction and slenderness of the structure were carried out in different records. The results of this research are as follows:

- The soil-structure interaction generally reduces the elastic and inelastic forces required in the structure. But for a structure with short-period, the inelastic forces required in the soft soil condition may be more than that of the hard soil condition.
- The interaction of soil-structure in the elastic range has a greater effect than in the inelastic range.
- In general, the behavior coefficient of soil is found to be lower for soft soil when compared to that of the rigid bed.

The studies of Ghannad and Jahankhah (2006) focuses more on the behavior coefficient by examining the parametric behavior of the non-elastic structure by increasing the interaction of the soil-structure. They found that the soil-structure interaction generally reduces both the elastic and inelastic force demand of the structure and the effect of the interaction decreases with increasing the inelastic susceptibility. Therefore, soil-structure interaction reduces the behavior coefficient.

Although the soil-structure interaction does not affect the behavior coefficient of the system on the hard soil, its effect on the structures on the soft soil can be remarkable. Therefore, the effect of soil-structure interaction for the design of structures located on soft soils should be considered. Also, in these studies, the spectrum of the design for obtaining the coefficient of behavior with regard to the shear wave velocity in the soil was presented.

2.7 History of Soil-structure Interaction Studies

Gutierres and Chopra (1973) proposed Ritz method for dynamic analysis of multi-story buildings with a soil-structure interaction. The system studied was a shear building located on a rigid circular plate connected to the half-space linear elastic surface. In this method, the structural changes to the normal vibration models of the building are transformed into a rigid structure. Bielak (1974) has studied the soil-structure interaction where he considered the buried foundation and material damping. Karabalis and Beskos (1986) obtained the dynamic response of buried structures by considering the effects of soil-structure interaction using finite element methods. Trifunac et al (2000) used both analytical and empirical approach to solve the problems of soil-structure interaction.

Xiaoming et al (2003) has considered the asymmetry and irregularities of earthquake waves, which led to non-uniform failures in the foundations of a flexible resilient building.

2.7.1 Cone Model for Surface Foundation

This type of cone is used for horizontal and vertical displacement transitions. Figure 2.4 shows the transient cone model. To obtain the height of the complete cone formed above the incomplete cone, use the static stiffness obtained from the cone model with the stiffness of a rigid plate on the half-space, according to the motion mode, and hence calculate the degree of opening of the cone head. This causes the cone model to match completely in the static and real mode.

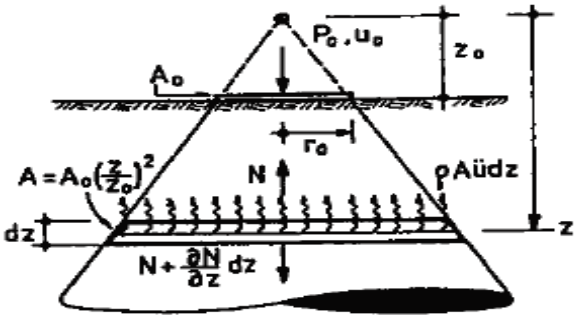

Figure 2.4: Translational Cone with Vertical Motion, Axial Distortion Wolf and Deeks (2004).

The coefficient of stiffness and damper can be obtained by using Wolf (1994):

$P_0(t) = Ku_0(t) + C\dot{u}_0(t)$

(Eq. 3)

$K = \frac{\rho v^2 A_0}{z_0}$ (Eq. 4)

$C = \rho v A_0$ (Eq. 5)

In which ρ, A_0, v, P_0, u_0 and $\dot{u}_0$ are soil density, foundation cross section, velocity, force, displacement, velocity of system, respectively.

Rotational cone type is used for rotational displacements including creep and torsional spin movements. Figure 2.5 shows the rotational cone model. The coefficient of hardness and damper can be obtained as follows:

$K_\varphi = \frac{3\rho v^2 I_0}{z_0}$ (Eq. 6)

$C_\varphi = \rho v I_0$ (Eq. 7)

Where I_0 and z_0 are moment of foundation in z deep and peak distance to the ground.

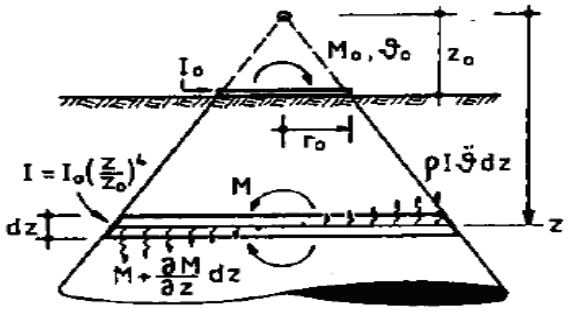

Figure 2.5: Translational Cone with Rotational Motion Wolf and Deeks (2004).

2.8 Background to Principles of Strength of Materials

In order to understand the principles of the strength of materials for analyzing the soil-structure interaction, it is found appropriate to provide a brief history of the development of method for finding resistance of materials. The pioneering reference (Ehlers 1942) published before 1942 shows the infinitely incomplete transitional cone for modeling a pivot on the surface of a homogeneous half-space for horizontal and vertical motion of a surface layer. A homogeneous half-space was investigated 30 years later in 1974 using shear distortions in a cone Meek and Veletsos (1974). A spring-damper-mass model with coefficients independent of the frequency of an additional degree of freedom has also been developed in this paper, which shows that the rotary cone is exactly the basis of the centralized parameter models. The torsional motion of a surface layer on a homogeneous half-space is analyzed using a cone model in Veletsos and Nair (1974). In all homogeneous half-space states, the key aspect of wave motion is the propagation to the outside of the waves far from source of turbulence in a surface that is propagated in a direction of propagation (an increase in the sub surface) with an infinitely incomplete cone. It takes more than 15 years for significant progress to be reported at three levels. First of all the formulation of the

infinite half cones become consistent then the application develops and finally the cone faces are better understood.

2.9 Previous Studies on the Effect of Soil-structure Interaction on the Response of Structures

Many studies have been done to investigate the effects of soil-structure interaction on the behavior of structural systems. Prasad and Veletsos (1989) carried out research on the effect of soil-structures interaction on structures with low frequency oscillations. However, these effects are also important for structures with moderate to high frequency oscillations when the period of the soil is high. They also investigated the effects of soil-structure interaction on the seismic response of structures affected by the Mexico City earthquake in 1985. In 2004, Kim and Rosset (2004) studied the effects of nonlinear behavior of the soil on the nonlinear response of structure. In their study they considered structures with varying height.

2.10 Consideration of Damage Indexes

There are various global and local damage indexes for evaluating existing buildings. Each of these indexes focuses on a parameter that is derived from the building structural modeling. Ductility of structure, drift of stories, rotation of joints and components and components of structure, dissipated energy, and fatigue of structure are parameters that are considered in damage assessment. An overview of the previously proposed damage indexes is shown in Table 2.1.

Table 2.1: Overview of Previously Proposed Damage Indexes.

Local damage indexes		Global damage indexes
Cumulative indexes	Non-cumulative indexes	
Park-Ang damage index	Plastic ductility	Maximum softening

(Park and Ang, 1985)	(Williams and Sexsmith 1995)	(DiPasquale and Cakmak, 1988)
Energy-based models (Elms *et al.*, 1989)	Inter-storey drift (Sozen, 1981; Roufaiel and Meyer, 1981)	Park-Ang damage index (Park and Ang, 1985)
Low cycle fatigue (McCabe and Hall 1989, Stephens1985)	Ductility ratio (Newmark and Rosenblueth, 1971; Ayala and Xianguo, 1995)	Global damage index (Chung *et al.*, 1987)

Williams and Sexsmith (1995) aimed to investigate seismic damage indexes, according to their use in decision making of structural rehabilitation. The purpose was to assess quantitative damage by using damage index which was calculated with the help of numerical methods in order to provide stability for concrete structures subjected to earthquake. The index may be defined locally for a structural member or for the global structure.

Most local cumulative indexes are in nature, reflecting the dependency of the damage on both the amplitude of vibration and the number of loading cycles. The main disadvantages of local damage indexes are the need for adjusting the coefficients for a particular structural type and the lack of calibration against different degrees of freedom of the member damage. The global damage index may be calculated by considering the weighted average of the structure's local index or by comparing the modal features of the structure before and after the earthquake.

They defined the structural damage in terms of plastic deformations, as shown in Eq.8. This index is defined as the weighted average in the member or using the maximum value of damage index in the story that can be also be expressed in global terms.

Simplicity and ease of use has made it one of the most popular indexes for engineers and researchers:

$$DI_{\mu} = \frac{u_{\max} - u_y}{u_{mono} - u_y} \quad \text{(Eq. 8)}$$

u_{max} is the maximum deformations, $u_y$is yield deformations and u_{mono} is maximum deformation capacity of the system under a monotonically increasing lateral deformation.

Drift ratio, which is one of the most practical indexes of damage among engineers, can be put into this category of indexes. This index is defined as the ratio between the maximum displacement of the structure at the target point and the story elevation and it is generally a global index (Sozen, 1981; Roufaiel and Meyer, 1981):

$$DI_{Drift} = \frac{\Delta_{\max}}{H} \quad \text{(Eq. 9)}$$

Park and Ang (1985) introduced their index for the first time in 1985. The index is a combination of ductility parameters and energy absorption capacity. After several years, Kunnath et al. (1992) modified the basic index which is presented in Eq.10:

$$DI_{PA} = \frac{\delta_m}{\delta_u} + \frac{\beta}{\delta_u P_y} \int dE_h \quad \text{(Eq. 10)}$$

δ_m is the largest displacement occurred, δ_u is equal to the final displacement of the building members, and P_y indicates the elastic stress for the element. The dE_h integral shows hysteretic energy dissipation by the element and β represents a constant value for the model. The value of this parameter is set to 0.025 in this thesis. Although this index was calibrated for concrete members, it can be used to assess the damage of both concrete and steel structures. It is an efficient index due to its clear physical concepts.

This thesis research work is about steel structures, and OpenSees software (2013) was used for analysis and design. However, Park-Ang damage index cannot be directly used for steal structure in OpenSees software (2013) and hence a code was writer to do that.

Based on the FEMA274, μ_u is assumed to be, $11\delta_y$.The Park-Ang damage index can be calculated for a member. Also, in the case of calculating μ and μ_u for the structure, the index can be used for the entire structure too.

One of the methods for assessing the global index of the structure is the use of correlation equations and as a result, the relationship among the member indexes can be defined by the energy absorbed by them. In this regard, the damage index of the story can be determined according to the damage index of members of a story and the energy absorbed by them. The global damage index of the structure can also be obtained from the relationship between the damage index and the energy absorbed by the stories:

$$DI_{story} = \sum (\lambda_i)_{element} (D_P)_{element}$$
$$(\lambda_i)_{element} = \left(\frac{E_i}{\sum E_i} \right)_{element} \quad \text{(Eq. 11a)}$$

$$DI_{overall} = \sum (\lambda_i)_{story} (D_P)_{story}$$
$$(\lambda_i)_{story} = \left(\frac{E_i}{\sum E_i} \right)_{story} \quad \text{(Eq. 11b)}$$

D_p and E_i are index of damage and hysteretic energy of the member or story, respectively, λ_i is the ratio of a member or story's energy to the total energy of members of a story or all stories of a building. The description of Park-And damage

index can be shown in Table 2.2, and based on the aforementioned equation can be calculated using seismic responses.

Table 2.2: The Definition of the Park-Ang Damage Index (1985).

Damage Index, DI	Description
DI<0.1	No damage
0.1≤DI<0.25	Minor damage
0.25≤DI<0.40	Moderate damage
0.4≤DI<1.0	Severe damage
1≤DI	Collapse

Bozorgnia and Bertero (2001a and 2001b) have introduced two developed damage indexes for inelastic SDOF system, as shown below:

$$DI_1 = \frac{(1-\alpha_1)(\mu-\mu_e)}{\mu_{mono}-1} + \alpha_1 \frac{\mu_H - 1}{\mu_{H_{mono}} - 1} \quad 0<\alpha_1<1$$
$$DI_2 = \frac{(1-\alpha_2)(\mu-\mu_e)}{\mu_{mono}-1} + \alpha_2 (\frac{\mu_H - 1}{\mu_{H_{mono}} - 1})^{0.5} \quad 0<\alpha_2<1 \qquad \text{(Eq. 12)}$$

The coefficients of α_1 and α_2 which are mentioned in their paper, vary between zero and one. If $\alpha_1 = 0$ and $\alpha_2 = 0$ specific conditions occur for two damage indexes that are directly related to the maximum plastic deformation, but if $\alpha_1 = 1$ and $\alpha_2 = 1$, the two assessed damage indexes have direct relations to hysteretic energy dissipation.

Maximum Softening Index is a combination measurement of both reduced stiffness and flexibility effect. The damage index based on period is given by:

$$D_m = 1 - \frac{T_{und}}{T_m} \qquad \text{(Eq. 13)}$$

Where, T_{und} is the period of undamaged structure and T_m is the maximum period of structure.

These parameters can theoretically demonstrate the real seismic behavior of existing buildings, but in most cases, these data are not accurate because they are derived by modeling. Providing a precise model for existing buildings that are damaged by earthquakes is not possible since the distribution of cracks and plastic hinges cannot be well known by these models. In addition, the effects of infilled-masonry, architectural configuration and irregularity in plan and elevation of the buildings are inevitable which affects the seismic behavior.

Considering these effects in nonlinear mathematical models or finite element models is also very complicated and time-consuming. Therefore, taking the above mentioned parameters into account suitable cannot be sufficient for damage assessment during earthquakes. In contrast, some parameters can show the real seismic behavior of these buildings, considering the effects described above Crisafulli and Carr (2007).

These effects can be well evaluated and observed if they are carried out using semi-natural tests on existing buildings. These are qualitative construction parameters that are carried out using semi-natural tests with accuracy, speed and cost-effectiveness. Destructive and non-destructive tests on concrete structures have been conducted in this research considering the static and dynamic features of the structure.

A correlation between the important and effective parameters of ground motion and the Park-Ang damage index is indicated in this paper and finally, a new damage index has been introduced (Yerli et al. 2003).

2.11 Near-field Earthquakes

Strong ground motions with relatively large magnitudes are the most dangerous seismic loadings that the structure must resist. Mohraz (1976) has divided earthquake records into three groups, using 1989 Loma Perita Earthquake data:

1) Near-field records: Distance less than 20 km to fault
2) Intermediate-field records: distance between 20 and 50 km to the fault
3) Far-field records: Distance greater than 50 km to fault.

The concept of modeling and simulating strong near-field ground motions, as well as structural characteristics of a structure that should show controlled behavior against these dynamic movements, are the two important issues in near-field studies. Of course, there are still many problems and uncertainties in understanding, describing, and predicting the near-field ground motions.

The first near-field record registered is the 1996 earthquake in Parkfield, California. Harner and Trifonac (1967) first saw the existence of pulses in this record in 1967.Since then, reported records of major earthquake events, have confirmed these pulses in areas near the faults, and also such potential for destruction when the causative fault is in the vicinity of urban areas.

Following the 1994 Northridge-USA and 1995 Kobe-Japan earthquakes, many modern structures in these areas, which were designed according to the regulations of those countries with more advanced criteria, have been seriously damaged or destructed. Occurrence of such events led the researchers to study these two earthquakes more rigorously. After extensive research, most of the damage to these buildings were attributed to the special features of the near-field earthquakes. This was

the starting point for researchers paying closer attention to near-field earthquakes. Near-field earthquakes have specific features that distinguish them from distant earthquakes.

Near-field earthquakes have higher acceleration with limited frequency than far-field earthquakes with high frequencies. These earthquake records have long pulses with large amplitudes, especially when exposed to the fault propagation direction, which is often seen at the beginning of the record. The fault propagation effect occurs when the propagation vector of the rupture front is directed towards the site and the rupture velocity is approximately equal to the shear wave velocity.

It was found in the studies conducted that the period of these pulses will increase by the magnitude of the earthquake and the pulse amplitude is a function of the earthquake magnitude and distance of the station to the causative fault of the earthquake. Due to the presence of such intense pulses in near-field records, the records of these earthquakes will not be broad band but pulse-like.

This means that in Fourier spectrum, maximum spectral amplitude occurs in a very small range or approximately within a certain period, instead of a large periodic range. Existence of these specific pulses transforms the response of the structure from waveform to modal, in which one or more modes determine the final response of the structure. In such a case the response of the structure is determined by the superposition of the waves passing through it.

The specific pattern of wave distribution due to the shear deformations in near-field areas makes the horizontal components perpendicular to the fault with larger amplitudes than the vertical components parallel to the fault direction.

At the beginning of the earthquake record pulses transfer large amounts of energy into the structure. Hence, in a short time, the distribution of nonlinear behavior of the structure is transformed in such a way that instead of developing nonlinear behavior and plastic hinges at the height of the structure, most of the earthquake energy will be absorbed in the first created hinges and the expansion and development of nonlinear behavior is not observed. This energy absorption causes large inter-story drifts, which is not observed in current patterns, for example, from the one that uses the first mode shape of the structure as a response.

Another impact of strong pulses in such earthquakes is the transmission of the maximum amplitude of the response spectrum towards short periods. Therefore ductile structures are within the range of stiff structures, whose design is controlled by increased base shear instead of velocity or displacement. As a result, the structure vibrates in a stiff way and does not have the chance of further displacement to dissipate earthquake energy and its apparent ductility decreases. Studies have shown that damages are inversely proportional to the distance from the source of the earthquake; therefore, structures suffer more damages in near-field areas than far-field regions.

For some period ranges, response spectrum of near-field earthquakes is generally higher than those values in Iranian design code and they also have larger values when compared with response spectrum of far-field earthquakes. When the structure is exposed to near-field, motions, the structural requirements will increase. Distribution

of parameters in the elevation of a structure, such as, story drifts, inter-story drifts, relative velocity, and absolute acceleration are greater in near-field areas Abdolahzade et al. (2014).

2.12 Tectonic Plate Zone of Mazandaran Province (North of Iran)

One of the important features of Iran plate is the young tectonic movements which show themselves in active faults, young volcanos and vertical movements. According to the tectonic maps prepared by Iran fault-plane, it can be seen that this plate has net mass of young and active faults. In most seismically active regions of the world where seismic history goes back to the ancient times, usually tectonic movements are horizontal so that they release their energy along slip faults. This can be found in the northern regions of Minor Asia and Central Asia. In Iran area, the young plates' movements do not follow a particular procedure. In most regions, especially in Alborz, horizontal movements are observed in addition to vertical movements along faults which demonstrate messy deformation. Abdolahzade et al. (2014) has studied the seismic hazard assessment of north regions and potential and active geo seismic resources. They have also analyzed different types of faults in the region and the movements of the seismic tectonic plates in this region.

2.13 Summary

Many seismic parameters were proposed to express the intensity of earthquakes, which have similar degrees of structural damage. The correlation between seismic parameters and structural damage factors has attracted the attention of many researchers. In this chapter, numerous past research carried out on the seismic parameter responsible for the structural failure were reviewed. In all those past studies, none of them considered the effects of seismic parameter on structural failure in the presence of soft soils. There are various software tools that can be used for analyzing the soil structure interaction

problem. In general, software based on finite element method, such as Diana, Abaqus, OpenSees, Ansys, SAP2000, etc., can analyze soil-structure interaction problems.

This damage pattern is of great importance since it provides a better selection of earthquake records by considering the required parameters to demonstrate the destructive effects in buildings on soft and hard soils. It also considers issues such as Park-Ang damage index. The Park-Ang index is so important because it is based on the consumed energy in members and includes the deformation of the elements.

Some of the responses which can be recorded are the output of displacement, velocity, acceleration, drift, shear of the stories, input energy of structures, damage and hysteretic energy of members. These responses should be first considered for each story of a structure and then for the whole structure. Given the large number of these outputs due to the number of records, the above mentioned outputs were limited to displacement, drift, shear of the stories and structural damage. The reason for choosing the damage output is that the damage index may include final deformations, yield or ductility of the members, and the energy absorbed by them. The other reason for selecting this response is that if few members reach the yield point, other outputs may not experience many changes but the damage index is so sensitive. Based on how the damage index is defined, responses can be dependent on the members yield, stiffness, their absorbed energy or the combination of them.

Chapter 3

METHODOLOGY

3.1 Introduction

In the Hazus-MH classification (2003), heights of steel buildings were categorized as LR: low-rise (1-3 stories), MR: mid-rise (4–7 stories) and also HR: high-rise (8+ stories), respectively. First of all the design of 2D steel bare framed structures with 3, 5, 8, and 12 stories were based on SAP 2000 software by using the tenth topic of the National Building Regulations of Iran (INBC, 2013 similar to AISC 360-10). Then the structural sections found as a result of SAP2000 designed were used to create the same frame models in OpenSees software. Each building has three types of models introduced: i) bare frame, ii) partially-infilled frame iii) fully infilled frame. For each infill wall, the external bay of the frame was introduced as an equivalent diagonal strut based on FEMA-356 (2000) in OpenSees software (Table B.1). Before the analysis carried out all models were verified by using the first six modes. More details about verification can be found in chapter 5. The nonlinear dynamic analysis method (Time History) was used and the structural response was calculated by considering the nonlinear behavior of materials and nonlinear geometric behavior of the structure. Since the main objective of this research is to compare structures with each other, the structural designs were considered the sections as optimal.

SeismoSignal software was used for the investigation of earthquake parameters. 23 intensity measures were introduced for an acceptable response of a tested three-story

reinforced concrete frame by Cao and Ronagh (2014). 20 intensity measures (IMs) were introduced in SeismoSignal but 32 IMs in total were used for the study presented in this thesis. The 12 remaining IMs were calculated using MATLAB software. The 32 intensity measures were determined for each one of the two sets of seismic ground motions. Hence in this study, the effects of underlying soft and hard soils on the nonlinear response of structures with and without infills and subjected to two sets seismic records is evaluated by using nonlinear dynamic time history analysis.

To investigate the influence of the soil-structure interaction on the structural behavior, cone model was used to analyze the soil environment. Analysis of models was carried out twice by using OpenSees software; once with the assumption of rigid support and the second time by considering the soil under the structure (both modes). Non-linear analysis (time history analysis) for steel frames was done in 2D. For creating the models with the soil-structure interaction, an equivalent degree of freedom system was used. In this study, the effect of soil-structure interaction on the near-fault earthquake was investigated.

It is known from past earthquakes and literature that pulse-like seismic records can cause severe damage to buildings. On the other hand, the response of the structure to pulse-like and ordinary seismic records can be considerably different. Investigation carried out within this study on the failure of steel moment resisting frames with infills and without them are presented in chapter 6 this thesis. Then brief description of the fragility curves and how to calculate them is elaborated. In this study using the available ground motion data, the relationship between the structures response and its failure with the parameters of the ground motion were examined. Two sets of ground motions, called "Ordinary Seismic Records (OSR)" (74 records) and "Pulse-Like

Seismic Records (PLSR)" (64 records), were used in nonlinear dynamic analyzes of steel moment frames with and without infills. Seismic behaviours were measured and evaluated for the above mentioned sets of records using three global damage indexes; modified Park-Ang index, maximum inter-story drift ratio index and maximum roof displacement index. The relationship between several pulsed and un-pulsed intensity measures and three damage indexes on steel moment resisting frames with and without infills were determined by using Spearman correlation coefficient.

In literature, mainly the assessments of the relationships between the damage index and seismic parameters are concentrated on RC frames with limited number of seismic records (Kostinakis et al 2015). The estimation of the two global damage indexes (modified Park-Ang and maximum inter-story drift ratio) for two sets of pulse-like (Table A.1) and ordinary earthquake records (Table A.2) can be found in the first part of this chapter. In order to increase the accuracy of the results, 12 different types of steel frames were used for this study (Figure 3.1).

138 earthquake accelerations were used as input ground motion records and they are categorized into two groups of PLSR and OSR. Pearson linear correlation coefficient, which shows a degree of correlation between the ground motion parameters, was approved, calculated and compared. Nonlinear dynamic analysis was performed on the steel frames and linear correlation coefficient between ground motion parameters and general index of global structural damage were calculated and analyzed.

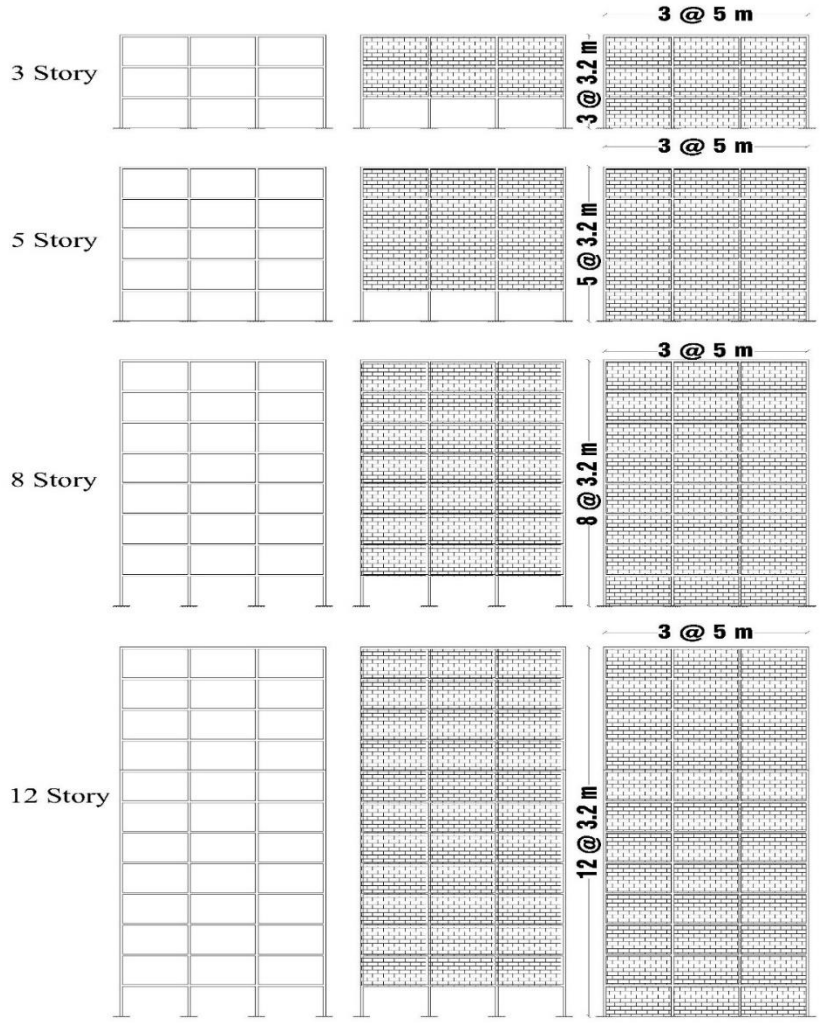

a) Bare Frame b) Partially-Infilled Frame c) Fully Infilled Frame

Figure 3.1: 3-, 5-, 8- and 12-story Bare, Partially Infilled and Fully Infilled Frames.

Soft Story: The soft story is usually present in buildings when a large number of nonstructural rigid components, such as masonry walls, are attached to the columns of the upper stories of structures while the first story is left empty of walls or with a reduced number of walls in comparison to the upper stories. There are different methods to calculate the stiffness of the story. For example, to calculate the stiffness of ith story, it is enough to restrain the columns in top and bottom of ith story.

F=k*d, for calculating k, apply force to ith story and then find displacement of ith story. k depend on the force, F and displacement, d. Arbitrary force is considered to be equal to 100 ton.

If the ratio of the force input to the displacement of ith story (stiffness of ith story) be less than 0.7 times stiffness of (i+1)th story, then this story is called soft story otherwise it is not soft story (Standard 2800). In this study the partially-infilled frames of all models do not have soft story.

3.2 Seismic Parameters of Near-fault Pulse-type Motions

For the effectiveness of ground motion parameters, two sets of pulse-like seismic records in the near-fault region and ordinary seismic records in soils with a shear wave velocity less than $360^{m}/_{s}$ were used in nonlinear dynamic time history analysis. These records were extracted from all over the world and selected from the PEER-NGA website. The selection of earthquake records were based on the shear wave velocity. They were selected by considering the type of soil C, PGV, magnitude (from 5 to 8) and epicentral distance. Table A.1 and Table A.2 are for earthquakes with PLSRs and OSRs, respectively. The earthquake selection had two components based on maximum acceleration.

3.3 Structural Analysis Methods

The first step to assess the behavior of a structure is to provide a mathematical model of the building, which includes all structural features, such as strength, stiffness, materials, support conditions, etc. Then, in order to determine the seismic effects on the members when subjected to earthquakes, the structure should be analyzed by using one of the following methods; linear static, linear dynamic, nonlinear static, and nonlinear dynamic according to the degree of importance and accuracy of their responses. In this study nonlinear dynamic time-history analysis was used.

3.4 Lateral Load Distribution

Lateral load distribution should be very similar to that occurring during the earthquake and create critical states of deformation and axial forces in the members. For this purpose, lateral load distribution by static method must be applied to the structure.

3.4.1 Lateral Load Distribution by Linear Static Method

Lateral load distribution by linear static method can be found from equation (Eq. 14)**:**

$$F_i = \frac{w_i h_i^k}{\sum_{j=1}^{n} w_j h_j^k} V$$

$$k = 0.5T + 0.75$$

$$T \leq 0.5 \rightarrow k = 1$$

$$T \geq 2.5 \rightarrow k = 2 \qquad \text{(Eq. 14)}$$

T= Fundamental period of the structure.

The value has no meaning in load distribution since it increases at any step, but the pattern and form of distribution is important.

Basic assumptions for the analysis and design of the initial models were carried out in accordance with the provisions of "Tenth Chapter of Construction National Regulations of Iran (INBC 2013)", which is related to the designs and execution of steel structures. Also Iranian code of practice for seismic resistant design of buildings, known as national standard No. 2800-2014 was used. It should be noted that the evaluation of the performance of these structures were based on FEMA-356 (2000) criteria.

3.5 Selecting the Initial Modeling Conditions

3.5.1 Material Properties and Sections of Steel Frames

Properties of materials and sections are required for the design of structures. In these buildings, author made the effort to use the specifications of materials similar to those used in common construction projects in the country. Material properties are presented in Tables 3.1 and 3.2.

For designing the main members of the building, such as the beam and the column, sections of the steel frame were designed by using Iranian steel design code (INBC 2013). In all designs, the structural analysis were carried out as bare frame and the soil-structure interaction was ignored (steel sections can be seen in Table 3.3).

Table 3.1: Properties of Materials

steel	
Weight per unit volume, W	$7850\ {}^{kg}/_{m^3}$
Modulus of elasticity, E_s,	$2.1 \times 10^6\ {}^{kg}/_{m^2}$
Poisson's ratio, ν,	0.3
Yield stress, F_y.	$2400\ {}^{kg}/_{m^2}$
Ultimate stress, F_x	$4000\ {}^{kg}/_{m^2}$

Table 3.2: Soil Properties (Standard 2800, 2014).

Soil type according to codes	Allowable stress,q_a	Subgrade Reaction Modulus ,k_s
Type III	$1.5\ {}^{kg}/_{cm^2}$	$1.8\ {}^{kg}/_{cm^2}$

Table 3.3: Steel Beam and Column Sections Used for the Steel Frames

Model	No. Story	Columns HEB (Number of Story)	Beams IPE (Number of Story)
1	3	220(1), 200(2), 180(3)	330(1), 300(2), 240(3)
2	5	280(1-2), 240(3-4), 220(5)	360(1-2), 330(3), 300(4), 240(5)

3	8	340(1), 320(2-3), 300(4-5), 280(6-7). 260(8)	400O(1-2), 360O(3-4), 330O(5-6), 300(7), 270(8)
4	12	450(1-3), 400(4), 360(5-8), 320(9), 280(10), 240(11-12)	400O(1-4), 400(5-7), 360(8-10), 300O(11-12)

3.5.2 Material Properties of Infill

For modeling the masonry-infilled in the structure, two equivalent diagonal struts were used in accordance with FEMA-356 (2000) and the width of these equivalent struts were calculated by using the Eq.1. The initial stiffness of a masonry-infilled wall, k_e (Sattar and Liel, 2010), is expressed as:

$$k_e = 2\left(\frac{E_{me} a t_{inf}}{r_{inf}}\right)(cos\,\theta)^2, \quad \text{(Eq. 15)}$$

When there is an increase in force on the masonry infill, the stiffness of the masonry-infilled frame decreases to α_h until failure occurs in the panels. For calculating the maximum strength of the masonry-infill Zarnic and Gostic (1997) proposed an empirical equation, which was later modified by Dolsek and Fajfar (2008):

$$F_{max} = \frac{0.818 L_{inf} t_{inf} f_{tp}}{C_l}\left(1 + \sqrt{{C_l}^2 + 1}\right), C_l = 1.925\frac{r_{inf}}{h_{inf}}, \quad \text{(Eq. 16)}$$

Dolsek and Fajfar (2008) proposed a cracking force (F_{cr}) of 0.55 times the maximum strength (F_{max}) and a wall strength (δ_{cr}) of 5.0 times the displacement (δ_{cap}). Struts have negligible tensile strength. The residual strength of the wall (F_r) is assumed to be 20% of F_{max}. Based on this experimental results, δ_{cap} is taken here as 0.25% drift (Manzouri 1995). The force-displacement relationship in Figure 3.2 indicates the initial stiffness (k_e), maximum strength, initial strain and ultimate strain.

Ibarra et al (2005) first introduced four parameters; stiffness, strength, reloading stiffness and post-capping strength for material and assigned them to the struts for infill.

Sattar and Liel (2016) used these four parameters to control the cyclic deterioration of material. . These four parameters can be used for infill walls with deformation and energy dissipation capacities similar to those used in this thesis.

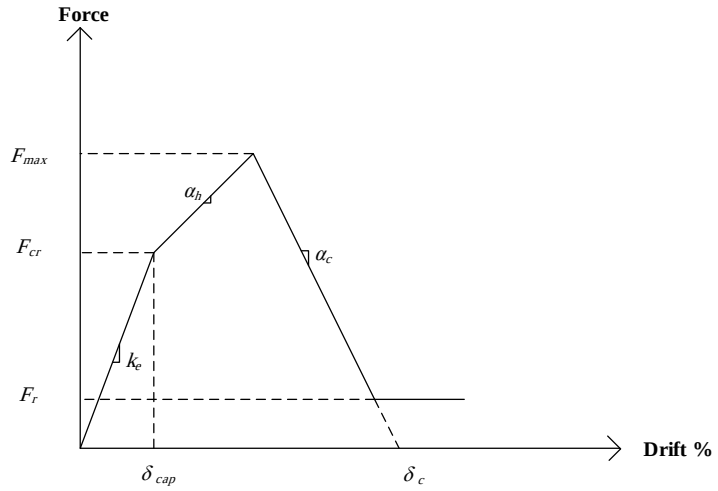

Figure 3.2: Model of Force-displacement Relationship Between Masonry-infill and Equivalent Diagonal Strut (Sattar and Liel 2010).

In Figure 3.3, the simulation model obtains material nonlinearities in beams, columns, beam-column connections, and masonry walls. P-Δ effects are incorporated in the model through a leaning column and large deformation geometric transformations, but not the contribution of the gravity system to the lateral resistance of the steel frame. Deterioration in the beams, columns, and connections were modeled with concentrated springs idealized by the tri-linear backbone and associated hysteretic rules developed by Ibarra et al. (2005), which was selected for its ability to simulate the strength and stiffness degradation experienced during seismic collapse.

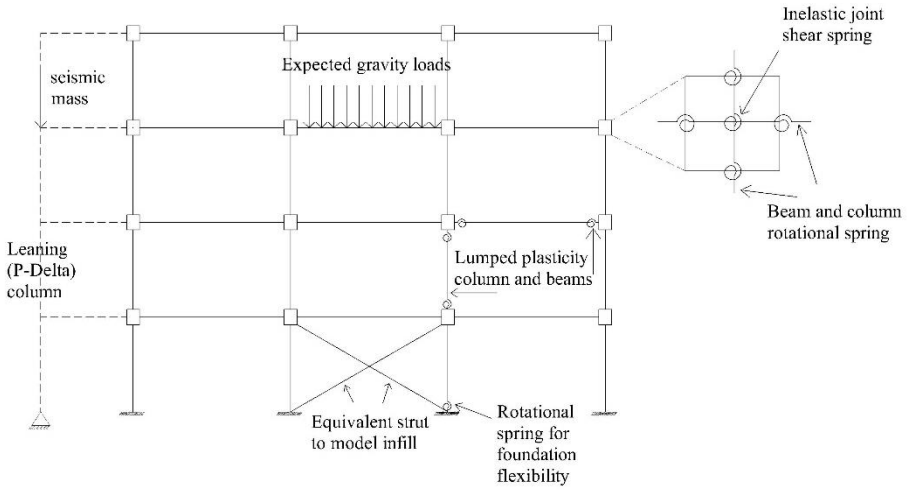

Figure 3.3: Schematic Archetype Building Model Showing Key Nonlinear Elements Used for Dynamic Analysis (Sattar and Liel 2010).

Calculating the Fundamental Period

Seismic loading of buildings were carried out in accordance with the regulations of designing buildings against earthquakes (Standard 2800, 2014).

Standard 2800 (Standard 2800, 2014) uses the following relationships to calculate the fundamental period of the structure:

A. For buildings with moment frame system

1. If infill walls are assumed not to prevent movement of the frames:

   • Steel frames $T = 0.08H^{\frac{3}{4}}$

   • Concrete frames $T = 0.05H^{0.9}$

2. If infill walls assumed to prevent movement of the frames:

   T is considered to be 80% of the above values.

B. For buildings with other framing systems

With the presence or absence of infill walls and in all cases, T is calculated by the using the following:

$$T = 0.05H^{\frac{3}{4}} \quad \text{(Eq. 17)}$$

Where, H is the height of the building in meters from the base. The fundamental periods of buildings are presented in Table 3.3.

Table 3.4: Assessment of Experimental Fundamental Period of the Models (Standard 2800, 2014).

Number of stories	Model height (m)	Experimental fundamental period (s)
3	$9.6m$	$T = 0.08H^{3/4} = 0.43\ S$
5	$16m$	$T = 0.08H^{3/4} = 0.64\ S$
8	$25.6\ m$	$T = 0.08H^{3/4} = 0.91\ S$
12	$38.4\ m$	$T = 0.08H^{3/4} = 1.23\ S$

Base Shear: Minimum base shear or the total lateral seismic force in each of the directions of the building is obtained from the following relationship (Eq.18):

V=CW (Eq. 18)

V= Base Shear force

W = total weight of the building, including all dead weight and the weight of fixed installations, plus a percentage of live load and snow load

C= seismic coefficient obtained from equation (Eq.19):

$$C = \frac{ABI}{R} \quad \text{(Eq. 19)}$$

In which:

A = Design base acceleration (in relation to gravity acceleration, g)

B = Response coefficient of the building obtained from the design response spectrum

I = Importance factor of the building, R = Behavior coefficient of the building.

Design Base Acceleration, (A): Design base acceleration ratio is different for the regions of the country, based on their risk of seismicity. The values are presented in Table 3.4. Since the modeled buildings are located in North of Iran, there design base acceleration of them is considered as 0.30.

Table 3.5: Design Base Acceleration Ratio for Different Seismic Areas (Standard 2800, 2014).

Region	Design Base Acceleration (g)	Description
1	0.35	Very high seismic relative hazard
2	0.3	High seismic relative hazard
3	0.25	Intermediate seismic relative hazard
4	0.2	Low seismic relative hazard

Response Coefficient of the Building, (B): Response coefficient of the building reflects how the building responds to the ground motion. This coefficient is obtained using relations (Eq.20):

$$0 \le T \le T_s \rightarrow B = 1 + S(\frac{T}{T_0})$$
$$T_0 \le T \le T_s \rightarrow B = S + 1 \qquad \text{(Eq. 20)}$$
$$T \ge T_s \rightarrow B = (S+1)(\frac{T_s}{T})^{\frac{2}{3}}$$

In which:

T= Fundamental natural period of vibration of the building in seconds

T_s, T_0, S = Parameters that depend on the type of soil and seismic hazard of the area.

The values of these parameters are presented in Table 3.5.

Table 3.6: Parameters for Calculating the Response Coefficient (Standard 2800, 2014).

Soil type	Low and intermidiate seismic relative hazard S	High and very high seismic relative hazard S	T_S	T_0
I	1.5	1.5	0.4	0.1
II	1.5	1.5	0.5	0.1
III	1.75	1.75	0.7	0.15
IV	1.75	1.75	1.0	0.15

Since modeled buildings are to be constructed on type III soil, the parameters related to the response coefficient are presented below:

$T_0 = 0.1$
$T_s = 0.5$
$S = 1.5$

Table 3.6 shows the calculation of the parameters related to response coefficient of the modeled 3, 5, 8 and 12 stories buildings.

Table 3.7: Calculation of the Buildings Coefficients (Standard 2800, 2014).

Fundamental period	Response coefficient
$T = 0.33 \leq T_s$	$B = S + 1 = 2.5$
$T = 0.57 > T_s$	$B = (S + 1)(\frac{T}{T_s})^{\frac{2}{3}} = 2.29$
$T = 0.77 > T_s$	$B = (S + 1)\left(\frac{T}{T_s}\right)^{\frac{2}{3}} = 1.87$

Importance Factor of the Building (I): The importance factor of the buildings, as described in Standard 2800, is obtained from Table 3.7 according to building classification. Since the modeled buildings are residential, they belong to Group 3 and their importance factor is 1.0.

Table 3.8: Importance Factor of the Building (Standard 2800, 2014).

Building Classification	Importance Factor
Group 1	1.4
Group 2	1.2
Group 3	1.0
Group 4	0.8

Behavior Coefficient of the Building, (R): The coefficient of behavior for the building includes the effects of factors, such as ductility, degree of indeterminacy and excessive resistance in the structure. The behaviour coefficient depends on type of lateral force resisting system of the building and according to Standard 2800 it is equal to 7.

The values for the seismic parameters A, I, and R used for the design are 0.3, 1, and 7, respectively. Parameter B can be calculated based by using Eq. 20 and Table 3.4. The values of B for 3, 5, 8, and 12 stories are calculated as 2.75, 2.75, 2.39, and 1.88, respectively.

3.6 Seismic Ground Motion Criteria of IMs

There are many seismic parameters introduced in past research which can be obtained directly from acceleration or indirectly by using time history analysis. Nonlinear time history analysis is performed using acceleration. The accelerometers used should represent the actual movement of the ground at the site. The SeismoSignal software introduces 20 seismic parameters for each record. 12 other parameters are calculated using MATLAB software. These seismic parameters are implemented in SeismoSignal and MATLAB software and summarized in Tables A.1 and A.2.

To determine the intensity of earthquake-induced seismic motions, a great number of IMs has been introduced in published research. A general definition for some IMs

based on their applications is presented by Kramer et al. (2006). All 32 parameters of ground motion intensity measures are listed in Table A.4. It should be noted that correlation between seismic intensity measures and damage state of the building has been previously evaluated by many researchers.

Ground motion parameters can be categorized into two groups. A group of earthquake parameters has been directly extracted. These parameters are PGA, PGV and PGD, which were used by many researchers to develop fragility curves. Parameters of the other group are determined indirectly by using computer analysis support. These parameters are S_a (T_1), S_v (T_1), S_d (T_1), EP, AI, etc. A detailed overview of the mentioned Ground Motion Intensity Measures (GMIMs) and their applications were done by Riddle (2007). Comparison of the response spectrum of two sets of earthquake records is shown in Figure 3.5. In these two spectra, it can be observed that the mean spectrum in a set of PLSRs is greater than the OSRs set.

These are important parameters for determining the potential ground motion damages. These seismic parameters may have a simple maximum value or be a combination of mathematical functions. Important seismic parameters are used in this study including PGA, PGV, PGD, velocity spectrum intensity (VSI), Housner Intensity (HI), sustainable maximum acceleration (SMA), sustainable maximum velocity (SMV), effective design acceleration (EDA), acceleration root mean square (A-RMS), velocity root mean square (V-RMS), displacement root mean square (D-RMS), Arias Intensity (AI), characteristic intensity (CI), specific energy density (SED), etc.

Features of the seismic parameters mentioned above are presented in Table A. 3. Selected seismic parameters include peak or maximum criteria (PGD and PGV),

spectral parameters, such as, response, energy, Fourier Spectral and energy parameters, such as, Arias intensity (AI), strong motion duration (SMD), SED, etc. Among the seismic parameters, CAV has showed a good relationship with structural damage in some of the past studies.

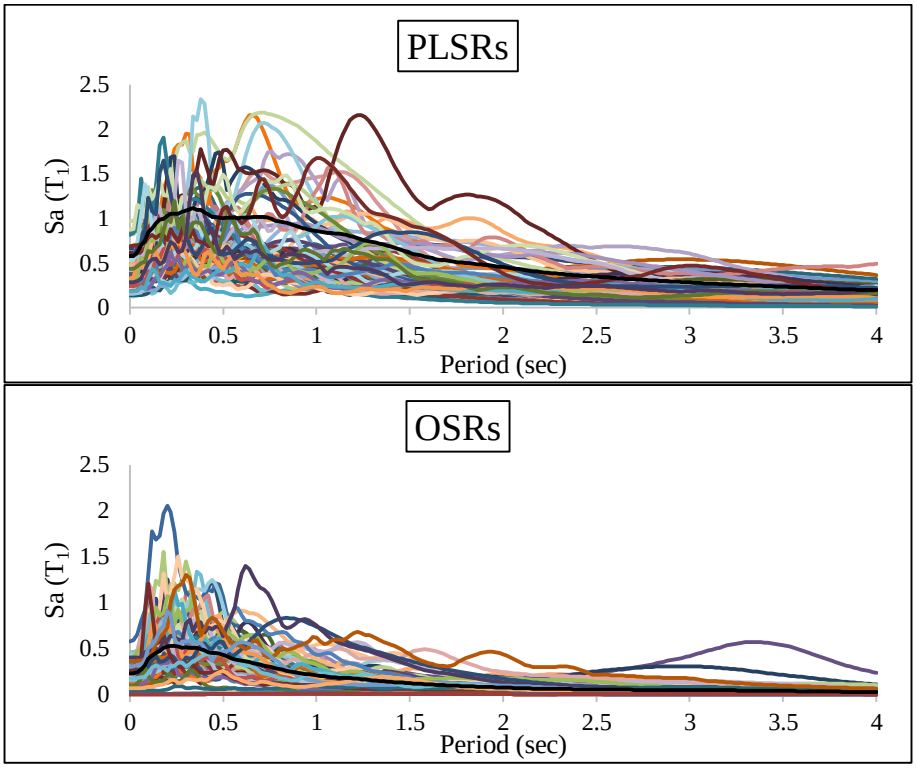

Figure 3.4: Comparison of the Response Spectrum of Two Sets of Earthquake Records.

Pseudo-Spectral acceleration and absolute spectral seismic input energy have strong interactions with these two models. On the other hand, PGA, central period and the strong motion duration determined after Trifunac et al. (2000), show a weak interaction with these two models.

Arias intensity (1970) and cumulative absolute velocity (CAV) are extracted according to the acceleration of time history. The average EPA is defined by spectral coordinates

according to the elastic acceleration response (5% critical value) over the period of 0.5-0.1 seconds, divided by the standard value of 2.5.

Arias intensity (AI) is the mass energy unit in a single degree of freedom (SDOF) system during the ground motion consumption process. CI is calculated according to amplitude and time dependent parameters (Park-Ang et al 1985). CI is a damage index with respect to maximum deformation and cyclic energy. I_f was proposed by Fajfar et al. (1990) after reviewing the two fundamental parameters of ground motion, including PGV and the duration of ground motion (t_d), based on 5 to 95 percent of Arias intensity (AI).

After introducing seismic parameters, Here we compare the Seismic parameters of Kocaeli earthquake record measured in two locations in Turkey was used. For each record, 20 and 12 seismic parameters were calculated with SeismoSignal and MATLAB software, respectively. The Kocaeli earthquake records at two different stations, Atakoy and Yarimca was used in this study (Figures 3.5 and 3.6). Figures 3.5 and 3.6 shows the acceleration, velocity and displacement for Atakoy and Yarimca stations, respectively.

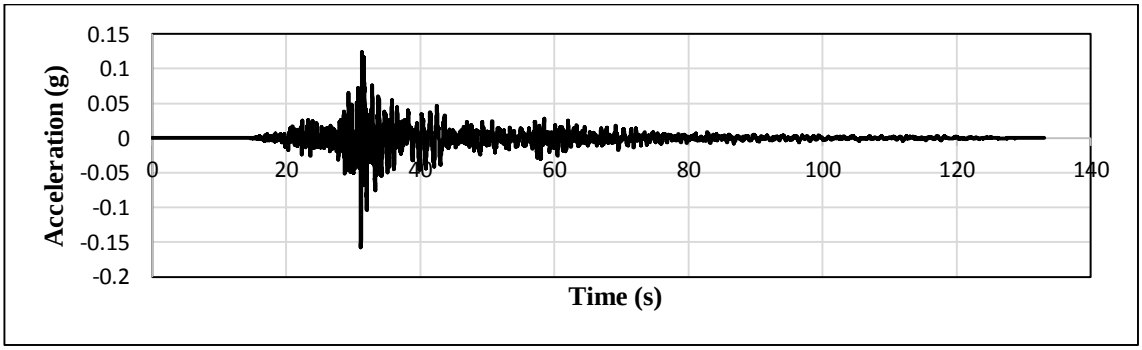

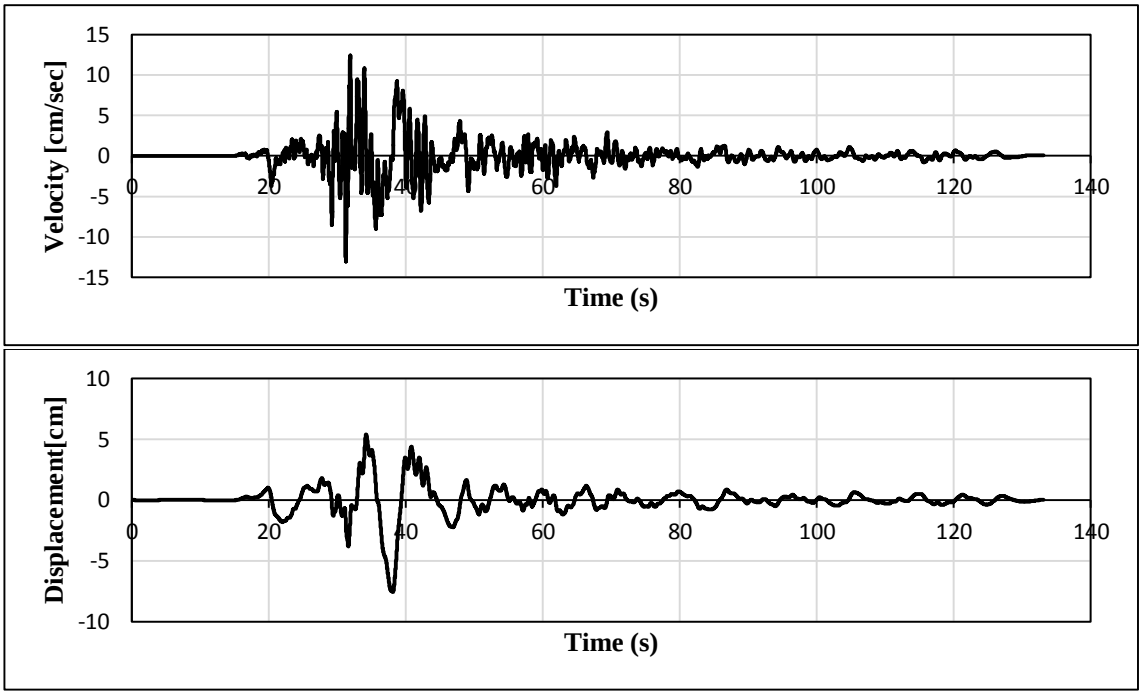

Figure 3.5: Acceleration, Velocity and Displacement of Kocaeli Earthquake in Atakoy Station.

As can be seen from Tables A.1 and A.2, the magnitude of this earthquake is high in both stations, but the distance to the fault line is different. Tables A.1 and A.2 shows that some records are close to the fault and large in magnitude, but they are in the OSRs category, which is not a factor in earthquake with pulses-like.

For example, Parkfeild earthquake and station: Parkfeild-Cholame. In Tables 3.8 to Table 3.9, the two records in Kocaeli-Turkey were calculated using SeismoSignal and MATLAB software. As can be seen the acceleration, velocity and displacement of the record with pulse-like are more than those of without pulse.

Table 3.9: Calculate of Accelerogram Kocaeli-Turkey in SeismoSignal Software.

No.	Accelerogram in SeismoSignal	IMs	Station Yarimca	Station Atakoy
1	Max Acceleration (g)	PGA	0.3445	0.15739
2	Max Velocity (cm/sec)	PGV	61.8466	13.06073
3	Max Displacement (cm)	PGD	39.9673	7.56145
4	Vmax/Amax (sec)	PGV/PGA	0.1830	0.08459

5	Acceleration RMS (g)	A-RMS	0.0495	0.01172
6	Velocity RMS (cm/sec)	V-RMS	16.4648	1.79941
7	Displacement RMS (cm)	D-RMS	11.7386	1.21576
8	Arias Intensity (m/sec)	AI	1.3214	0.28161
9	Characteristic Intensity	CI	0.0652	0.01463
10	Specific Energy Density (cm^2/sec)	SED	9486.7569	431.01168
11	Cum. Abs. Velocity (cm/sec)	CAV	997.0724	695.09400
12	Acc Spectrum Intensity (g*sec)	ASI	0.2140	0.143390
13	Vel Spectrum Intensity (cm)	VSI	168.6097	52.25290
14	Housner Intensity (cm)	HI	177.3293	48.57029
15	Sustained Max.Acceleration (g)	SMA	0.2046	0.11692
16	Sustained Max.Velocity (cm/sec)	SMV	59.4027	10.82017
17	Effective Design Acceleration (g)	EDA	0.3253	0.16357
18	A95 parameter (g)	A95	0.3402	0.15620
19	Predominant Period (sec)	T_p	1.4000	0.30000
20	Significant Duration (sec)	SD	15.8350	31.79000

Table 3.10: Calculate of Accelerogram Kocaeli-Turkey in MATLAB Software.

No.	Accelerogram in MATLAB	Yarimca Station	Atakoy Station
1	S_a (T_1)	0.4126	0.2208100
2	S_v (T_1)	55.6604	30.9660200
3	S_d (T_1)	8.6447	4.6229200
4	I_f	150.4187	44.3620870
5	I_a	1.5147	0.8035936
6	I_d	130.7231	38.6068560
7	I_v	51.1515	28.3163750
8	EPA	0.2114	0.1411463
9	EPV	33.6264	9.5741625
10	Ω	0.3062	0.4922386
11	T_m (sec)	1.3392	0.6627200
12	P_d	6.1989	0.0569820

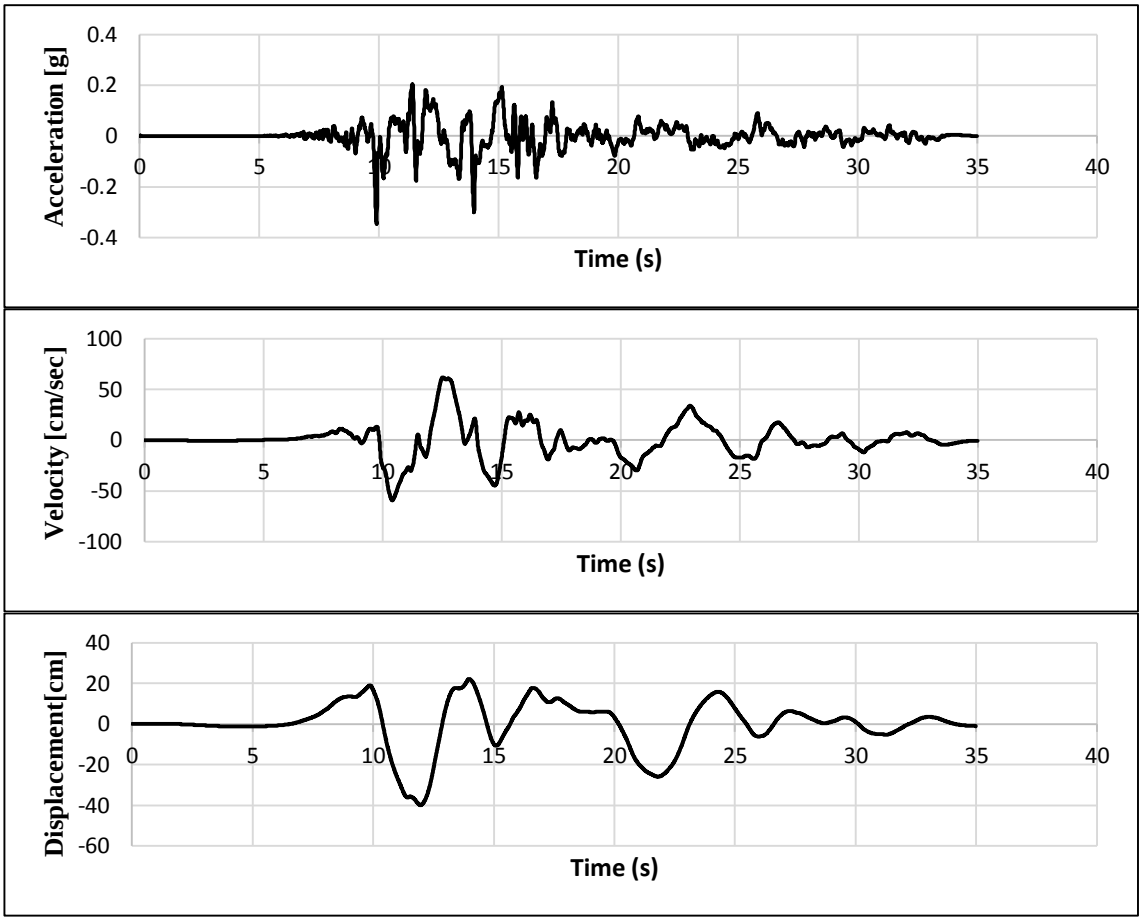

Figure 3.6: Acceleration, Velocity and Displacement of Kocaeli Earthquake in Yarimca Station.

3.7 Introduction of the Database

The entire database contains 138 data pairs (building-earthquake), each pair representing a building with at least one acceleration record. Pulse-like ground motion records are obtained from non-pulse ground motion records using logistic regression. Panella et al. (2017), with the help of logistic regression, introduced the Impulsivity Index (IP_R) with respect to PGV and L_v in the following relation:

$$IP_R = \frac{1}{1+e^{(5-0.45PGV+0.01L_v)}} \quad \text{(Eq. 21)}$$

The index has numerical values between zero and one, and the closer to the one, the earthquake is indicative of the directivity characteristics and the presence of a strong

pulse. High values of IPR> 0.7, as well as PGV> 30 cm/s (Panella et al. 2017) are selected earthquake with a directive pulse.

Bazzurro and Luco (2007) examined the engineering importance of earthquake with an intensity of $M_w > 5$. The intensity-focal distance diagram of the earthquake is shown in Figure 3.7.

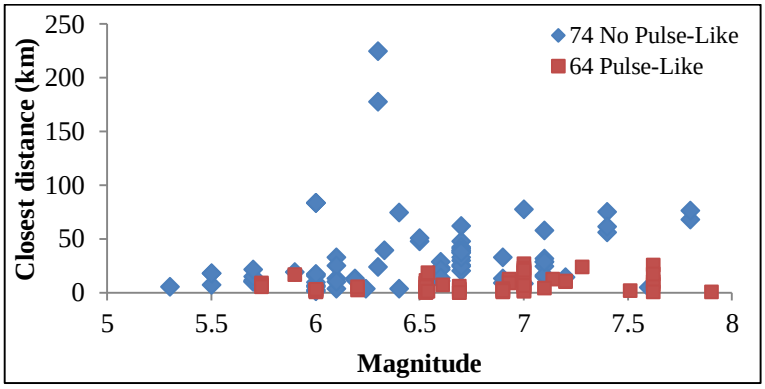

Figure 3.7: Intensity-focal Distance Diagram of Earthquakes.

The intensity (M_w or M_L according to PEER website) varies from 5.0 to 8.0, which include famous earthquakes, such as, San Fernando in 2/9/1979 (intensity 6.6), Loma Perita in 10/17/1989 (intensity 6.9), Lenders in 6/28/1992 (intensity 7.2) and Northridge earthquake in 1/17/1994 (intensity 6.5). Focal distances were in the range of 2 to 230 km (Figure 3.7). According to the two categories of records, the expected parameters in each earthquake record are shown in Figure 3.8.

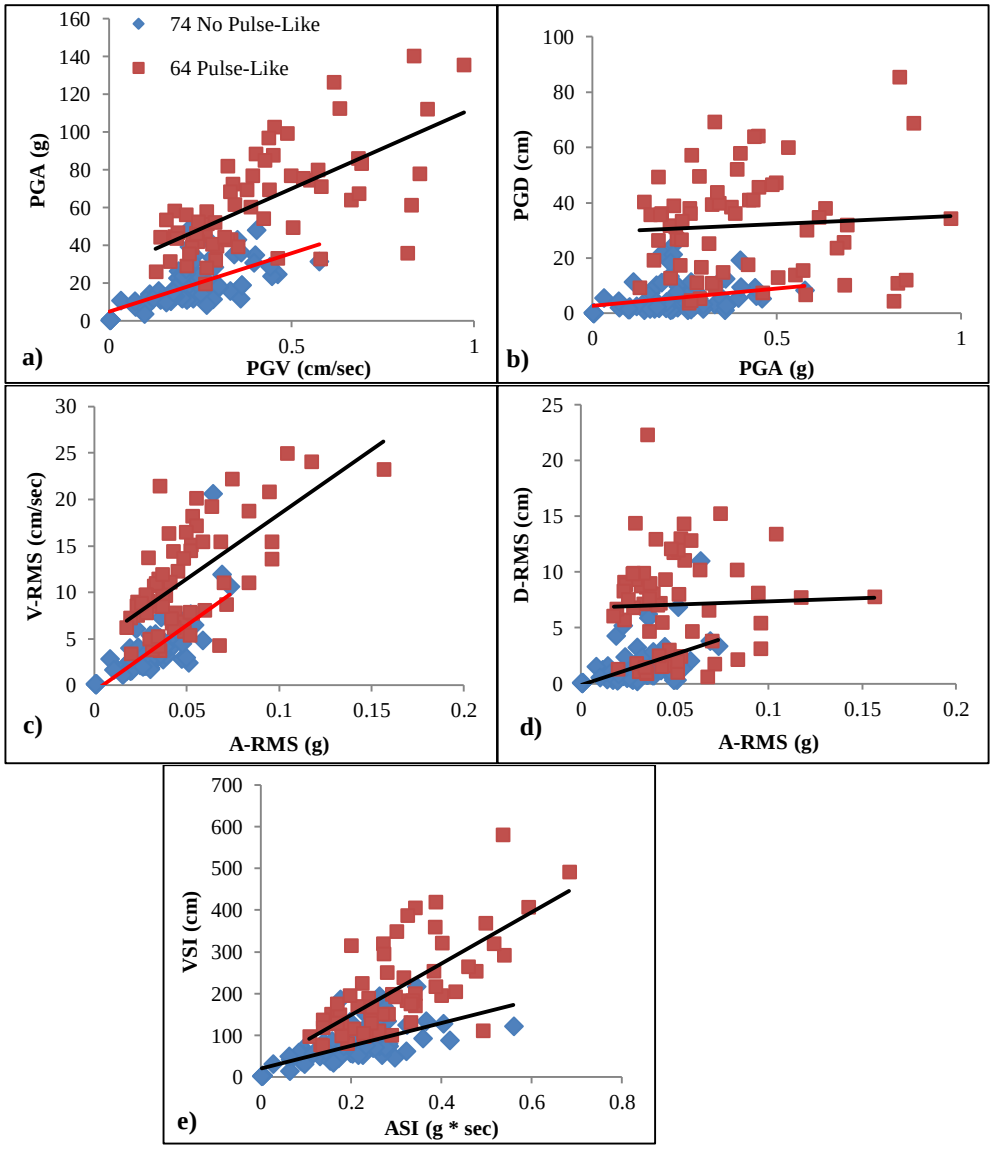

Figure 3.8: Comparison of the Two Sets of Earthquake Records Parameters.

In order to increase the accuracy of data used in damage index, despite the fact that they are not independent, the important horizontal directions of the earthquake record were considered separately. Finally 1656 data sections were processed, which are described here. The seismic performance of the buildings was assessed using the following steps:

a) The Maximum Inter-story Drift Ratio (MIDR)

b) The Roof Drift Ratio (RDR)

c) The Global Structural Damage Index (GSDI).

GSDI can generally show the efficiency of the global structural index and nonlinear steel buildings index. One of these indexes is the maximum inter-story drift. To calculate RDR for each building, lateral roof displacement should be divided by the total height of each building. In addition, the Global structural damage index (GSDI) is also defined for buildings. It should be noted that the damage index was estimated numerically and seismic damage rate for each component was evaluated as displacement and damage in the whole building. In previously published work, GSDI was considered as a weighted average of the damage indices (Elenas 2000).

Chapter 4

VERIFICATION OF SOIL-STRUCTURE INTERACTION (SSI)

4.1 Introduction

It is expected that when a structure faces an earthquake, such as, a design earthquake then the structural displacement will be more than the displacement expected in its elastic state. Therefore, the maximum structural displacement should be based on the limitation of the design code. During recent years, researchers have estimated the inelastic displacement factor by using the maximum demand for elastic and inelastic displacement. In different codes, these displacements are achieved in a variety of ways. For example, the amount of roof displacement is determined by the displacement method and the pushover analysis method as mentioned in the FEMA356 (2000) and FEMA440 (2005), respectively. In another study, the relationship between the maximum inelastic and elastic displacement (Veletsos and Newmark 1962) was observed by studying single-degree-of-freedom (SDOF) systems with cyclic behavior of elasto-plastic material. The results indicated that the ratio of inelastic displacement to elastic displacement is considerably greater in the short period region while the same ratio is almost equal to one in long period region and this is known as "equal displacement rule".

Hall et al. (1995) investigated the consequences of near-fault seismic ground motions on the inelastic behavior of the structure, irrespective of the effect of soil-structure

interaction. The seismic failures of structures rely on the characteristics of the ground motions and have strong dependence on the dynamic behavior of the structures (Baker 2008). In another study, Azarhoosh and Ghodrati (2010) studied the elastic behavior of SDOF system with soil subjected to pulse-like ground motions. They indicated that the structures subjected to pulse-like ground motion had similar responses. The effects of inertial soil-structure interaction on the constant strength inelastic displacement ratios of degraded systems have not yet been investigated. Hassania et al. (2018) studied the effects of foundation flexibility on the degraded super-structures by demonstrating that the effects of the SSI with the hysteresis stiffness degrading model can significantly change the inelastic displacement related to the non-degrading system. These changes were most pronounced during short-period region.

In this section of thesis, the inelastic displacement ratio of a SDOF system with degrading behavior under pulse-like seismic records (PLSRs) and ordinary seismic records (OSRs) were investigated. The aim was to compare the system period ranged from 0.1 to 5 seconds with a different behavior of the soil-structural interaction. Based on these analyses, two sets of PLSRs and OSRs, were evaluated under the influence of soft soil and the results were compared. Finally, statistical regression analysis was used to estimate the inelastic displacement ratios of SSI models with a set of pulse-like seismic records.

4.2 Soil-structure Interaction Models

During an earthquake the seismic behavior of the structure is strongly related to the soil-structure interaction and hence the soil beneath the structure should be considered to understand the structures seismic response. Determining the soils effective dynamical stiffness is regarded as the main purpose of analyzing the vibration of

foundation in soil-foundation interaction. In this regard, there are precise methods, such as, finite-element, cone method or equivalent methods in order to calculate the dynamic stiffness of the foundation under the influence of seismic excitation (Wolf 2004). In the cone method, the dynamical system of the soil is modeled in a homogeneous half-space based on the material resistance method by using a shaft-axis rod, where the cross-sectional characteristics of the rod can be shifted along the axis (Wolf 2004). Based on the cone model, the soil is substituted by discrete linear models, involving horizontal, vertical and rotational movements to simulate sway and rocking move as a mechanical system. A rigid and inflexible disk is considered as the foundation m_f and the polar moment of inertia I_f, as well as the soil beneath in a homogeneous half-space (Figure 4.1).It is worth noting that in the cone model, the shear wave velocity in the horizontal and torsional states was deformed under the shear and the dilatational wave velocity for the momentary and rotational states which were oscillating axially. Soil damping values, poisson ratio and mass density of half-space were assumed to be 0.25, 0.4, and 1800, respectively.

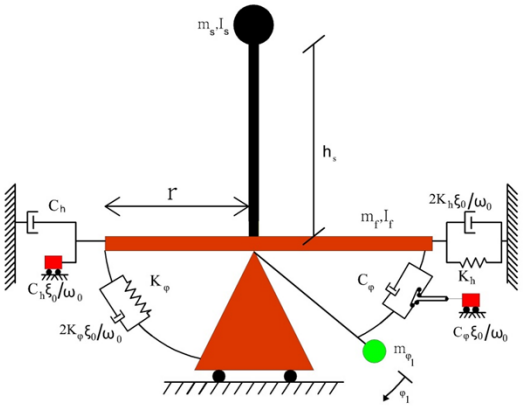

Figure 4.1: SDOF System of Soil-structure Interaction (Wolf 2004).

As illustrated in Figure 4.1, the soil support was replaced by a system with four springs and damping. In addition, it was modeled to simulate energy dissipation and viscous

damping in soil with materials and radiation damping. The adopted coefficients of the soil-foundation model are as follows (Wolf 2004):

$$k_h = \frac{8\rho {V_s}^2 r_0}{2-\upsilon} \quad , \qquad c_h = \pi\rho V_s {r_0}^2 \qquad \text{(Eq. 22)}$$

$$k_\varphi = 8\rho {V_s}^2 {r_0}^3 \quad , \qquad c_\varphi = \frac{\pi\rho V_p {r_0}^4}{4} \qquad \text{(Eq. 23)}$$

$$m_\varphi = \frac{9\rho\pi^2 {r_0}^5(1-\upsilon)}{32}\left(\frac{V_P}{V_S}\right), \ \Delta M_\varphi = 0.3\pi\left(\upsilon - \frac{1}{3}\right)\rho {r_0}^2 \quad \upsilon \geq \frac{1}{3} \qquad \text{(Eq. 24)}$$

Regardless of horizontal motions in almost incompressible soil (0.33≤ ν ≤0.5), two features occur in vertical and rocking movements including V-axis speed which was converted to $2V_s$, a trapped mass ΔM and a trapped mass moment of inertia ΔM_φ, which should be added under the rigid foundation for the rocking degree of freedom.

In section, the effect of soil-structure interaction on the structure's response was evaluated by considering seismic excitation in the pulse-like seismic records and ordinary seismic records.

4.3 Key Parameters for Soil-structure Interaction Analysis

The dynamic behavior of the system depends directly on the height, length, and width of the structure, as well as the characteristics of the site-soil, which relies on the choice of ground motion. These basic non-dimensional parameters can be presented as follows:

The dynamic stiffness coefficient (the dimensionless frequency) of the structure-foundation is equal to:

i) $a = \frac{\omega_s H_0}{v_s}$

ii) The aspect ratio of the structure equals $\frac{H_0}{r}$

iii) Structure-to-soil mass ratio index is defined as $\overline{m} = \frac{m_{tot}}{\rho r h_s}$

iv) The foundation to structure mass ratio is $\frac{m_f}{m_{tot}}$.

The two parameters a_0 and H_0/r are the parameters which influence the structures response. When a_0 is considered to be zero, the structure is considered as fixed-base structure and it becomes more than one variables as a structure with the soil-structure interaction in flexible soil state. The H_0/r ratio is introduced as the slenderness of structure. Poisson's ratio and soil damping ratio were 0.4 and 5%, respectively.

4.4 Structural Performance with Various Degradation Materials

Understanding the behavior of elements in building design and the influential factors on this behavior is important. Elemental behavior can be determined in the behavior of the section and the moment-curvature relation of the section. The stress and strain relationship of materials is usually nonlinear, but different nonlinear behavior is observed according to the properties of materials. The use of simple material models is essential, even if advanced mathematical models are used to make the conclusions more easily interpretable and easier to analyze. It is very important to use simple material models in computations to achieve results with different convergences. In this section of thesis, three different hysteretic models including bilinear (BL), Giuffre-Menegotto-Pinto (GMP), and degraded stiffness (DS) were considered.

Regarding the BL model with a kinematic hardening, no change occurs in the strength and stiffness of materials, and these materials are considered as basic materials. Model calibration parameters should be fully defined in order to describe the mechanical properties of the material. The initial stiffness (k), the yield strength (F_y), and the strain-hardening parameter (α) are introduced in this model (Otani 1981). For the first time, Giuffrè and Pinto (1970) introduced elastoplastic behavior without hardening,

then it was modified by the Menegotto and Pinto (1973) with hardening, and later it was modified by Filippou et al. (1983) with isotropic hardening. This model was introduced by Işık and Özdemir (2017). Ramberg–Osgood model is regarded as one of the uniaxial steel models which can simulate the strain-hardening of steel materials (Ramberg et al. 1943). The bilinear degraded-stiffness (DS) hysteresis materials are shown based on degrading the global stiffness behavior in the structures at unloading and reloading branches. Comparisons of the three hysteresis models with their corresponding parameters are shown in Figure 4.2.

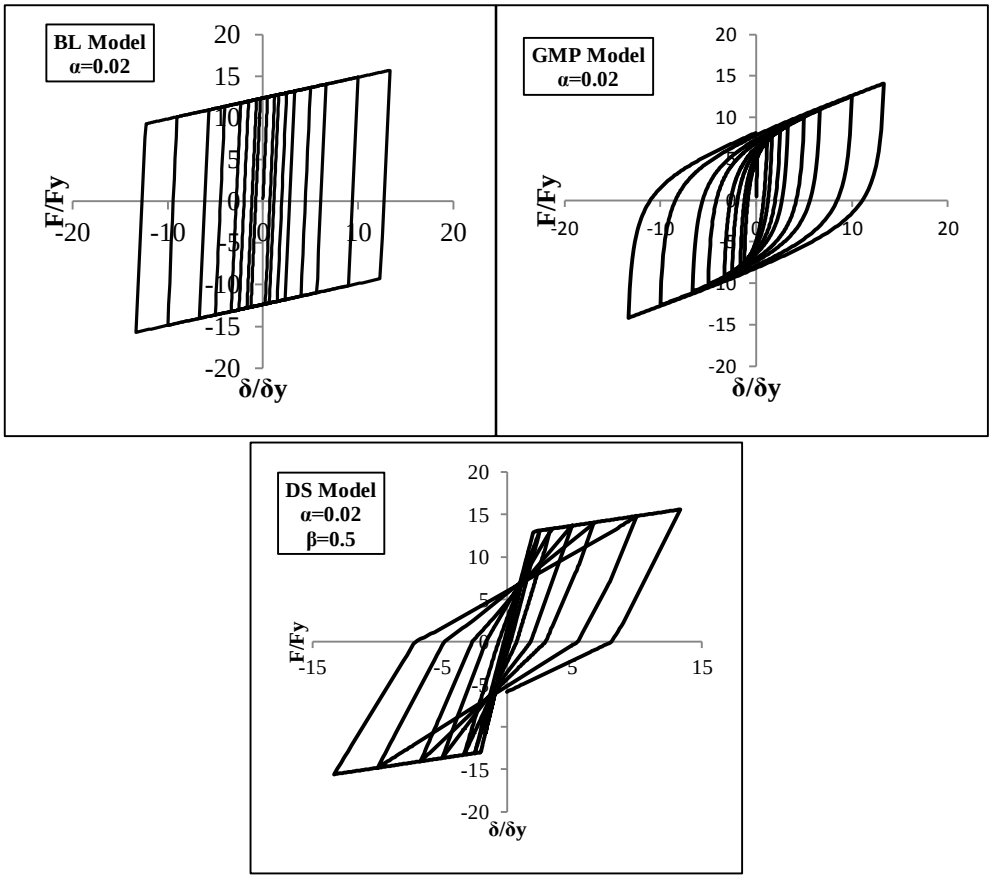

Figure 4.2: Hysteretic Load-deformation Curves Obtained from Three Materials.

4.5 Inelastic Displacement Ratios

In the performance-based earthquake engineering method, the inelastic displacement demand of the structure exposed to a seismic ground motion is of particular importance

(NEHRP 1997). The coefficient method was used to determine the target displacement at a level of risk in nonlinear static analysis (NEHRP 1997). Inelastic displacement ratio,C_R, is defined as the ratio of the maximum inelastic displacement demand (S_i) to the maximum elastic displacement (S_e) on SDOF system. In addition, García and Miranda indicated the inelastic displacement ratio, C_R, in constant strength with different periods as follows (Ruiz-García 2003):

$$C_R = \frac{S_i}{S_e} \quad \text{(Eq. 25)}$$

The lateral strength coefficient (constant parameter, R) is obtained from the ratio of required resistance (F_e) to yield strength (F_y):

$$R = \frac{F_e}{F_y} \quad \text{(Eq. 26)}$$

4.6 Results of Statistical Analysis

Nonlinear dynamic analysis of degrading structure was conducted to evaluate the effects of SSI on the inelastic displacement ratio. The entire spectrum obtained in the following sections is based on the average results of two sets of recorded ground motions as shown in Tables A.1 and A.2.

In this regard, for a given ground motion, a large number of SDOF soil structure models were considered including several predefined key parameters, such as, SDOF models with fixed-base and flexible-base systems, which range from 0.1 to 5 seconds, three aspect ratios (H_0/r = 1 and 3), three non-dimensional frequency values (a_0 = 1, 2 and 3) and 3 levels of strength reduction factors (R = 2, 4 and 8). The nonlinear dynamic analysis was compared by using the OpenSees software.

The already described material models BL and GMP and DS hysteresis models, were used. The damping ratio ξ for all systems was equal to 5% and the strain hardening ratio α was equal to 2%. For validation of numerical models, the models were subjected to Northridge earthquake and the results were compared with Hassania et al. (2017) (Figure 4.3).

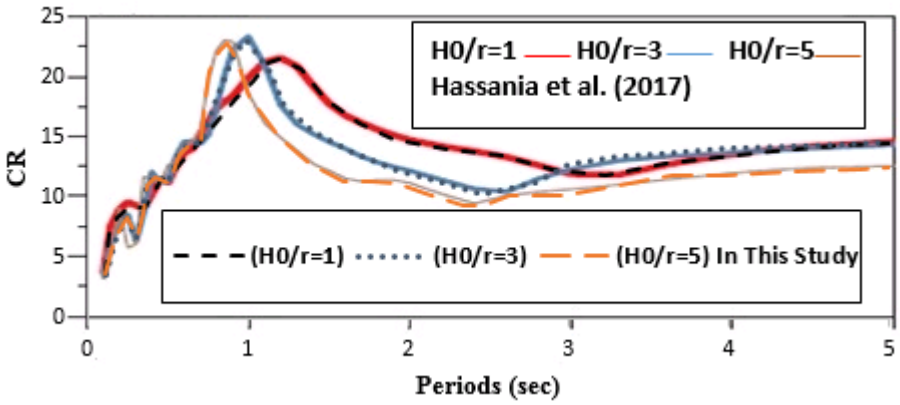

Figure 4.3: Verification of Soil-structure Interaction in this Study and Hassania et al. (2017).

4.7 SDOF Effect for Fixed-base System

Figure 4.4 illustrates the mean C_R range for fixed-base systems with strength reduction factor under two sets of earthquake records. The spectrum follows a regular process in different periods in two sets of records. Obviously, the maximum inelastic displacement of the systems is significantly greater than the maximum elastic displacement during a short period region. In the mean spectrum of pulse-like seismic record (PLSRs), this displacement is observed more than the average spectrum (OSRs), while the trend is roughly equal to 1 by increasing the period.

These variations rely heavily on the deteriorating materials in reducing the spectrum due to an increase in the period. As shown, the obtained results from these graphs can

be used to better understand the effects of different variables on the maximum inelastic displacement to maximum elastic displacement.

Further, in the short period region an increase in reducing the strength of factor value leads to an increase in the C_R value in both sets of records. Obviously, the behavior of different types of degradation materials does not affect long period structures (Chenouda and Ayoub 2008).

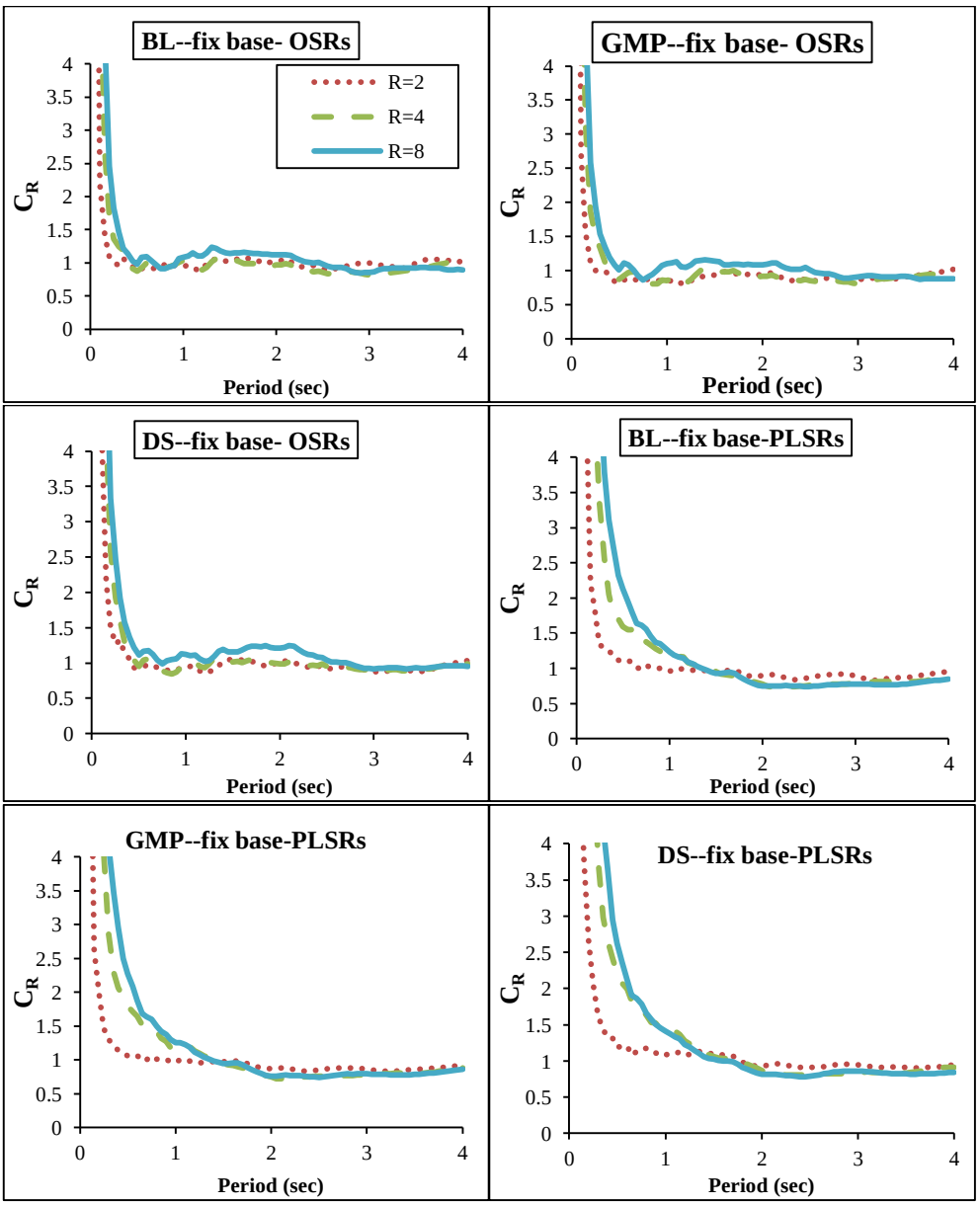

Figure 4.4: Inelastic Displacement Ratios without SSI Systems with Various Hysteresis Models.

Figured 4.5 to 4.7 illustrate the average of inelastic maximum displacement ratio to the maximum elastic displacement of the system for different strength reduction factor in the two sets of PLSRs and OSRs. As shown, different trends in the hysteresis model in C_R are largely related to two sets of records. The C_R ratio for the DS hysteresis model is higher than that of the GMP and BL over a period of less than 1.5 seconds in the PLSRs set. However, these changes are insignificant for OSRs.

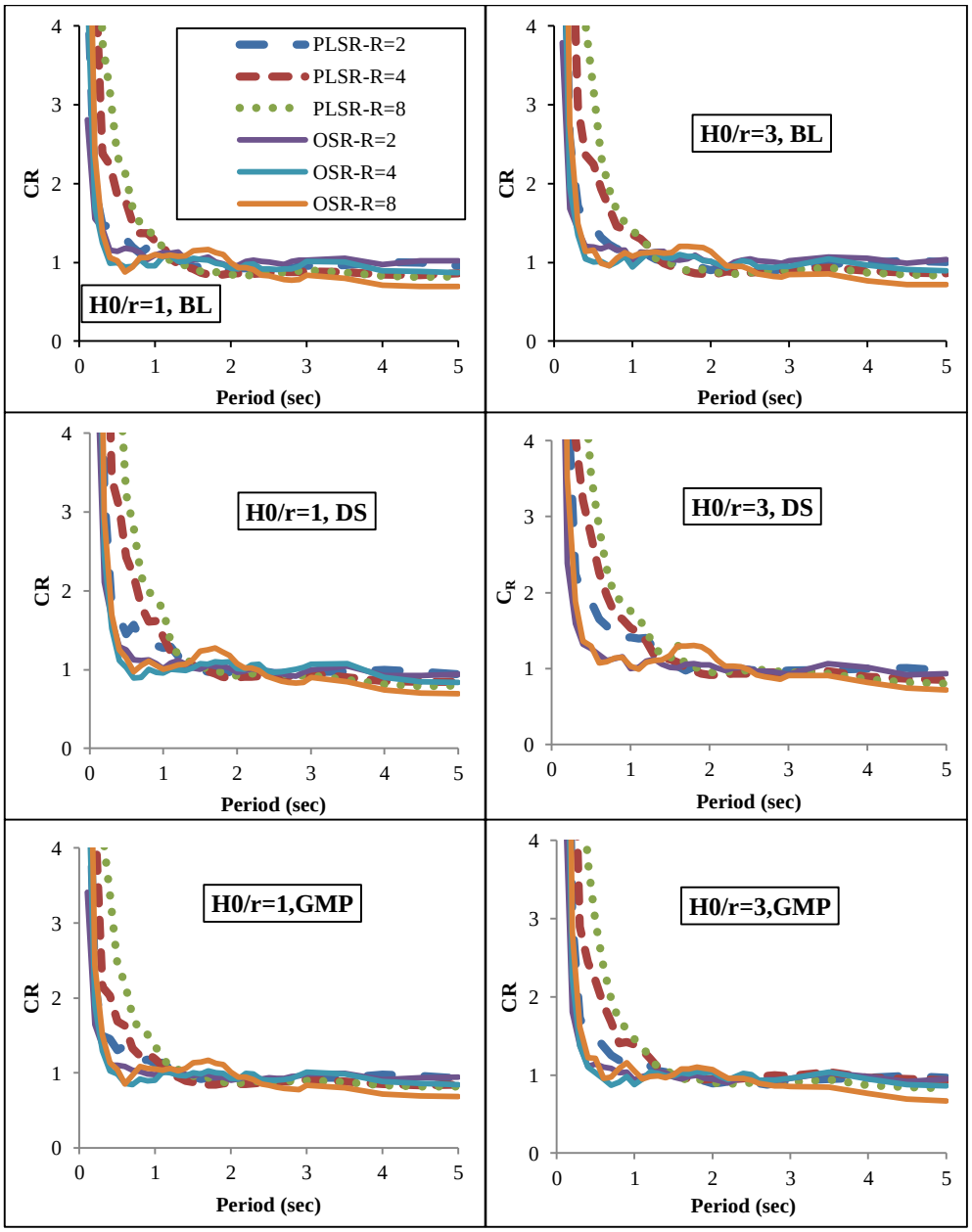

Figure 4.5: Inelastic Displacement Ratios with SSI Systems with Various Hysteresis Models for a_0=1.

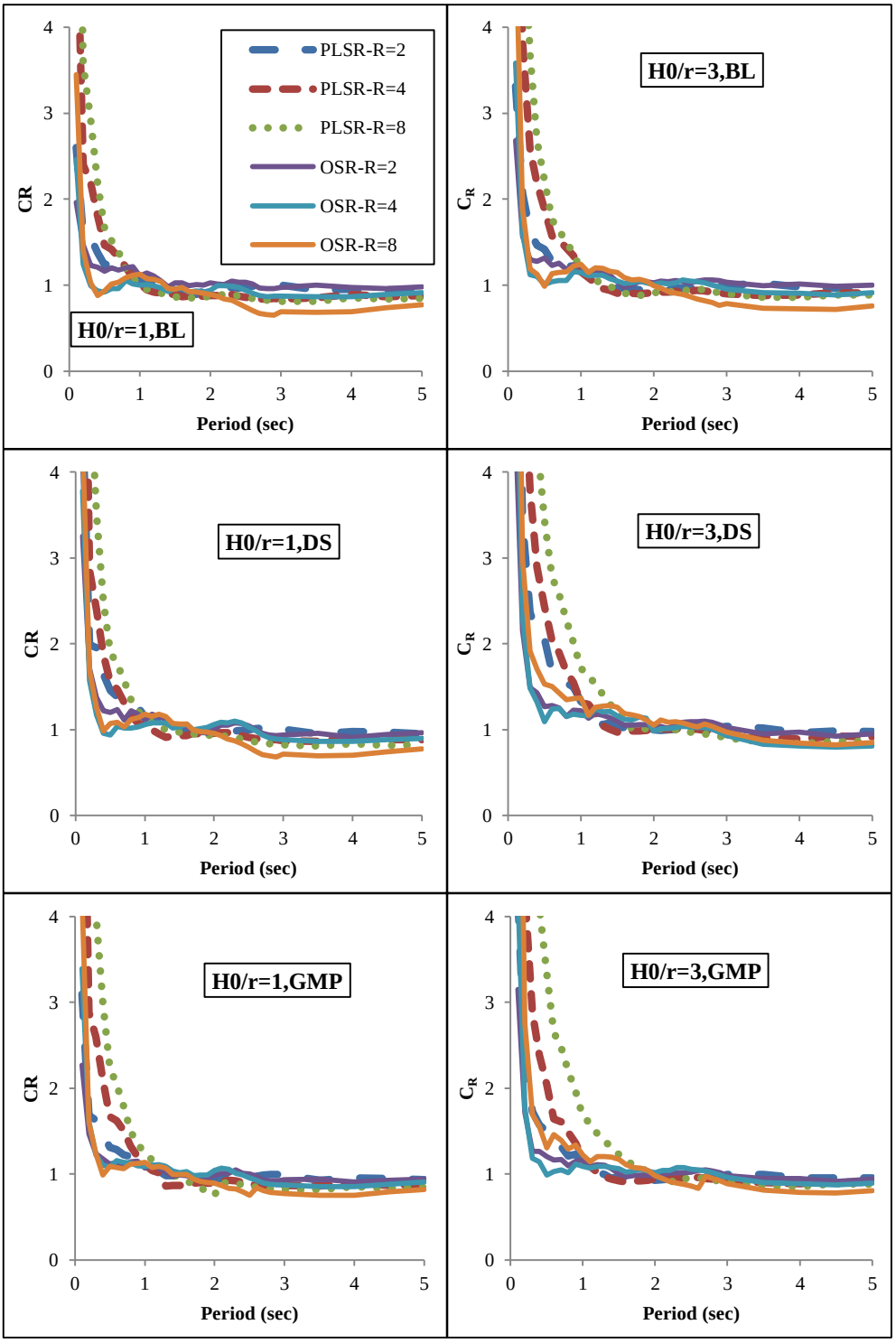

Figure 4.6: Inelastic Displacement Ratios with SSI Systems with Various Hysteresis Models for a_0=2.

By increasing the non-dimensional frequency (a_0), the C_R value in the PLSRs set increases, compared to that of OSRs in SDOF system (Figured 4.5 to 4.7).

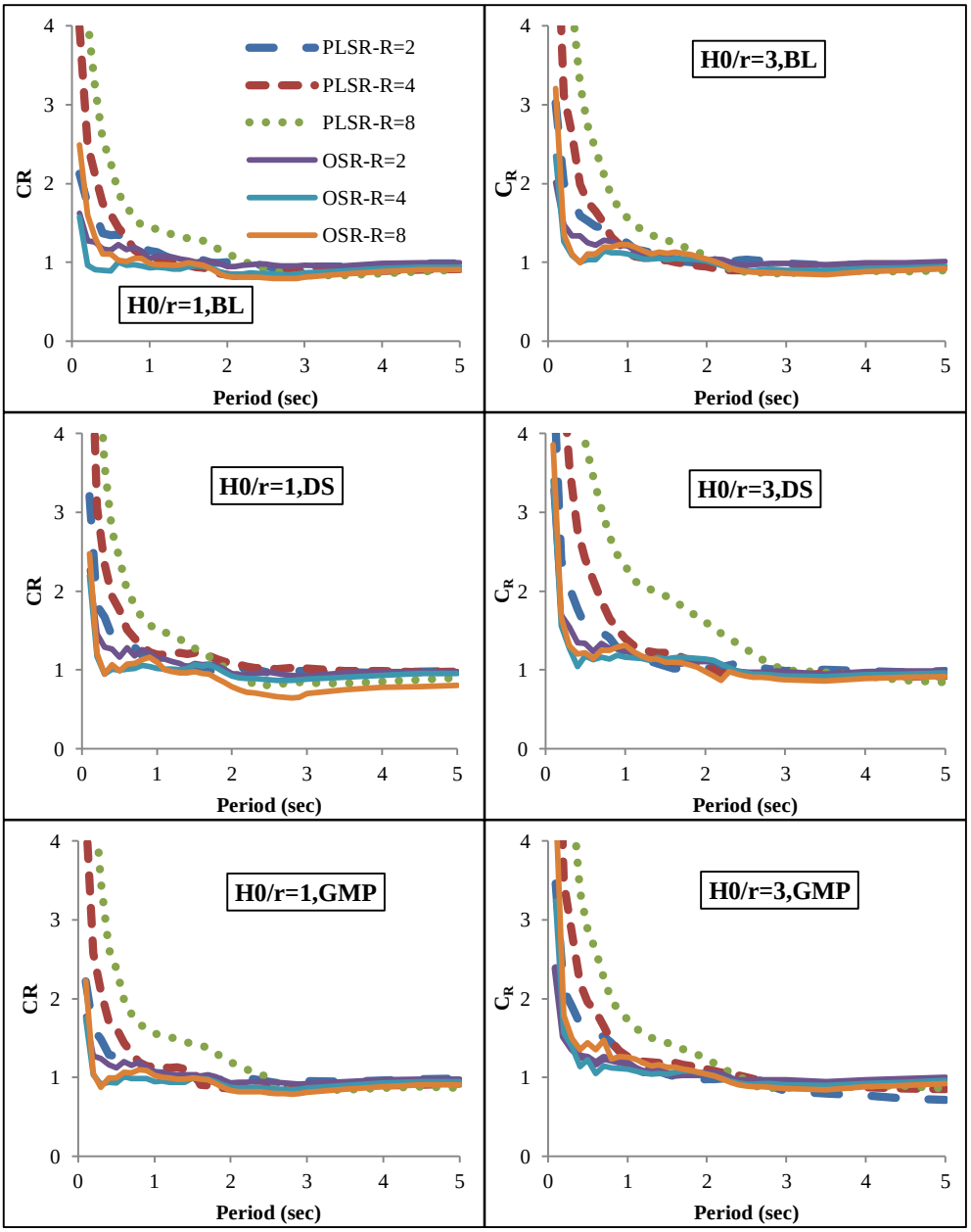

Figure 4.7: Inelastic Displacement Ratios with SSI Systems with Various Hysteresis Models for a_0=3.

In ASCE-41-17 (2017), the modification coefficient C_1 is related to the maximum inelastic displacement demand with elastoplastic hysteresis behavior with respect to the displacement for linear elastic response. Coefficient of C_1 is calculated as the target displacement in the nonlinear static procedure (NSP), which is defined as follows:

$$C_1 = 1 + \frac{(R-1)}{aT_e^2} \qquad \text{(Eq. 27)}$$

where a indicates a constant dependent on the soil conditions, and T_e represents the effective fundamental period for the building in the desired direction in seconds. In addition, Garcia and Miranda (2003) proposed correction coefficient $C_{G\&M}$ based on soil conditions:

$$C_{G\&M} = 1 + \left[\frac{1}{a\left(\frac{T}{T_S}\right)^b} - \frac{1}{c}\right](R-1) \qquad \text{(Eq. 28)}$$

The coefficients a, b, c and T_s for soil type D are equal to 57, 1.85, 60 and 1.05, respectively. Eqs. (27) and (28) were extracted based on site location and strength reduction factor. Since the use of Eqs. (27) and (28), suggested for structures with fixed-base, it is not appropriate to compute inelastic displacement coefficient for SSI. Furthermore, Figure 4.8 displays the comparison between the Eqs. (27) and (28) with fixed-base and C_R coefficients with the SSI with bilinear material behavior.

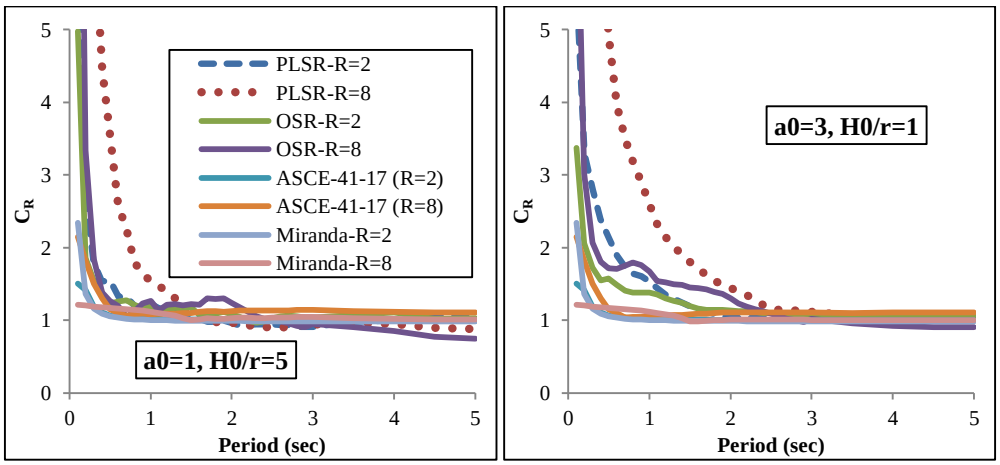

Figure 4.8: Comparison of C1 Coefficient in ASCE-41-17 with C_R for Systems with BL Hysteresis Model.

4.8 A Practical Procedure to Estimate C_R of Soil-structure Models with Three Hysteresis Models

Performance based seismic design is considered as a new procedure to earthquake resistant design. During the recent years, displacement-based design has been used to

reach the level of acceptable damage to the design earthquake, and these methods are considered as new tools for performance-based design.

This method has a simple estimation process of the average inelastic displacement ratio, which then allows for estimating the maximum inelastic displacement demand. Nonlinear regression analysis was performed to extract a simple expression to estimate the average displacement ratio for SDOF systems for soil-structure models with three hysteresis models. Then, Levenberg-Marquardt regression analysis was conducted by using MATLAB software. In ASCE-41-17 (2017), the modification coefficient C_1 was developed to incorporate SSI effects. The proposed function of the SSI effective parameters including parameters a_0, H_0/r, T_{fix} and R is as follows:

$$C_R = a + \left(\frac{m}{nT_{fix}^{d}+0.01}\right) \quad \text{(Eq. 29)}$$

Where, the constant coefficients of functions *a*, *d*, *m* and *n* were obtained based on the aforementioned key parameters as shown in Table 4.1.

These constant coefficients were first obtained based on each of the key parameters a_0, H_0/r and R by using Eq. 29 for soil-structure systems with PLSRs set. Regarding various parameters, the constant coefficients were separately calculated for each hysteresis material.

As illustrated in Figure 4.9, the average C_R values were computed by using Eq. 29 and the numerical analyses of different models. As displayed on Figure 4.1, the equation provides good approximations with analytical data.

Table 4.1: Estimation of Coefficients C_R for Three Hysteresis Models.

	Hysteresis Models		
	BL	**DS**	**GMP**
a	$1.1-0.12a_0-0.04\frac{H_0}{r}$	$0.96-0.01\frac{H_0}{r}+0.01R$	$0.99-0.05a_0-0.04\frac{H_0}{r}+0.02R$
d	$1.6-0.4a_0+0.03\frac{H_0}{r}+0.03R$	$2.2-0.33a_0$	$1.73-0.29a_0+0.02\frac{H_0}{r}+0.04R$
m	$5.8+0.35a_0-0.25\frac{H_0}{r}-0.45R$	$1.04+0.62a_0+0.15\frac{H_0}{r}+0.5R$	$2.89+0.09a_0+0.25R$
n	$26.2-2a_0-2.5R^{0.85}-1.3\frac{H_0}{r}$	$26-0.6a_0-2.8R^{0.84}-1.35\frac{H_0}{r}$	$28-1.35a_0-6.9R^{0.52}-0.47\frac{H_0}{r}$

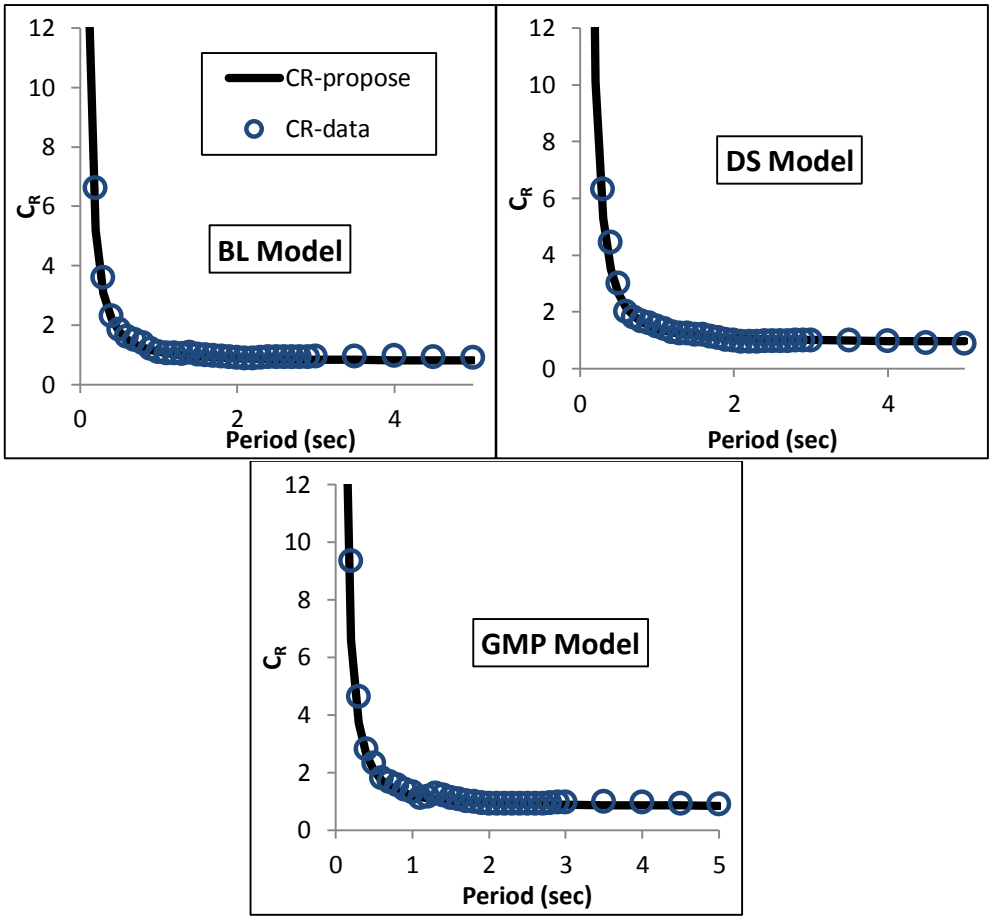

Figure 4.9: Comparison of Eq. 29 with Available Data with Regard to a_0=1, H_0/r=5 and R=4.

Chapter 5

VERIFICATION OF STEEL FRAMED MODELS WITH AND WITHOUT INFILL WALL

5.1 Verification of Steel Framed Models by using SAP2000 and OpenSees

The effect of the infill has long been known on the strength, hardness and shape of the frames. In conventional design of structures the infills are considered as part of the non-structural members and they are ignore during structural modeling. The existence of various effective parameters, the variability of the infill hardness and its dependence on the construction and the uncertainty about the dynamic behavior of the infill during earthquakes are some of the important aspects that are investigated in the systems. In addition, although there are so many different approaches for introduction of the masonry-infilled, the way infill is introduced should provide conditions for interaction between the infill and the frame (FEMA 356). Due to the reasons mentioned above, to determine the ultimate capacity of the structure, it is necessary to consider the infill in the structure.

The building frames are designed and analyzed in two-dimensions. These buildings are regular in elevation. Buildings have typical 3 bays each with 5 meters width and typical floor height of 3.2 meters. The SAP2000 and OpenSees software were used to design buildings. The first six modes of each structure observed by using SAP2000 and OpenSees software (2013) can be seen in Table 5.1 and Figure 5.1. It can be seen

that the periods of these structures obtained from the two software are in very good agreement. Hence the geometrical model was accepted as being reliable. All models are analyzed in the first mode.

Table 5.1: Fundamental Period of Vibration for the First Six Modes of Bare Frame using OpenSees and Sap2000 Software.

3Story		5Story		8Story		12Story	
OpenSees	Sap2000	OpenSees	Sap2000	OpenSees	Sap2000	OpenSees	Sap2000
0.87	0.90	0.96	0.99	1.41	1.45	1.86	1.88
0.36	0.40	0.35	0.37	0.61	0.63	0.71	0.72
0.19	0.18	0.19	0.20	0.37	0.40	0.43	0.45
0.08	0.07	0.12	0.13	0.24	0.25	0.30	0.33
0.08	0.07	0.08	0.08	0.18	0.19	0.23	0.24
0.06	0.05	0.08	0.08	0.14	0.14	0.18	0.19

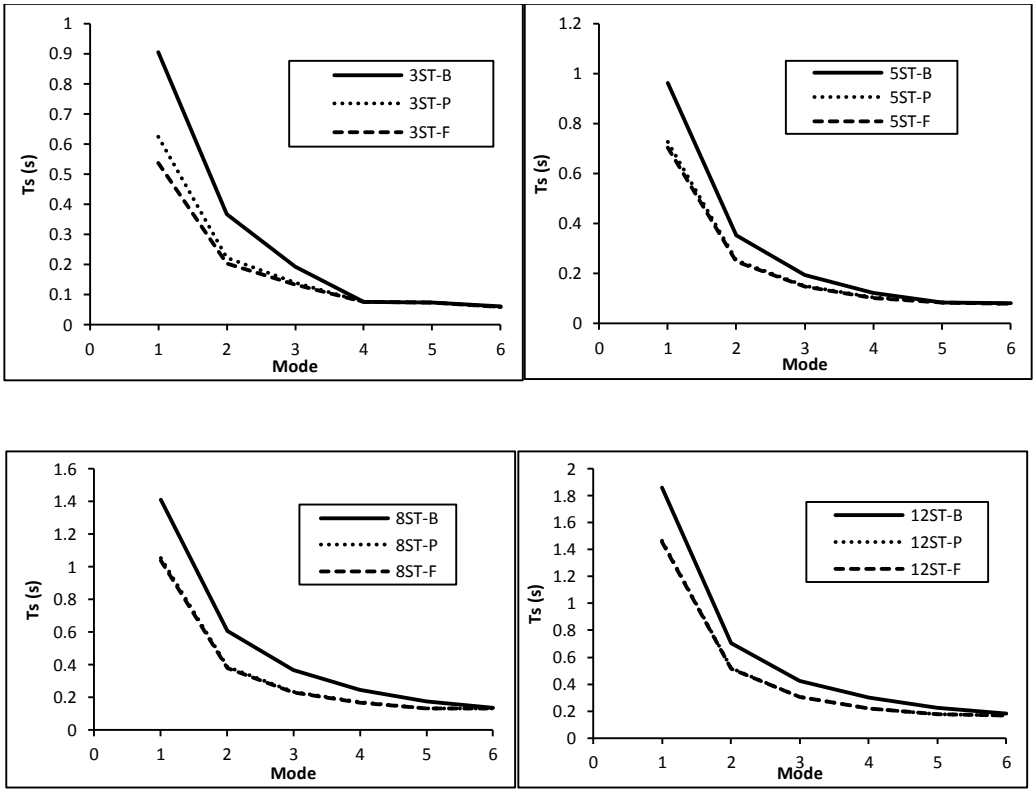

Figure 5.1: Fundamental Period of Vibration for the First Six Modes of Bare, Partiall and Fully Infilled Frames using OpenSees Software.

5.2 Verification of Steel Framed Models by using Experimental Results and OpenSees

Kappos and Ellul (2000) has conducted studies on steel and concrete frames with infill. In this study, it was observed that the frames and infill were integrated to the moment and the cracks formed around the infill. This followed by diagonal cracks that were observed on the masonry-infill. Smith (1962) carried out an experimental test on a steel frame with infill. This test led to the conclusion that the infill could be replaced with an equivalent diagonal strut. Models of an equivalent diagonal strut of FEMA-356 (2000) is based on models developed by Smith (1962).

Twelve samples of one story and one bay with a half-scale (bare and infill frames), as well as two sample frames of half-scale (infill frame, subjected to cyclic loads) were tested by Mehrabi et al. (1996). They showed that the strength and stiffness of structure with infill would be more than without infill. An equivalent diagonal strut based on macro model was verified by using experimental results and hysteretic material model which was developed by Ibarra et al. (2005). By using a macro-model in frames, one can consider the effect of various damage modes which can occur in the masonry-infill frame.

In this study, OpenSees software was used to statically analyze the equivalent diagonal strut model subjected to cyclic loading as in the experiment with and without cyclic deterioration in properties of strut. The analytical results were compared with the experimental ones in Figure 5.2. The difference between the two data from numerical and experimental results shows that strut model need to illustrate cyclic deterioration for modeling of the masonry-infill (Figure 5.2).

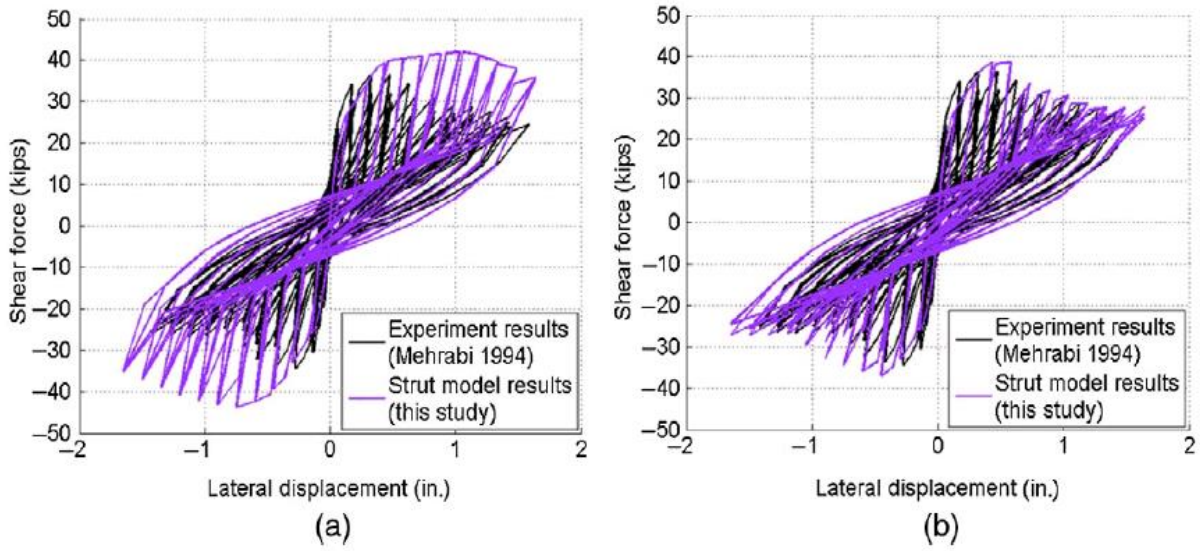

Figure 5.2: Hysteresis Load-displacement Curves for Experimental and Numerical Specimen with (a) no Cyclic Deterioration and (b) Calibration of the Cyclic Deterioration by using Sattar and Abbie 2016.

Four parameters for the cyclic deterioration of material used by Ibarra et al. (2005) was used with the equivalent diagonal compression struts. Those parameters can be used for masonry-infill walls with consideration of the energy dissipation capacities and deformations (Sattar and Abbie 2016). Mirtaheri et al. (2017) was evaluated a masonry-infilled steel frame building against progressive collapse. They verified experimental data for infill model based on Ibarra et al. (2005) and compared the experimental and numerical results by using OpenSees software. Numerical results for the validation model infill in bare frame has good agreement with experimental results. Tasnimi and Mohebkhah (2011) were investigated the seismic behavior of masonry-infilled steel frames with and without openings. They carried out experimental study on six real-scale, one-story one-bay steel frames with and without infill. They were tested under static conditions by applying cyclic lateral loading to the frame. The tested typical steel frame had 2200 mm bay width and 1870 mm story height (Figure 5.3). The average mortar compressive strength was 10.1 MPa, based on the mortar cube

compression tests. The mean prism compressive strength was 7.63 MPa. Frame column and beam steel sections were IPE140 and they had a yield stress of 315 MPa. In order to calculate the equivalent compression strut width Eq.1 and Eq.2 (FEMA356, 2000) were used (Table 5.2).

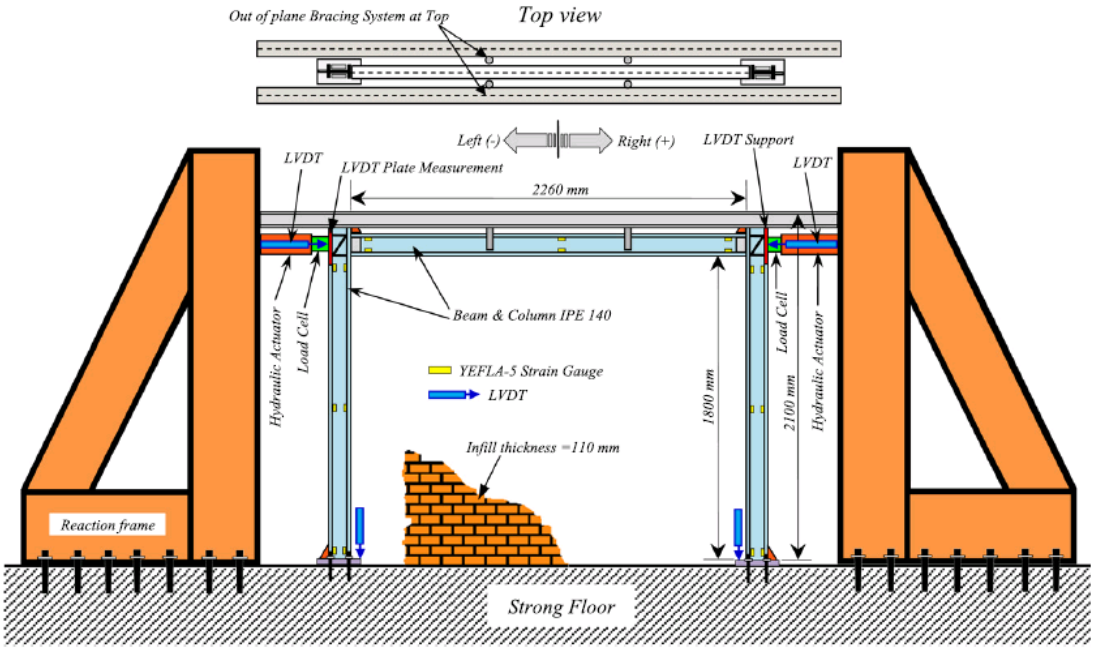

Figure 5.3: Details of the Experimental Setup and Steel Frame Specimen for Tasnimi and Mohebkhah 2011.

Table 5.2: Calculate the Equivalent Compression Strut Width by using FEMA356 (2000) Eq. 1 and Eq. 2.

Properties of structure	Value
h_{col}	187 cm
h_{inf}	180 cm
E_{fe}	2.24E+06 kg/cm^2
E_{me}	53410 kg/cm^2
I_{col}	541 cm^4
r_{inf}	289 cm
t_{inf}	11 cm
θ	0.672578783 deg
λ_1	0.071619176
A	26 cm

For validation of models in this study, the experimental results of Tasnimi and Mohebkhah (2011) were used. They tested two models, bare frame and masonry-infilled frame. As can be seen in Figure 5.4, the blue solid line was obtained from the experimental model and the red dashed line was obtained from the OpenSees software. The yield stress, modulus of elasticity (E), Poisson's ratio, density (ρ) and strain hardening of steel from experimental models were 315 MPa, 200 GPa, 0.3, 7850 kg/m3 and 2%, respectively. Both hysteresis load-displacement curves for infilled-frame specimen and bare frame specimen shows very good agreement between the experimental and numerical results.

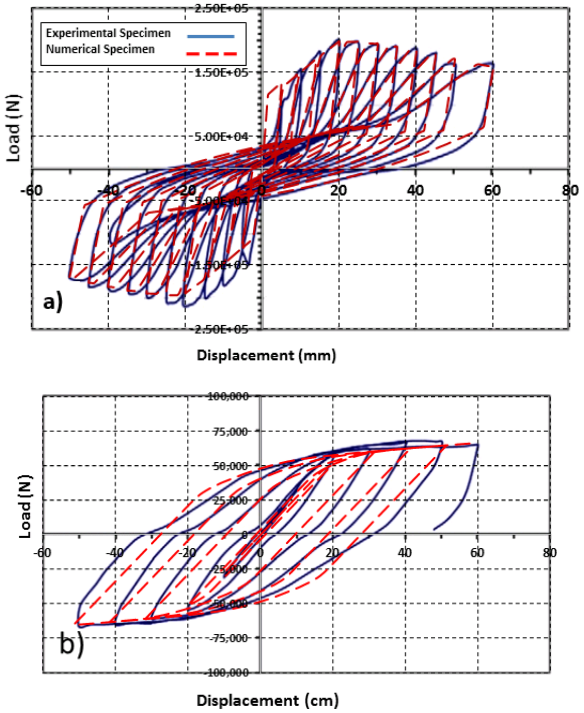

Figure 5.4: Hysteresis Load-displacement Curves for Experimental and Numerical by OpenSees: a)Infilled-frame Specimen b) Bare frame Specimen (Tasnimi and Mohebkhah 2011).

Hence, considering both verifications detailed in sections 5.1 and 5.2 and the good agreements in their results then it can be concluded that the numerical modeling used for all structural models in this study can be considered reliable.

Chapter 6

RELATIVE EVALUATION OF RESULTS

6.1 Consideration of Building Performance

It is a well-known fact that the effect of rupture directivity is one of the main causes of pulse-like strong motions. It should be noted that not all near source ground motions contain directivity pulses, not even all those satisfying the theoretical geometric prerequisites with respect to the rupture geometry. The effect of forward directivity also decreases with distance from the fault as seismic waves scatter, such that near-fault pulse-like ground motions are unlikely to occur more than 10 to 15 km away from the rupture (Baker 2007). The behavior of a specific member from the 2-D 3-story B, P, and F steel frame, which is subjected to two sets of seismic records, is investigated (Figure 6.1). The structures were modeled with material and geometric nonlinear features necessary for simulating the onset of earthquake. The analytical models are subjected to a database of two sets of records, pulse-like ground motion and ordinary ground motion. In this study, one of the OSR records of Whittier-Narrows earthquake of Bell Gardens-Jaboneria station (Table A.1) and one of the PLSR records of Kocaeli-Turkey earthquake of Yarimca station (Table A.2) were used to carry out the nonlinear time history analysis. Both of these records were obtained from stations that were located at less than 10 km from the fault line. Since the 74 OSR and 64 PLSR records are used then, as an example, only a part of a specific beam member behavior was considered in order to avoid dealing with too much data.

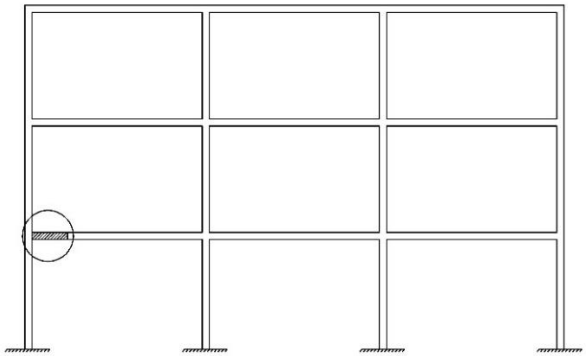

Figure 6.1: The Indicated Part of a Beam Member Was Investigated to Understand its Behavior when Subjected to Two Sets of Records.

The hysteresis behaviour of part of a beam on the first story, as displayed in Figure 6.1, was considered and subjected to two sets of OSR and PLSR records. Figure 6.2 shows the hysteretic force-displacement curves of the beam subjected to two sets of earthquake records with and without SSI. It can be observed that the load-displacement hysteretic behaviors of the beam subjected to two types of records are different. This is particularly valid for the PLSR record rather than the OSR record. The effect of including SSI in the PLSR record is particularly critical in structural beam elements (Figure 6.2). It should also be noted that all frames B, P and F are almost achieved the same displacement when OSR is used without SSI whilst the same record with SSI shows considerable variation in displacement among the frames the F frame achieving the highest displacement and the lowest displacement was achieved by the B frame. This order was also valid when PLSR record was used with and without SSI too. However, the variation among B, P and F was not as high as the OSR without SSI.

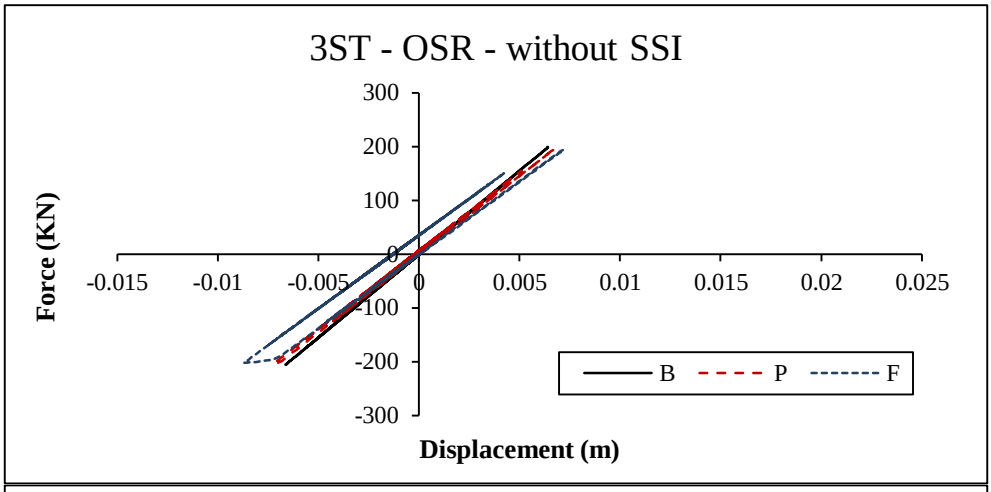
3ST - OSR - without SSI
Force (KN)
Displacement (m)
B
P
F

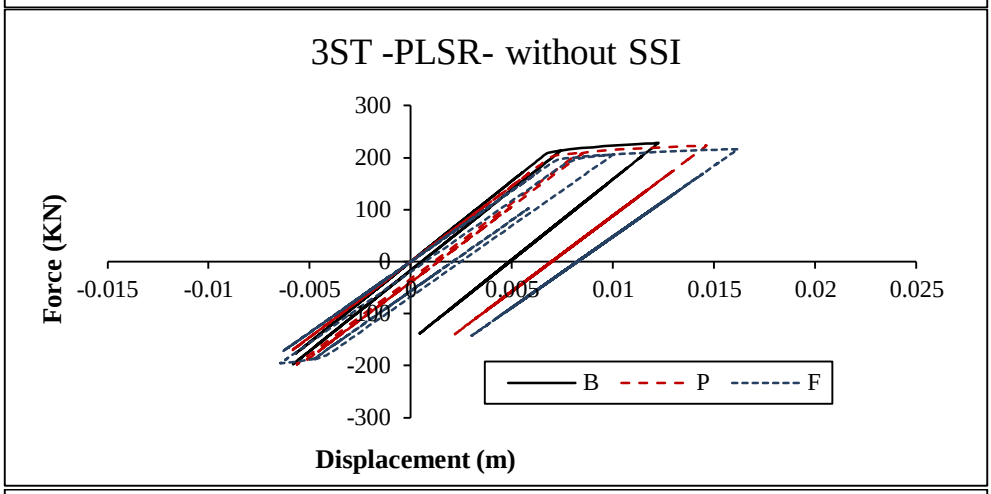
3ST -PLSR- without SSI
Force (KN)
Displacement (m)
B
P
F

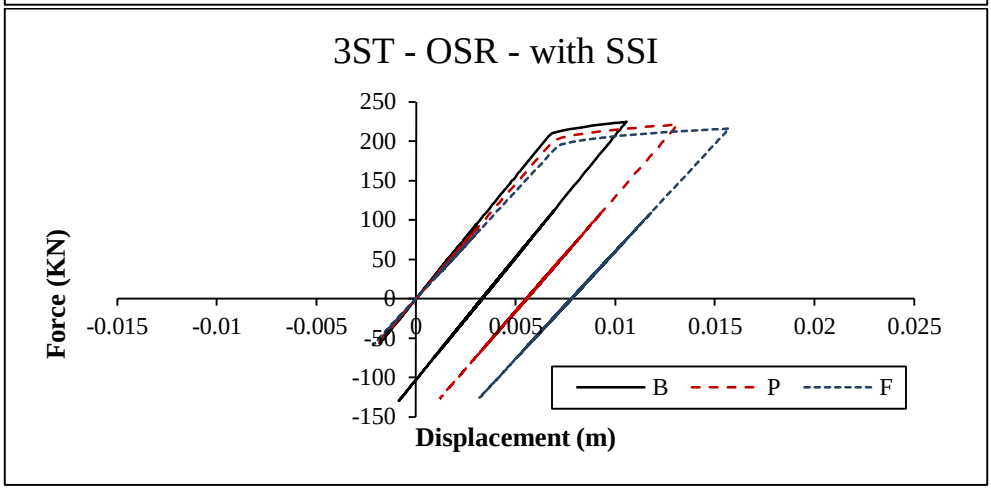
3ST - OSR - with SSI
Force (KN)
Displacement (m)
B
P
F

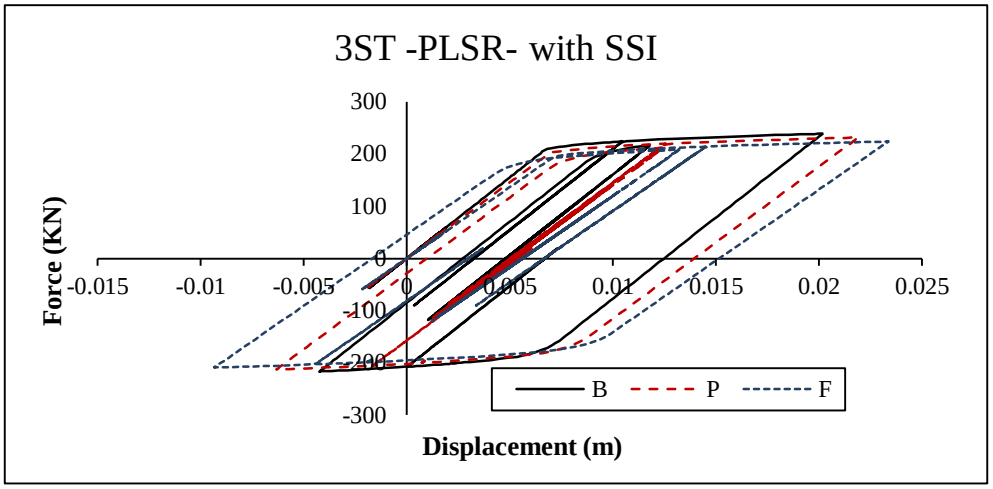

Figure 6.2: Hysteretic Curves of Force-displacement of Beam Subjected to Two Sets of Earthquake Records with and without SSI.

In this part the quantification of the impact of near-fault directivity on building seismic behaviour through nonlinear dynamic analysis of structural simulation models were done. Damage indices have been extensively used to express condition of the structure in seismic events. Park and Ang (1985) proposed a damage index as a relation between the ratio of maximum to ultimate deformation and hysteretic energy.

Damage Index (DI): One of the methods for calculating the structure total index is to use correlation equations and consequently find the relationship between the structural member indices and the energy absorbed by them. For this purpose, according to the damage index of members in a story and the energy absorbed by them, the story damage index could be obtained and the damage index of the total structure could also be calculated from the relation between the stories' damage indices and energy absorption with reference to Eq. 11. The description of Park-And damage index and the damage categories of structures exposed to seismic load can be found in Table 2.2. In this table based on the calculated damage index, there are five categories to define the damage level of a structure subjected to earthquake loads. Table 2.2 shows that the no damage state of a structure is when Damage Index (DI_{P-A}) is less than 0.1 whilst

DI_{P-A} = 1.0 indicates total collapse for a structure. It can be noticed that the value of δ_m is often non-zero. Therefore, even if a member has no damage, DI_{P-A} has a non-zero value.

Figures 6.3 and 6.4 show the damage index of GSDI in two record sets for 3 and 5 story structure, 8 and 12 story structures, respectively. Also, in these figures, five categories of failure are shown as horizontal lines. The rate of failure of the structures with PLSR set is more visible than OSR set. In Figure 6.5, comparison of seismic performance of buildings for two sets records by using Park-Ang index (GSDI) is shown. The failure of structures in three state of no damage, minor damage and moderate damage is shown to be more due to OSR set while the failure of structures in two state of severe damage and total collapse is more due to PLSR set.

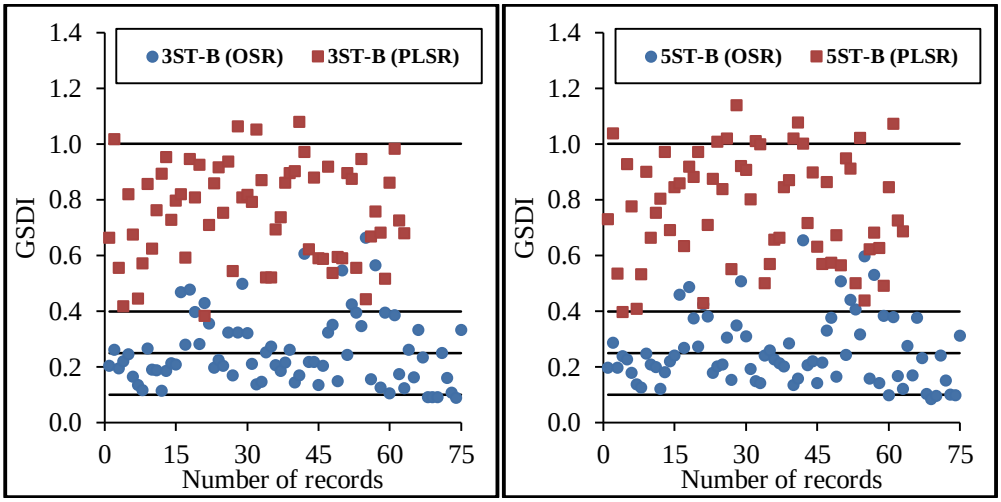

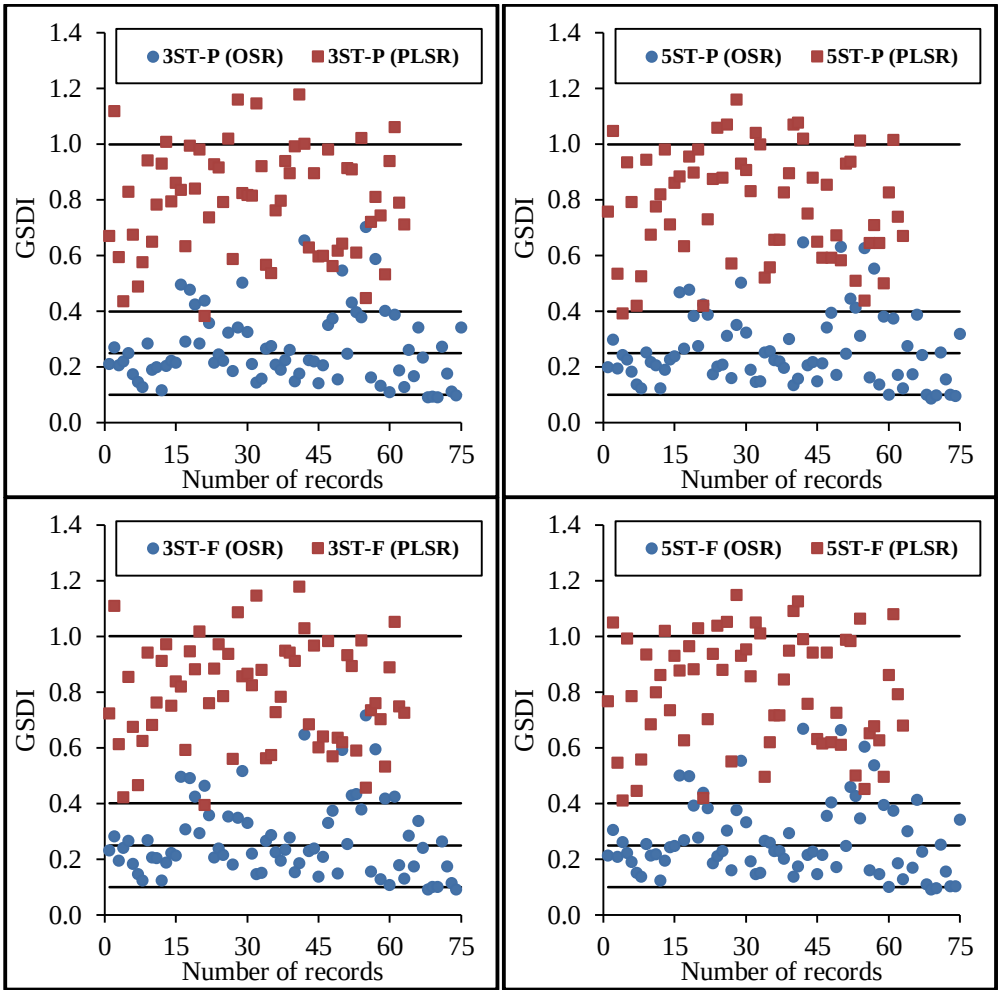

Figure 6.3: Considering of Seismic Performance of Buildings for 3 and 5 Stories by using Park-Ang Index (GSDI) without SSI.

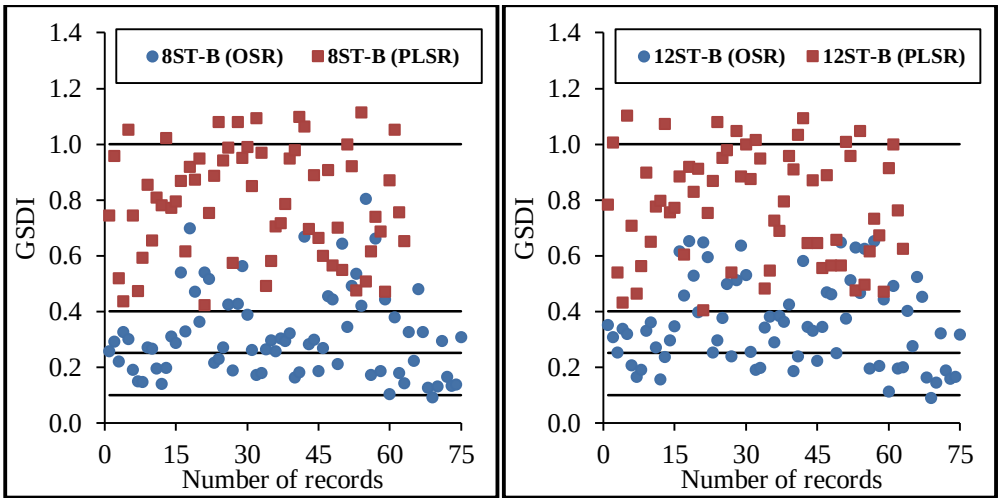

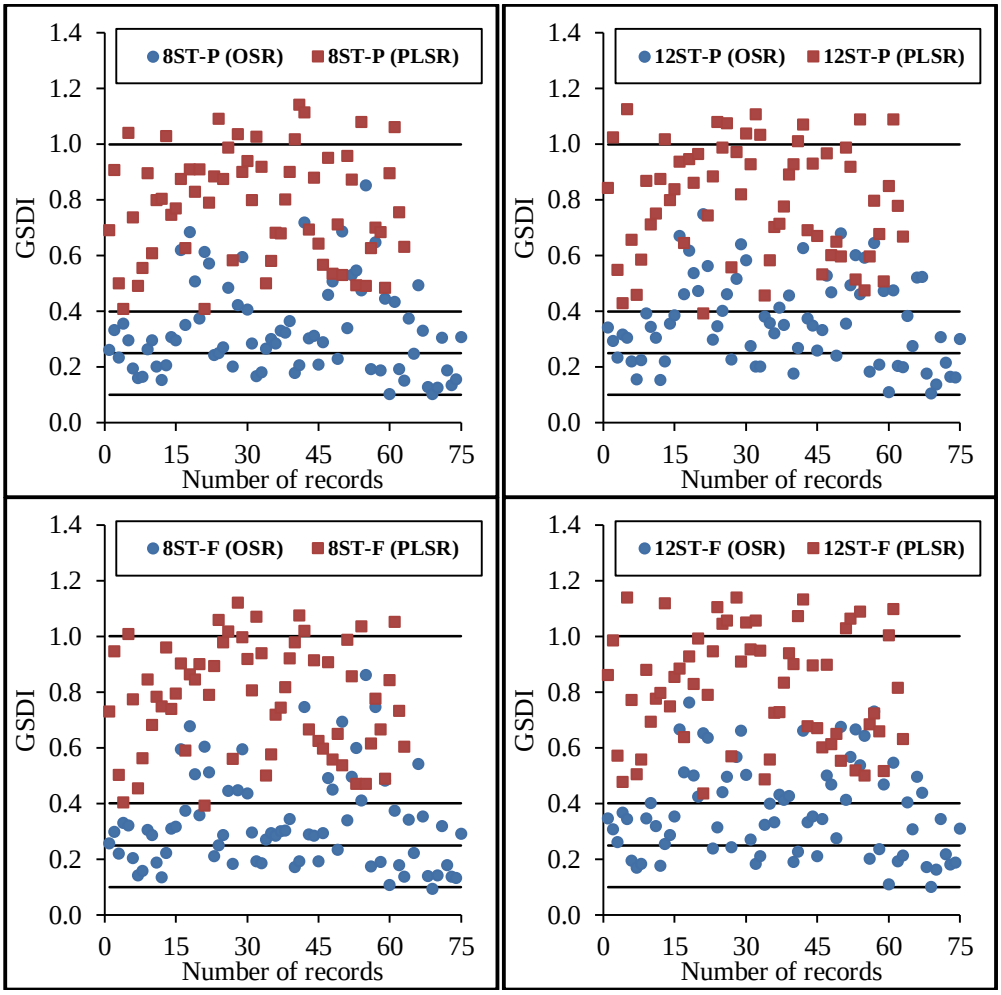

Figure 6.4: Considering of Seismic Performance of Buildings for 8 and 12 Stories by using Park-Ang Index (GSDI) without SSI.

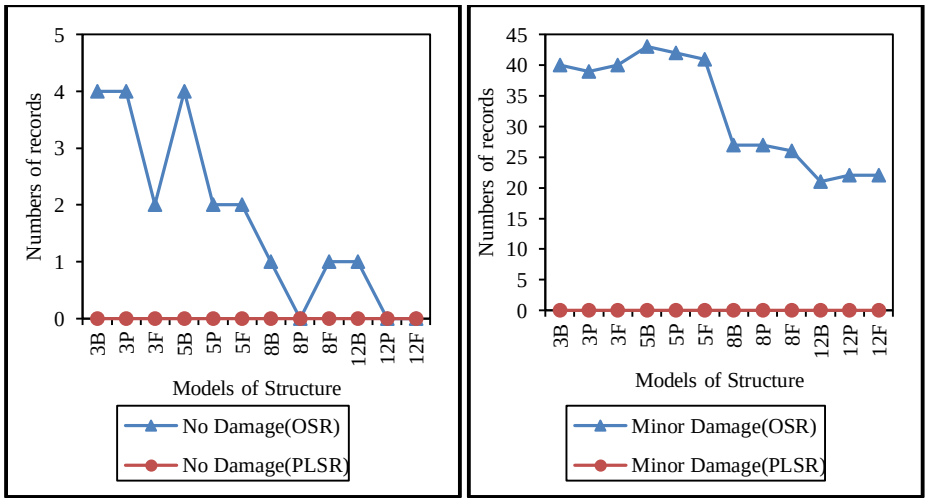

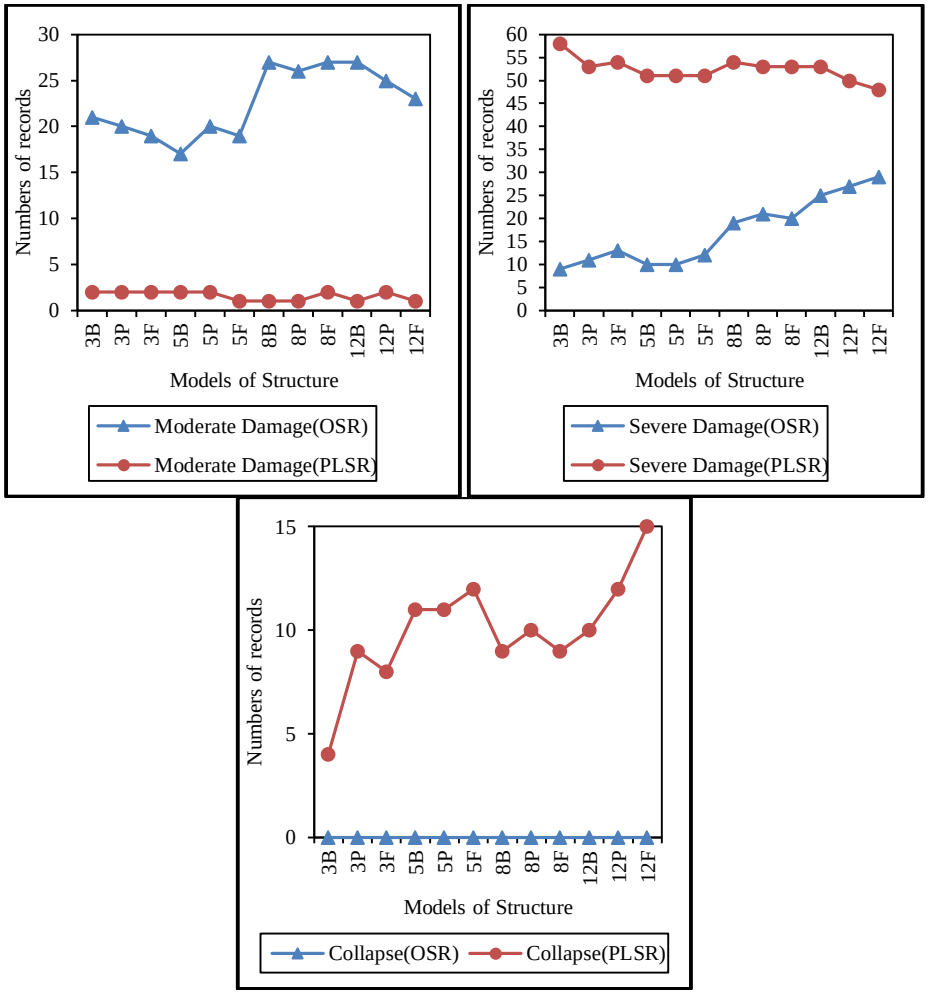

Figure 6.5: Comparison of Seismic Performance of Buildings for Two Sets Records by using Park-Ang Index (GSDI) without SSI.

6.2 Comprehensive Analysis of Correlation Coefficients

The correlation coefficient values are used to determine the relationship between intensity measure (IMs) of ground motion and degree of damage to buildings. First of all Kolmogorov–Smimov model (Jan 2018) was used to identify the input parameters and then to obtaining the normal distribution. For the ground motions selected, Kolmogorov–Smimov model shows that the data used are correct but it follows the normal distribution with 5% error. Therefore, to evaluate the correlation among the parameters used, the Spearman correlation coefficient was applied.

Spearman correlation coefficient

Spearman correlation coefficient is used as indicator to evaluate the relationship between the two variables, a and b, which are described by using monotonic function. The value of Spearman correlation coefficient ranges between -1 and 1 and they illustrate that each variable have a complete monotonic function. They also show the dependency between the parameters. However, value of 0 indicates that there is no association between the two variables. The spearman rank-order correlation coefficient between the two variables, a and b, are expressed as follows:

$$\rho_{spearman} = 1 - \frac{6 \sum_{i=1}^{N} d^2}{N(N^2-1)} \quad \text{(Eq.30)}$$

d, indicates the difference between a_i and b_i corresponding values and N indicates a set of pairs of values (a, b).

6.3 Correlation between Earthquake Intensity Criteria

Tables 6.1 and 6.2 shows Spearman's rank correlation coefficients of ground motion IMs. As explained in chapter 3, twelve different models were prepared and analyzed to evaluate the correlation between the parameters in both ordinary seismic records (OSR) and pulse-like seismic records (PLSR). The numerical evaluation of IMs indicate that the correlation coefficient defined by using this approach differ in two models. It should also be noted that the correlation coefficients for $S_d(T_1)$, $S_v(T_1)$ and $S_a(T_1)$ were not presented in tables, since they are dependent on the building analysis, with and without soil-structure interaction. It can be seen from Table 6.1 that SMV, VSI, AI, SED and EPV and from Table 6.2 A95 and EDA have the highest correlation with IMs. In summary, PGV/PGA and D-RMS have the lowest correlation with IMs. It will show that the correlation between velocity related criteria and drift related criteria is very high.

Table 6.1: Correlation Coefficients between Parameters of the Ground Motion in OSR.

	PGA	PGV	PGD	PGV/PGA	A_RMS	V_RMS	D_RMS	AI	CI	SED	CAV	ASI	VSI	HI	SMA	SMV	EDA	A95	Tp	SD
PGA	1																			
PGV	0.71	1																		
PGD	0.4	0.79	1																	
PGV/PGA	-0.46	0.17	0.31	1																
A-RMS	0.83	0.75	0.51	-0.23	1															
V-RMS	0.57	0.86	0.82	0.2	0.8	1														
D-RMS	0.3	0.67	0.92	0.23	0.51	0.81	1													
AI	0.81	0.81	0.64	-0.16	0.9	0.77	0.61	1												
CI	0.84	0.81	0.6	-0.18	0.96	0.8	0.58	0.98	1											
SED	0.5	0.84	0.91	0.25	0.64	0.91	0.89	0.79	0.74	1										
CAV	0.55	0.69	0.7	-0.01	0.66	0.7	0.72	0.88	0.81	0.85	1									
ASI	0.91	0.73	0.48	-0.38	0.87	0.63	0.44	0.9	0.91	0.58	0.68	1								
VSI	0.69	0.94	0.78	0.13	0.79	0.88	0.66	0.82	0.83	0.83	0.66	0.72	1							
HI	0.6	0.92	0.84	0.21	0.72	0.91	0.74	0.78	0.78	0.9	0.7	0.64	0.97	1						
SMA	0.77	0.74	0.54	-0.21	0.81	0.64	0.49	0.92	0.9	0.67	0.76	0.86	0.75	0.68	1					
SMV	0.66	0.9	0.85	0.12	0.78	0.9	0.76	0.86	0.85	0.9	0.77	0.74	0.92	0.92	0.79	1				
EDA	0.99	0.73	0.43	-0.41	0.84	0.61	0.35	0.82	0.85	0.53	0.57	0.93	0.72	0.63	0.77	0.69	1			
A95	1	0.7	0.39	-0.46	0.83	0.57	0.3	0.81	0.84	0.49	0.54	0.91	0.69	0.6	0.77	0.66	0.99	1		
Tp	-0.23	-0.01	-0.03	0.56	-0.15	0.03	-0.06	-0.17	-0.18	0.01	-0.15	-0.24	-0.02	-0.02	-0.28	-0.08	-0.18	-0.23	1	
SD	-0.62	-0.33	-0.05	0.51	-0.5	-0.22	0.06	-0.31	-0.41	0	0.05	-0.52	-0.37	-0.24	-0.42	-0.29	-0.62	-0.63	0.34	1

Table 6.2: Correlation Coefficients between Parameters of the Ground Motion in PLSR.

	PGA	PGV	PGD	PGV/PGA	A_RMS	V_RMS	D_RMS	AI	CI	SED	CAV	ASI	VSI	HI	SMA	SMV	EDA	A95	T_p	SD
PGA	1																			
PGV	0.64	1																		
PGD	0.03	0.62	1																	
PGV/PGA	-0.56	0.23	0.61	1																
A-RMS	0.82	0.58	-0.03	-0.39	1															
V-RMS	0.4	0.8	0.73	0.34	0.53	1														
D-RMS	-0.02	0.53	0.9	0.6	0.05	0.8	1													
AI	0.77	0.83	0.4	-0.11	0.65	0.59	0.29	1												
CI	0.86	0.79	0.26	-0.24	0.86	0.61	0.22	0.94	1											
SED	0.23	0.77	0.91	0.53	0.14	0.8	0.83	0.62	0.47	1										
CAV	0.25	0.63	0.6	0.31	0.07	0.43	0.44	0.75	0.53	0.77	1									
ASI	0.88	0.57	-0.01	-0.49	0.71	0.27	-0.06	0.77	0.81	0.2	0.34	1								
VSI	0.77	0.8	0.23	-0.17	0.76	0.56	0.15	0.86	0.88	0.43	0.48	0.7	1							
HI	0.72	0.85	0.33	-0.07	0.71	0.64	0.26	0.84	0.85	0.51	0.5	0.65	0.98	1						
SMA	0.84	0.62	0.12	-0.39	0.73	0.39	0.06	0.84	0.86	0.32	0.44	0.88	0.76	0.72	1					
SMV	0.39	0.78	0.76	0.3	0.31	0.81	0.7	0.68	0.58	0.86	0.67	0.34	0.56	0.64	0.49	1				
EDA	0.99	0.62	0	-0.57	0.82	0.37	-0.05	0.75	0.85	0.2	0.23	0.88	0.77	0.72	0.83	0.36	1			
A95	1	0.63	0.03	-0.56	0.82	0.4	-0.02	0.76	0.85	0.22	0.25	0.88	0.77	0.71	0.84	0.38	0.99	1		
T_p	0.1	0.38	0.15	0.24	0.27	0.38	0.13	0.26	0.27	0.25	0.18	0	0.43	0.43	0.02	0.29	0.12	0.1	1	
SD	-0.54	-0.12	0.42	0.54	-0.65	-0.06	0.34	-0.13	-0.35	0.35	0.49	-0.48	-0.38	-0.33	-0.4	0.13	-0.57	-0.54	-0.04	1

6.4 Correlation between Damage Criteria

6.4.1 Considering in Fix-base State

Spearman correlation coefficient is used to check correlation between different building criteria and damages when frame had fixed-base, without SSI. In Figures 6.6 to 6.8, correlation coefficients were calculated for the highest values of damage criteria. These figures indicate that damage indexes of MIDR and RDR have good correlation with each other but each one have the lowest correlation with GSDI. These results are due to MIDR and RDR being calculated by considering displacement demand while GSDI was determined by the deformation demand of building. In some cases, the correlation coefficients are very similar which shows that there is good correlation between displacement and deformation demands. Furthermore, it should be noted that GSDI has higher correlation with MIDR when compared to that of RDR. In most of the damage indexes, the correlation coefficients in the PLSR set were higher than the OSR set. The following are further discussions by considering the results of correlation coefficients without SSI.

Consider correlation of damage indexes MIDR and RDR (Figure 6.6):

- As the number of stories increase the correlation reduces and the OSR correlations reduce more than the PLSR.
- 3 and 5 stories have very similar correlation both for OSR and PLSR. On the other hand 8 and 12 stories have similar correlation but compared to 3 and 5 stories they are marginally lower. This is generally valid for Bare (B), Partially Infilled (P) and Fully Infilled (F) frames. Only for Bare model correlation appears to be better for 12 story frame.

Consider correlation of damage indexes MIDR and GSDI (Figure 6.7):

- As the number of stories increase the correlation generally increase except for F frame for both PLSR and OSR.
- OSR correlation is lower for 3 story B frame and same for 3 story and higher for 5, 8 and 12 stories for P frame when compared to those of PLSR.
- OSR and PLSR correlation is almost same as those in MIDR and RDR correlation when F frame is considered.

Consider correlation of damage indexes RDR and GSDI (Figure 6.8):

- As the number of stories increase the correlation either stays the same or increase, particularly for PLSR for all frames.
- OSR correlation is lower for 3, 8 and 12 stories and higher for 5 story B frame when compared to those of PLSR.
- OSR correlation is almost same as PLSR for all stories except for 5 story for P and F frames.

6.4.2 Considering in Soil Structure Interaction State

Spearman correlation coefficient was used to investigate the correlation between different building parameters with SSI and building failures. In Figures 6.6 to 6.8, the correlation coefficient for the damage criteria with SSI are given. These figures indicate that damage indexes of MIDR and RDR have good correlation with each other but each one have the lowest correlation with GSDI. These results show that, with regards to the SSI, the structures behavior was considerably different when compared to the behavior of fixed-base structure. In this section, there are two factors that play a very important role in the structures response. First of all the structure was modeled by using the soft soil, and secondly, the infilled-masonry had significant effects on the

stiffness of the structure. These factors affected the structures response. As can be seen from Figures 6.6 to 6.8, the two MIDR and RDR failure indicators are closely related, due to the fact that damage indexes of MIDR and RDR are calculated by considering structure displacement demands, but the GSDI is determined based on the demands of deformation of building elements. But in some cases, correlations with GSDI also show similarity, which may indicate that for such cases there is a good relationship between the demands for displacement and deformation. In addition, it should be noted that GSDI has higher correlation with MIDR than RDR. The correlation coefficients with the effect of the SSI were reduced by about 10-20% when compared with the same model with a fixed base. As can be seen in figures, the correlation coefficient decreases with increasing the number of stories. The following are further discussions by considering the results of correlation coefficients with SSI.

Consider correlation of damage indexes MIDR and RDR (Figure 6.6):

- As the number of stories increase there is more severe drop in correlation between 3, 5 stories and 8, 12 stories for PLSR.
- When OSR is considered generally the correlations drop as the number of stories increase. This is valid for all the frames.
- On the other hand, numerically there is slight drop in correlation for both OSR and PLSR moving from B to F frames.

Consider correlation of damage indexes MIDR and GSDI (Figure 6.7):

- As the number of stories increase there is generally decrease correlation for all frames for PLSR. The behavior is very similar and the correlation values only slightly lower than damage indexes MIDR and RDR for PLSR (Figure 6.6).

- The OSR correlation of 3 story is considerably lower for B frame and improves for P and F frame. Generally all OSR correlations are lower than PLSR and those obtained from correlation of damage indexes MIDR and RDR (Figure 6.6).

Consider correlation of damage indexes RDR and GSDI (Figure 6.8):

- As the number of stories increase the PLSR correlation is almost same for 3 and 5 stories for all frames and it considerably drops for 8 and 12 stories for P and F frames.
- OSR correlation is lower for all frames and follow similar pattern where correlations is generally best for 5 story frame for all infill options except 12 story is best correlation for P frame.

6.4.3 Comparing the Correlations with and without SSI

- OSR correlation generally becomes similar to PLSR as the number of stories increase, particularly for P and F frames of 8 and 12 stories.
- P frame with SSI has a different behavior than the rest of the other models.
- The displacement and deformation of the structure with IMs have weaker relationship with the structures in the absence of soil-structure interaction.
- OSR correlations are generally same or lower that the PLSR with and without SSI except 5 story B and P frame for damage indexes MIDR-GSDI and RDR-GSDI and F frame RDR-GSDI without SSI. Simply 5 frames out of 72 frames of all B, P and F frames with and without SSI.
- When SSI is considered there is bigger drop in OSR correlation, particularly for B frames in all three comparisons except for 5 story building. This phenomena corresponds well without SSI for damage indexes MIDR-GSDI

and RDR-GSDI where the OSR correlation of 5 story frame is higher than PLSR. Simply OSR correlation for 5 story frame is higher than the frames with other stories without SSI and RDR-GSDI with SSI. So this may indicate that damage indexes MIDR-GSDI and RDR-GSDI without SSI is almost excellent for 5 story building for all B, P and F frames.

- Comparison of all damaged indexes indicate drop in OSR and PLSR correlation values with SSI when compared to without SSI. This is important needs to be further investigated for better understanding of the more realistic behavior of structural B, P and F frames.

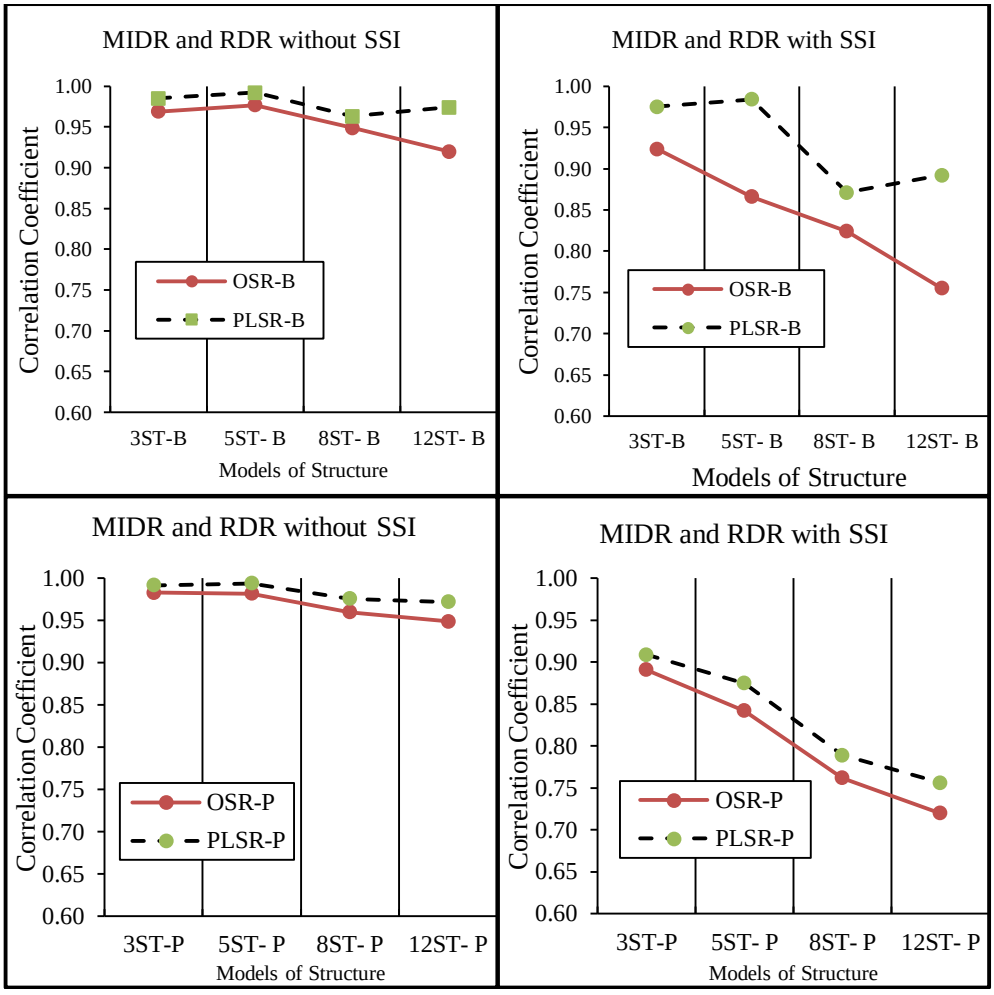

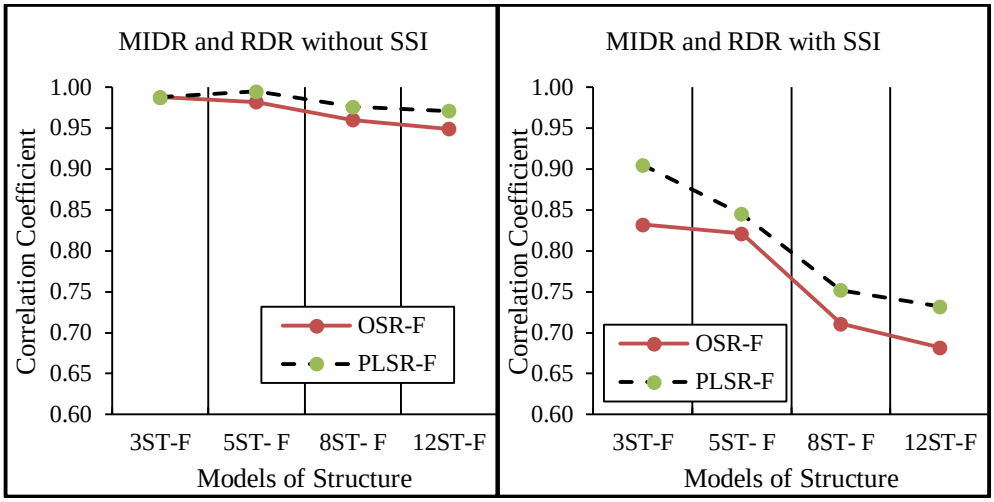

Figure 6.6: Correlation Coefficient between MIDR and RDR with and without SSI.

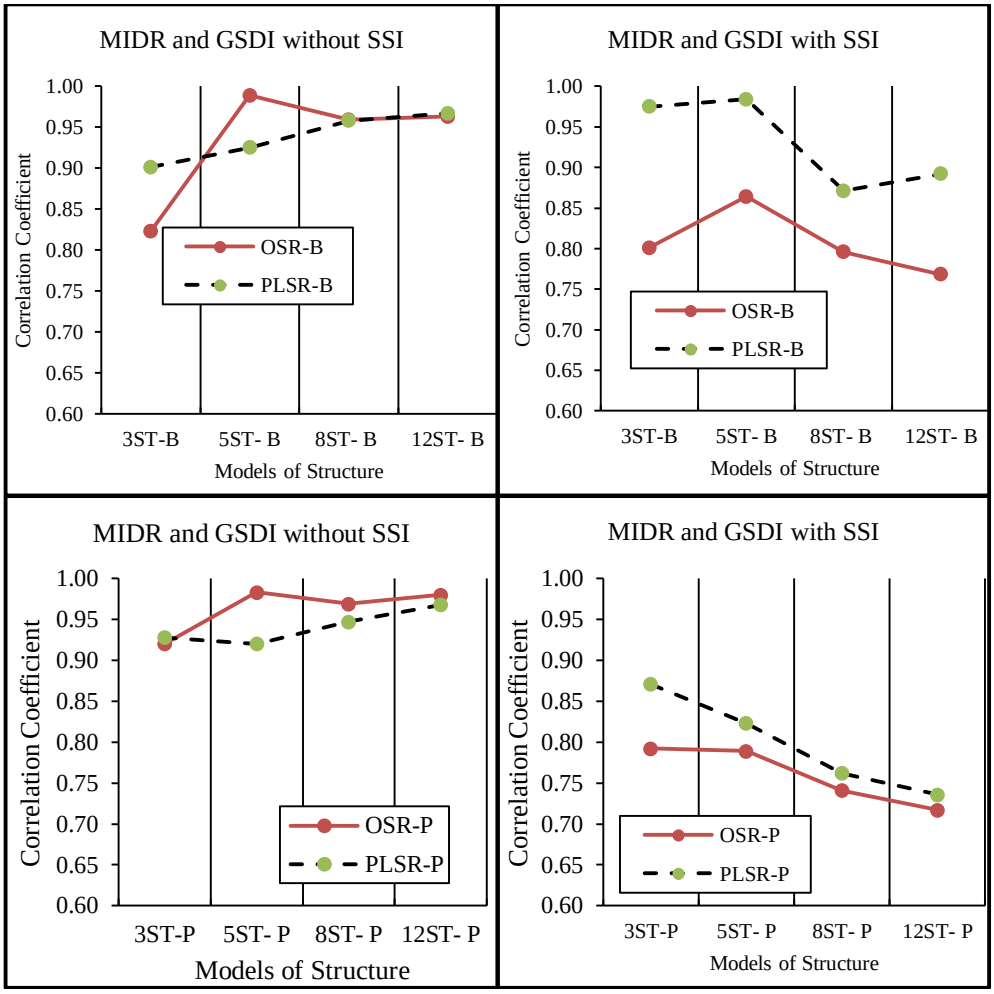

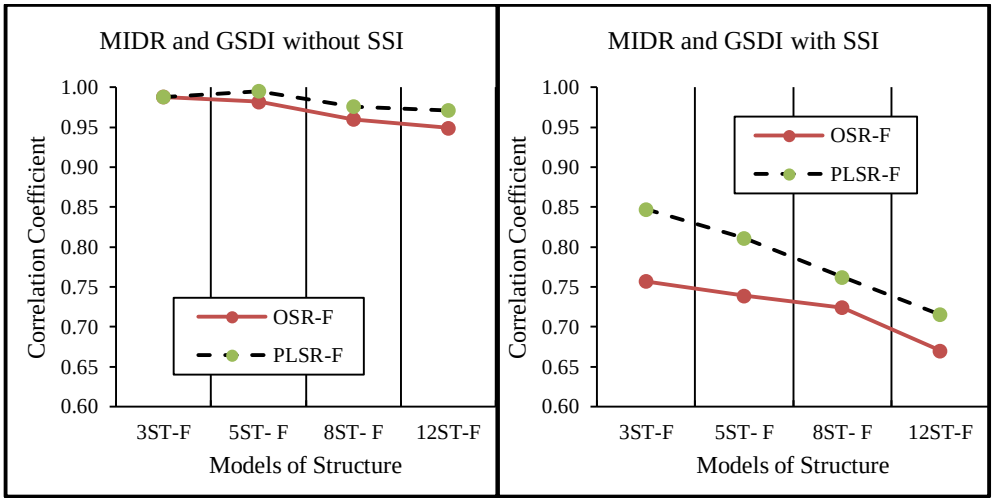

Figure 6.7: Correlation Coefficient between MIDR and GSDI with and without SSI.

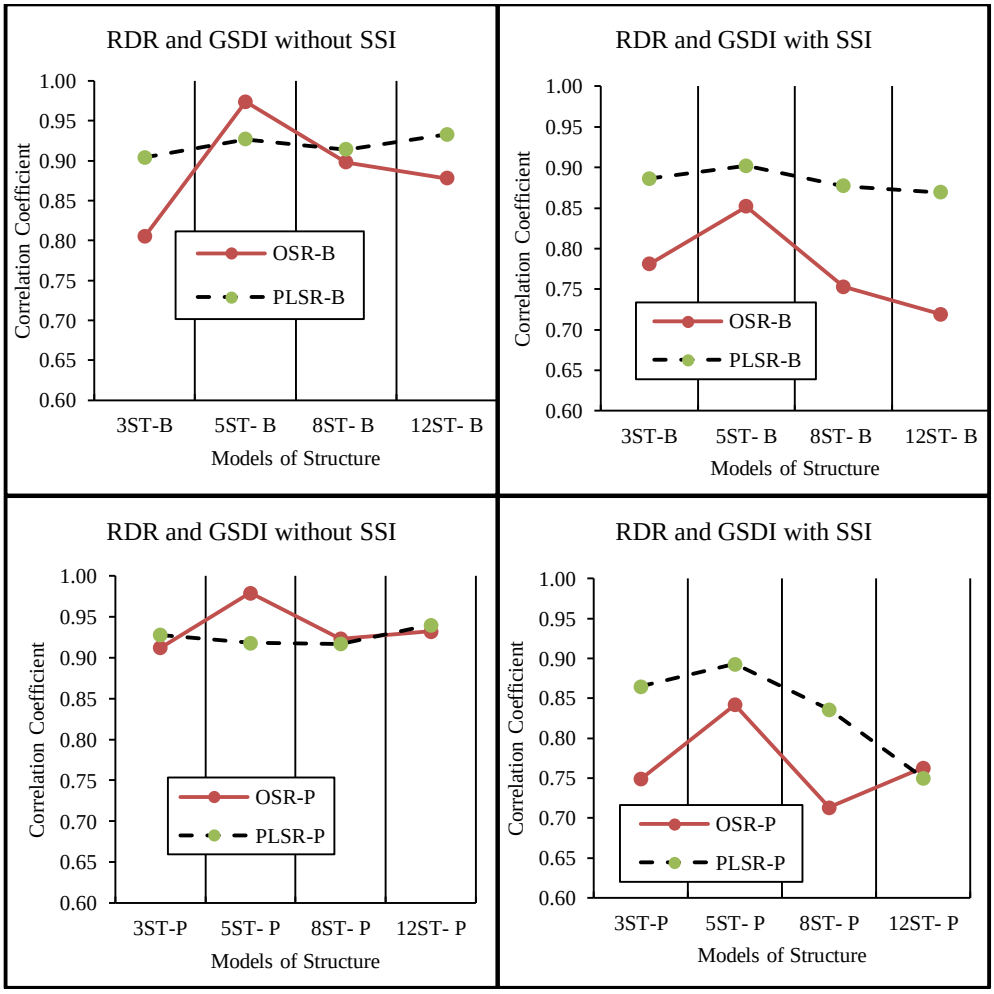

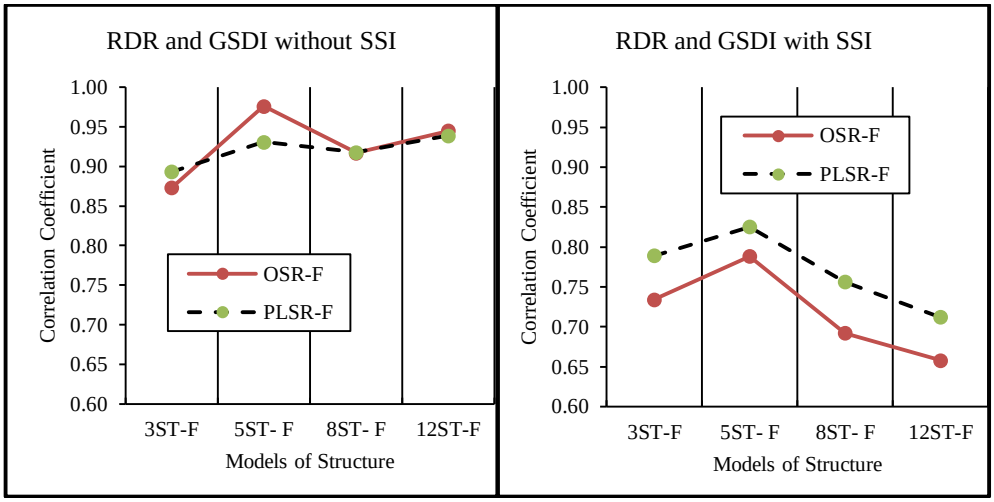

Figure 6.8: Correlation Coefficient between RDR and GSDI with and without SSI.

6.5 Correlation between Earthquake Intensity Criteria and Structural Response

Spearman correlation coefficient evaluates quality and accuracy of seismic IMs as an indicator of structural responses. Especially for the highest values of each damage criteria, Tables 6.1 and 6.2 based on the IMs, is stated and is created in chapter 3. Figures 6.9 to 6.12 give correlation coefficients between damage indexes and 16 seismic IMs indicators for both PLSR and OSR mode. It should be noted that a large part of IMs are correlated with damage index of building by using these tables and MIDR and RDR have the highest values of correlation. In Figures 6.9 to 6.12, the correlation coefficient of I_v, I_d, I_a, I_f, SMW, CAV, V-RMS, D-RMS, SED and PGD parameters on damage index like GSDI, RDR and MIDR, in OSR mode is higher than PLSR. But correlation coefficient of T_m, Ω, SD and T_p parameters in PLSR set is higher than OSR. It is interesting to know that D-RMS in PLSR mode and T_m, Ω, T_p, PGA/PGV in OSR mode have the correlation coefficient lower than the other parameters. For 8 and 12 stories models, damage index between MIDR and GSDI has stronger correlation than the RDR. But on 3 and 5 stories, relationship between three damage index correlation coefficients are very close.

Spearman Correlation for 3 Story frames:

- GSDI correlation with OSR was generally lower than and for some IMs similar to MIDR and RDR for all types of frames.
- Generally MIDR and RDR have almost identical correlation with IMs both for OSR and PLSR modes.
- GSDI have closer correlations with MIDR and RDR for PLSR mode and and for some IMs it has even slightly better correlation than MIDR and RDR.
- Generally OSR and PLSR coefficients individually follow the same pattern for B, P and F frames. The highest correlation for OSR and PLSR mode for all damage indexes is with S_a (T_1) except GSDI for OSR mode for F frame where I_f marginally achieves the maximum correlation. Correlation of MIDR, RDR and GSDI with S_a (T_1) at OSR mode drops by about 12% from B to F frame. This trend is almost same for the PLSR mode.
- The lowest correlation of damage indexes at OSR mode is with PGV/PGA, T_p, Ω, T_m and PLSR mode is with D-RMS, I_d.
- Generally OSR mode correlation is better than PLSR for all frame types with 3, 5, 8 and 12 stories.

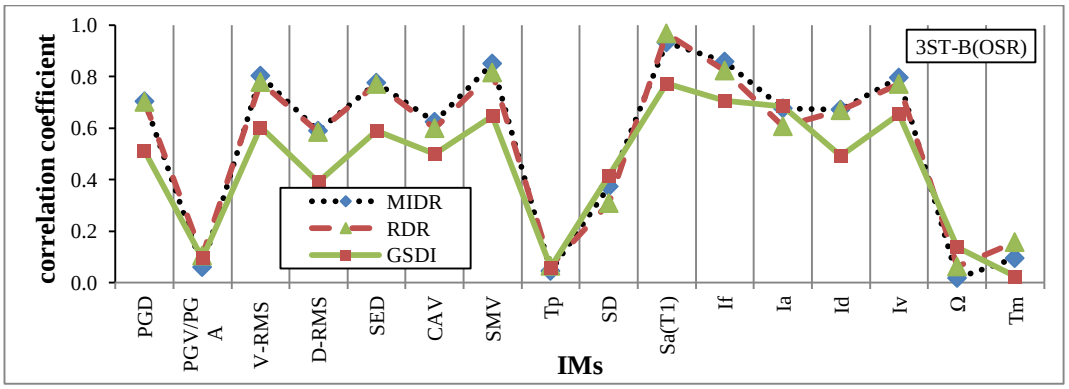

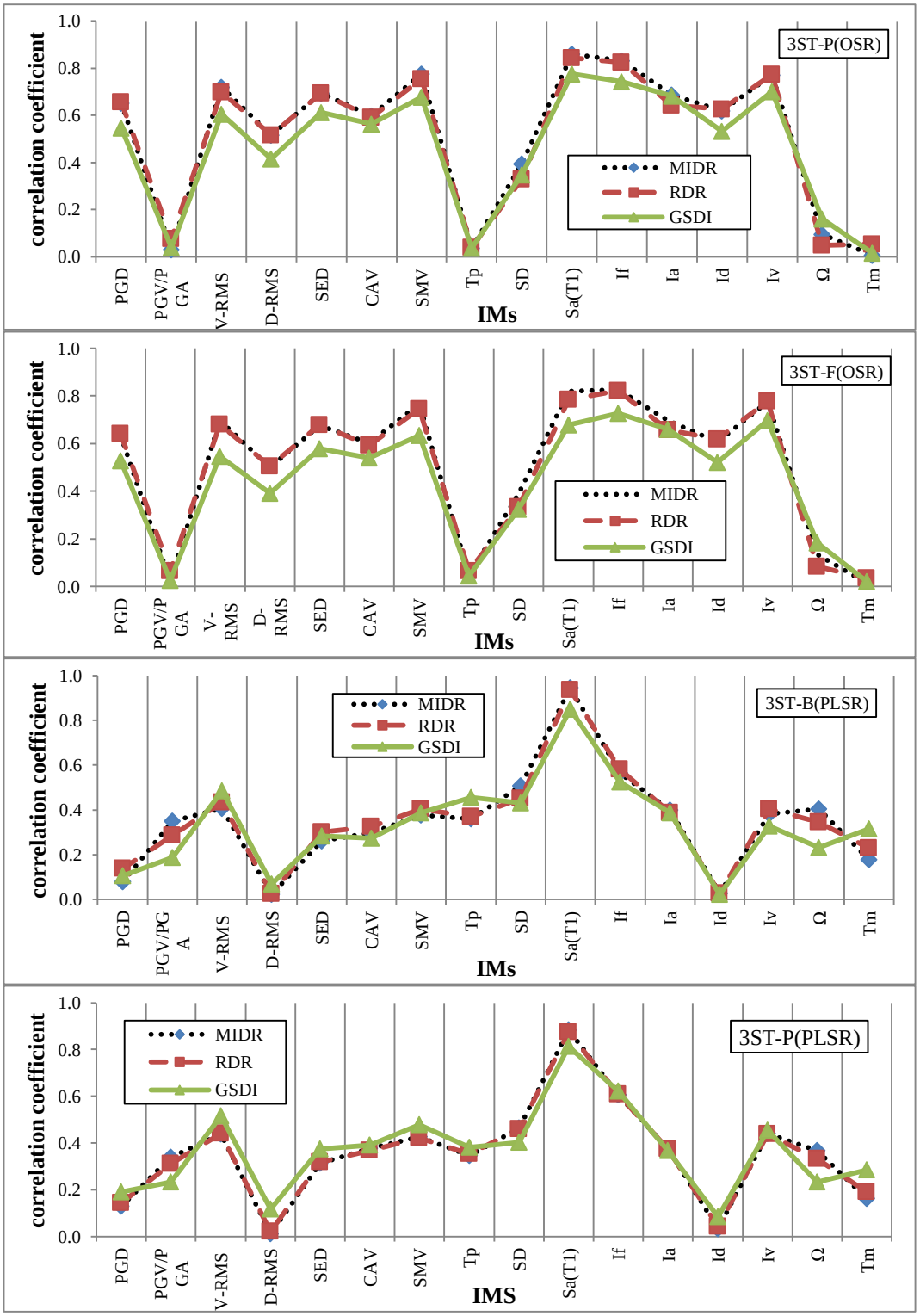
3ST-P(OSR)
3ST-F(OSR)
3ST-B(PLSR)
3ST-P(PLSR)
MIDR
RDR
GSDI
correlation coefficient
1.0
0.8
0.6
0.4
0.2
0.0
PGD
PGV/PGA
V-RMS
D-RMS
SED
CAV
SMV
Tp
SD
Sa(T1)
If
Ia
Id
Iv
Ω
Tm
IMs
IMS

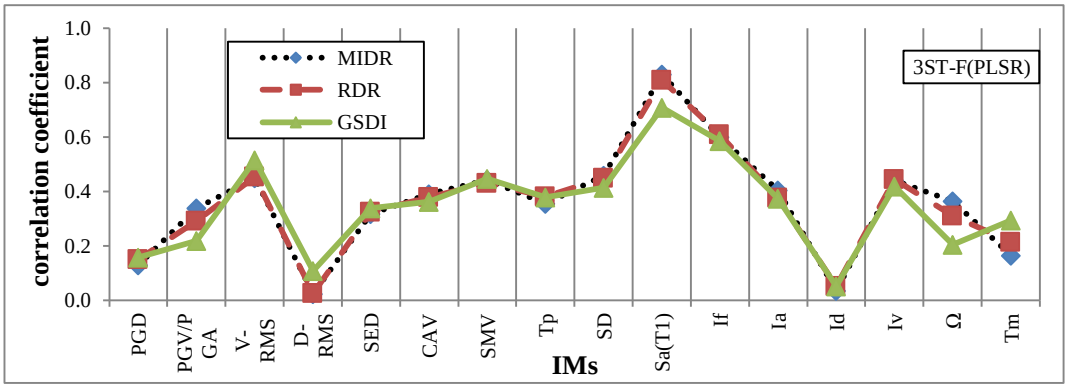

Figure 6.9: Spearman Correlation Coefficient between Seismic IMs and Damage Index in the Three-story Building.

Spearman Correlation for 5 Story frames:

The observations for 3 story frame is generally valid for this frame too with one exception that correlation of GSDI for OSR mode is very similar to those of MIDR and RDR for all frame types. As for PLSR mode the correlation of GSDI is also closer to MIDR and RDR and the best correlation is with F frame. The highest and lowest correlations of OSR and PLSR mode is with the same IMs as those for the 3 story case.

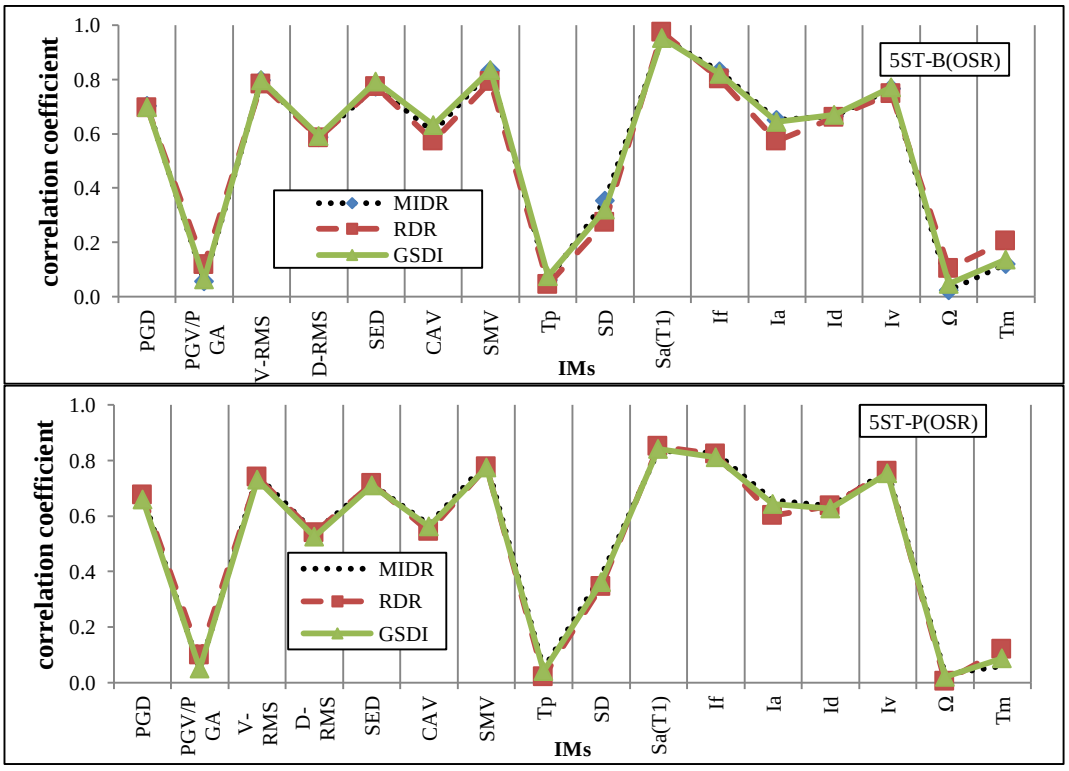

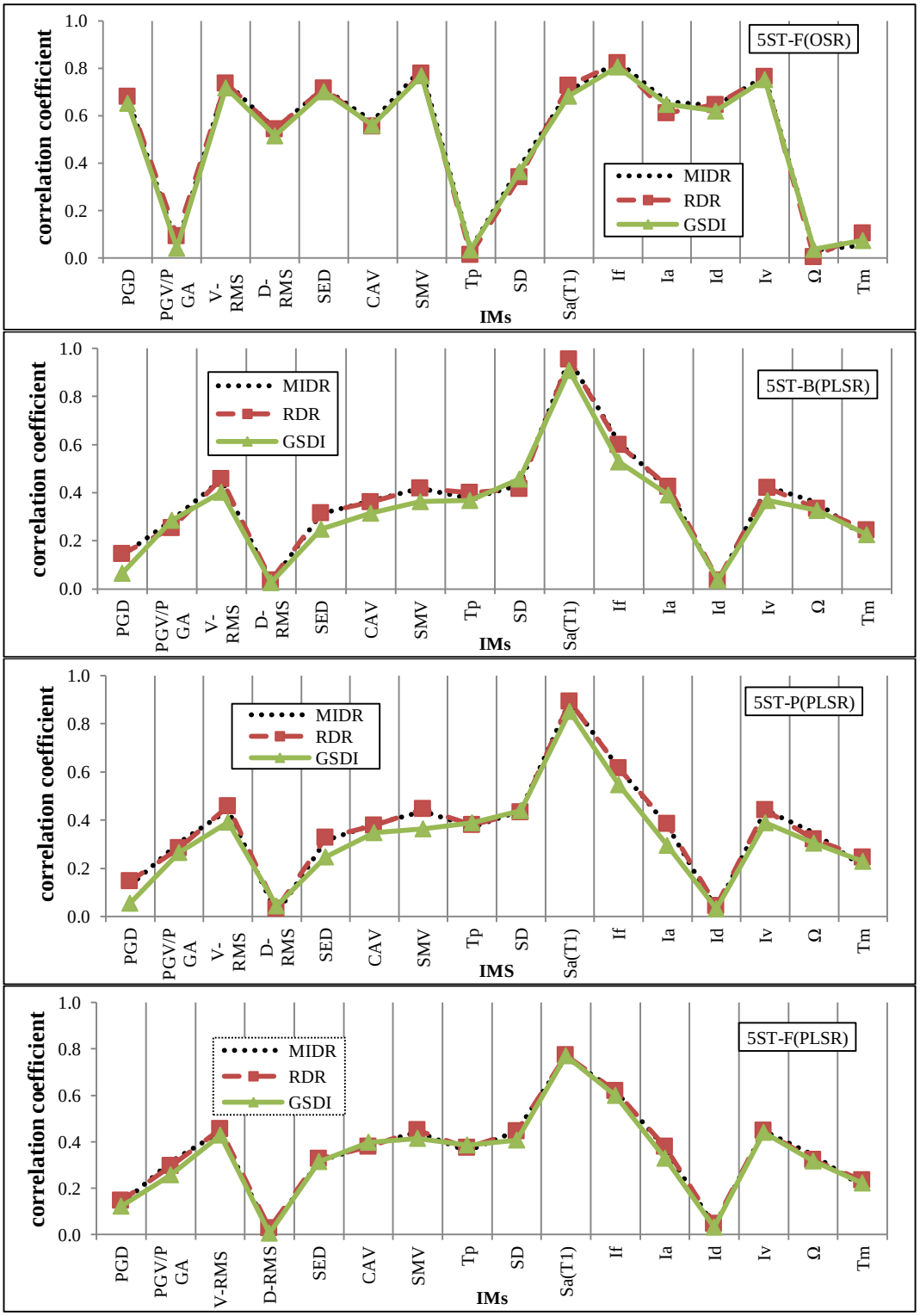

Figure 6.10: Spearman Correlation Coefficient between Seismic IMs and Damage Index in the Five-story Building.

Spearman Correlation for 8 Story frames:

The observations for 3 and 5 story frame is generally valid for this frame too with an exception that MIDR and RDR correlation are no longer identical. All three damage indexes are slightly separated from each other and the OSR mode of RDR correlation is more than MIDR for some IMs and particularly for the maximum one, S_a (T_1). The PLSR mode of MIDR-RDR together had the highest correlation with S_a (T_1).

There is one difference in 8 story frame when compared to 3 and 5 story. The lowest correlation for OSR mode is clearly with T_p for all frame types. On the other hand the lowest correlation for PLSR mode is with PGV/PGA and Ω for B frame whilst they are changed to D-RMS and I_d for P and F frames.

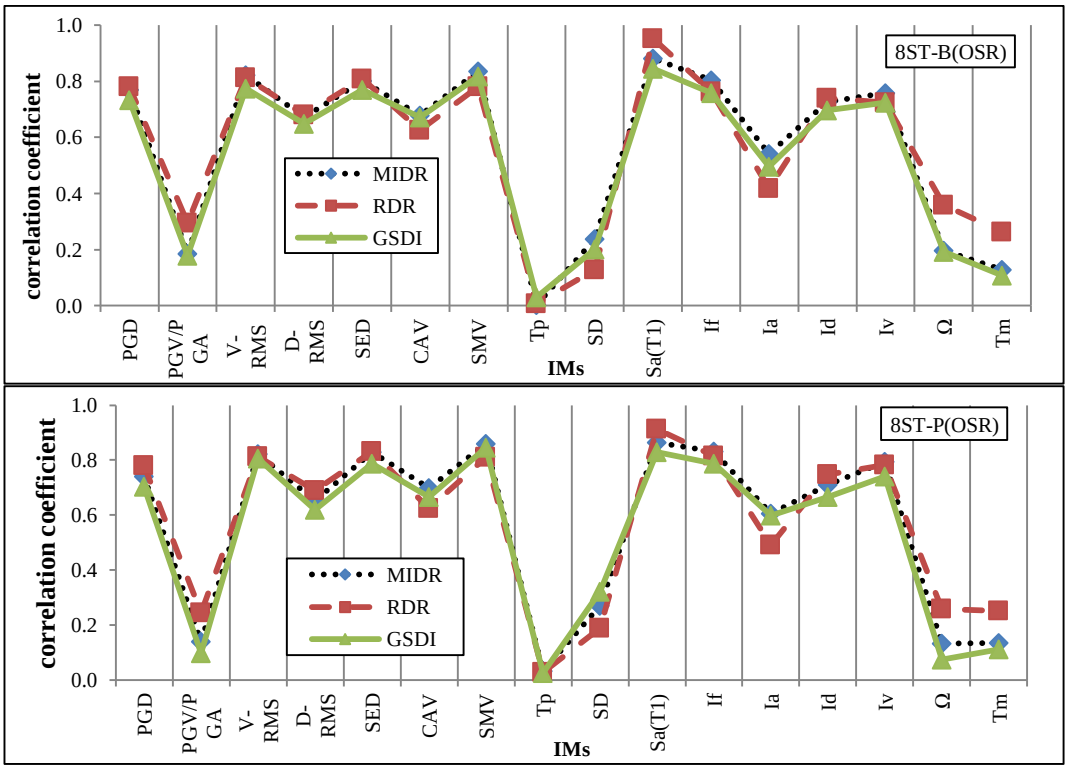

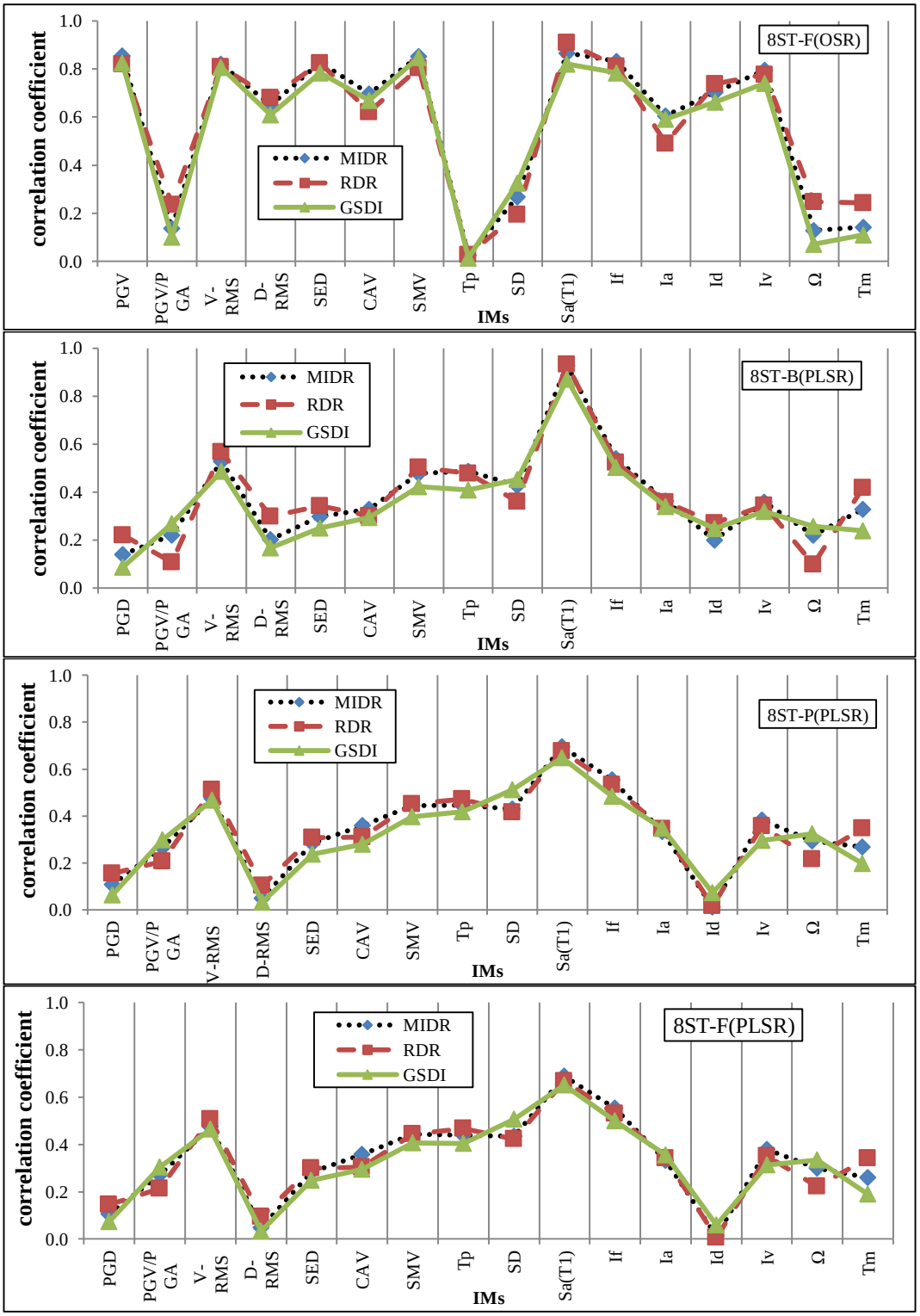

Figure 6.11: Spearman Correlation Coefficient between Seismic IMs and Damage Index in the Eight-story Building.

Spearman Correlation for 12 Story frames: The observations for 8 story frame is generally valid for this frame too but with the following differences:

- The highest correlation for OSR mode is with RDR and S_a (T_1) for B frame, GSDI and I_f for P frame, GSDI and S_a (T_1), MIDR and I_f for F frame.
- The highest correlation for PLSR mode is with all damage indexes and S_a (T_1) for B frame, MIDR and S_a (T_1), GSDI and I_f for P frame, GSDI and I_f for F frame.
- The lowest correlation for OSR mode is with MIDR, GDSI and T_p for B frame, GSDI and T_p, RDR and PGV/PGA for P frame, MIDR, GDSI and T_p for F frame.
- The lowest correlation for PLSR mode is with MIDR, GDSI and Ω for B frame, all damage indexes and Ω for P frame, GSDI and I_d, MIDR, RDR and PGV/PGA for F frame.

When compared to 3, 5 and 8 story frames OSR mode correlation of damage indexes with IMs are almost the same shape. However, for PLSR mode the damaged index to IMs correlation shape has changed for all frame types, particularly for P and F frames. Generally the correlation of damaged indexes are better with the IMs.

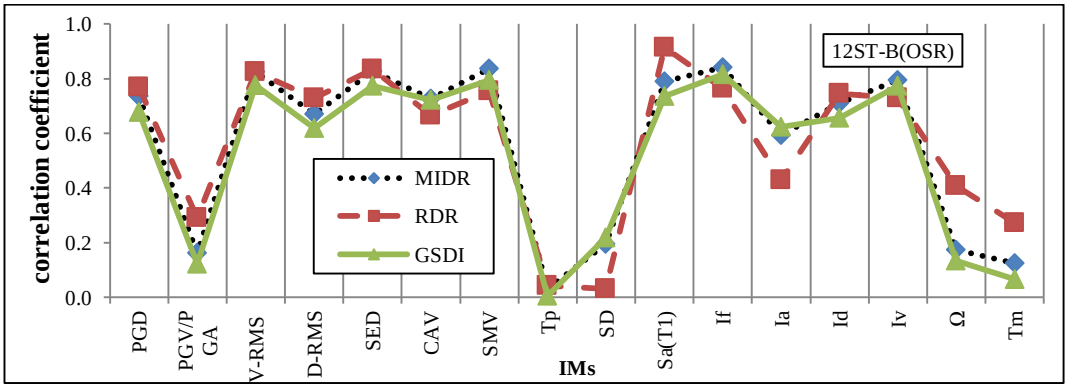

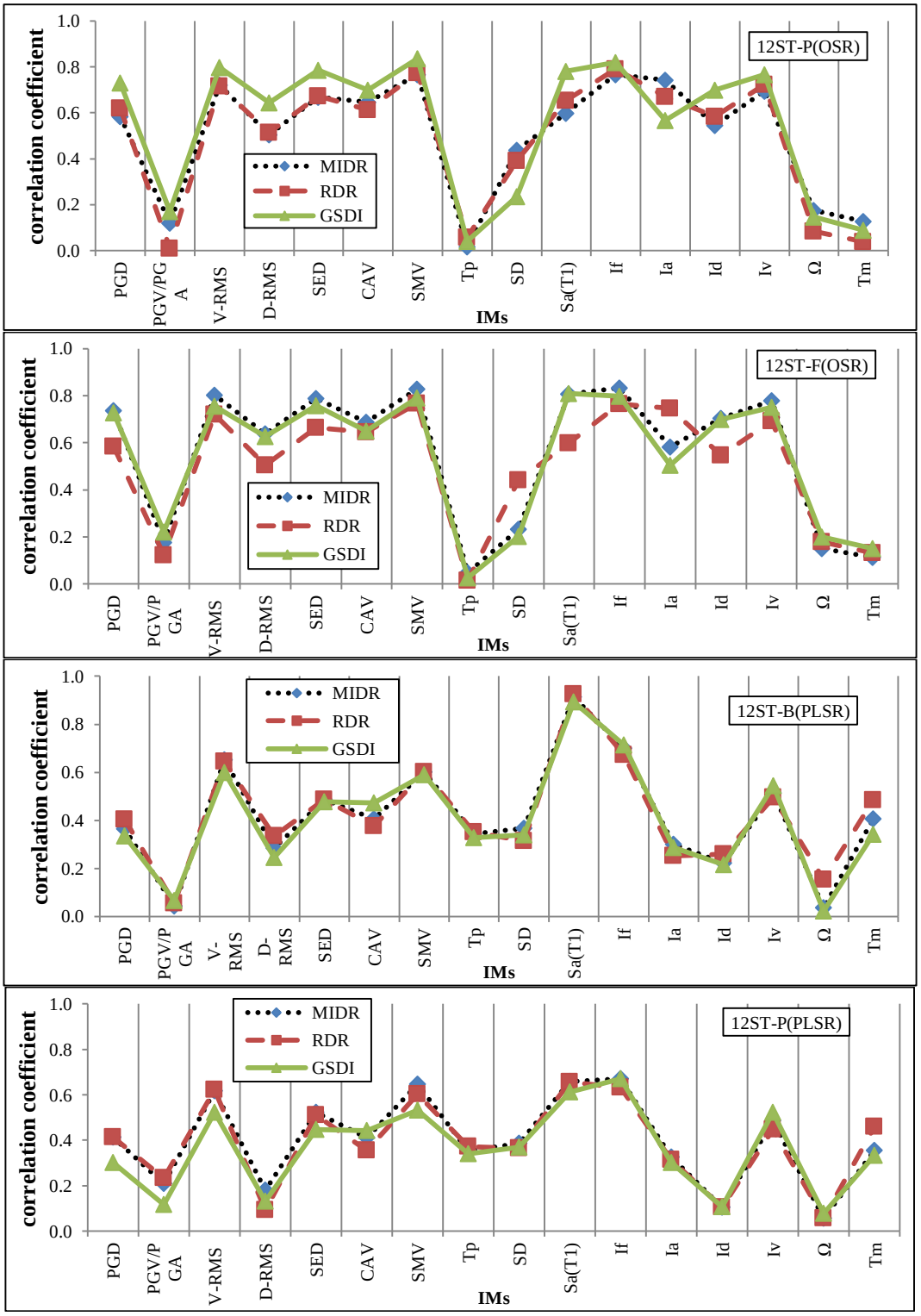
12ST-P(OSR)
12ST-F(OSR)
12ST-B(PLSR)
12ST-P(PLSR)
MIDR
RDR
GSDI
correlation coefficient
IMs
1.0
0.8
0.6
0.4
0.2
0.0
PGD
PGV/PGA
V-RMS
D-RMS
SED
CAV
SMV
Tp
SD
Sa(T1)
If
Ia
Id
Iv
Ω
Tm

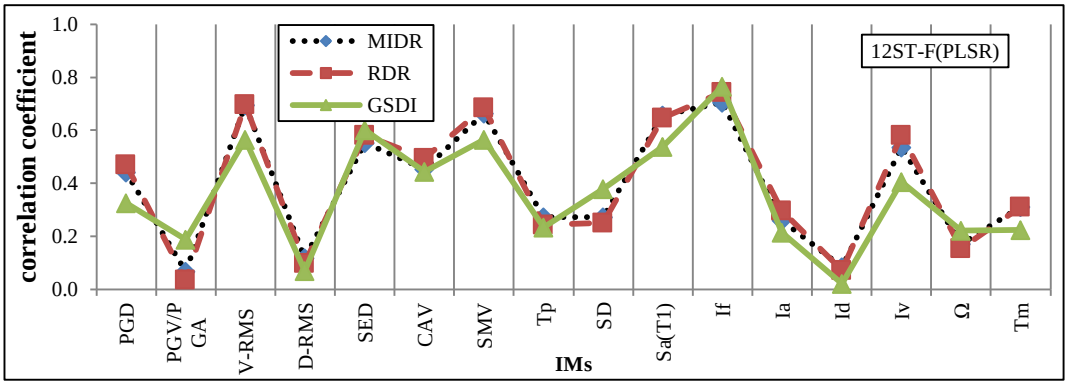

Figure 6.12: Spearman Correlation Coefficient between Seismic IMs and Damage Index in the Twelve-story Building.

In order to evaluate the IMs separately in the range of linear relationships (y = ax + b), the constant values *a* and *b* are assumed to be in the linear response range. Also, Spearman correlation coefficient with square root of R^2 calculated for linear fit. Figure 6.13 show the average curve for all structural models. Since the damage indicator MIDR showed a good correlation in the last sections, the results show that the effect of SSI has a reducing effect on correlation coefficient with MIDR and linear and exponential relations.

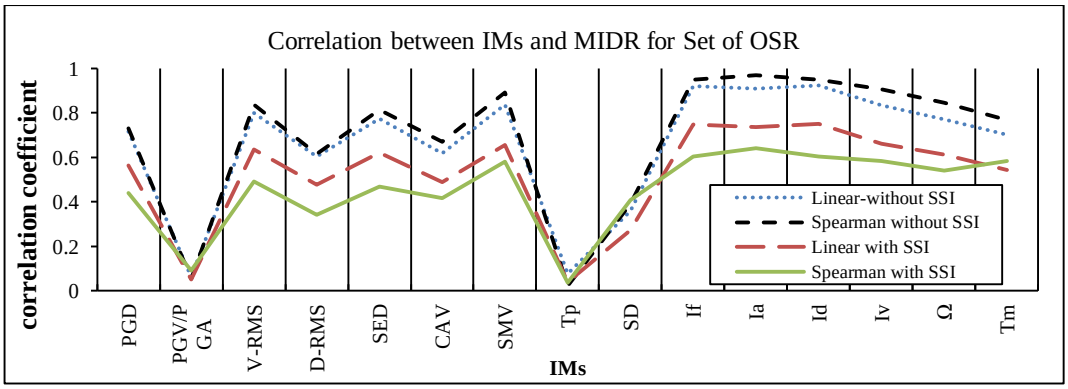

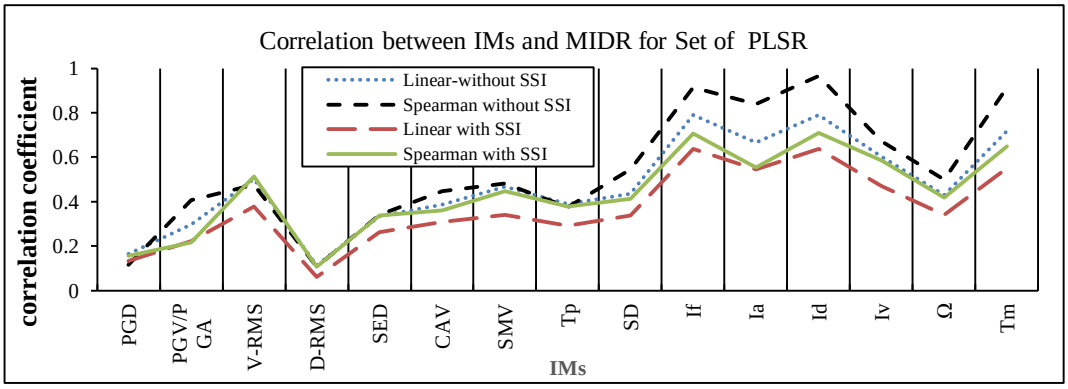

Figure 6.13: Correlation of Ground Motion IMs and MIDR with and without Considering SSI (OSR).

Chapter 7

SUMMARY, CONCLUSION AND RECOMMENDATIONS FOR FUTURE WORK

7.1 Summary

In this research, the effect of soil flexibility, underlying the foundation, on the response of 3, 5, 8 and 12 story high 2-D steel frames without (bare) and with partially infilled and infilled walls under pulse like and ordinary seismic records was studied. The structures had 12 models; In this regard, a cone model was used for soil modeling. The selected soil is type D. Using the OpenSees software, the soil was modeled as equivalent springs and dampers under structures of three, five, eight and twelve stories with a steel moment frame. OpenSees software was used to investigate the nonlinear dynamics of structures against PLSRs and OSRs, and the damage index of structures once with the assumption of rigid support in structures and again considering the effect of SSI. For further investigation of PLSRs and OSRs, the effect of SSI on the response of structures was considered.

The first limitation is the assumption of linear behavior of soil in structural analysis. With this assumption, the soil under foundation is homogeneous and for which behavior is considered linear, and so the strain is small. The second limitation is the selection of the earthquakes. In this research, pulse like seismic records and ordinary seismic records were applied to fixed-base of the structure. In the analysis, it was assumed that the connection of the structure to the ground is rigid, but in general, this

assumption is incorrect unless the structure is placed on very strong materials, such as rocks. When the structure is placed on hard soil, seismic excitation moves directly to the structure without changing its content. But in real terms, when the structure is constructed on soft soils, there are two fundamental changes in system analysis: First, the seismic excitation will change after the construction of the structure. Secondly, a structure on a soft soil is a different system than a hard soil. So, the structures prefer to interact with the surrounding soils. In some cases, it can be said that consideration of the effect of SSI will make the design of the structure economically feasible according to the type and characteristics of the soil and structure.

7.2 Conclusions

Nonlinear time history analysis was used with OSR and PLSR earthquake ground motions with and without SSI for analysis. The seismic performance of the buildings was evaluated using the general indicators of damages. The following are the conclusions of this research:

1- As an overall conclusion, the use of PLSR is important, particularly when SSI is considered, since it generally negatively effects the correlation of damage indexes. Furthermore, when SSI is considered, there is considerable change in the behavior of partially infilled and fully infilled frames with respect to bare frames and high rise with respect to low rise frames.

2- Acceleration-related criteria showed significant correlations with each other as bare frames for all stories. The correlation of the velocity criteria in PLSR were good and were similar to the acceleration-related criteria. In 8 and 12-story P and F frames under PLSR set, there has been a decrease in acceleration-related criteria while this caused an increase in displacement-related criteria,

parameters PGD and D-RMS. This will lead to a negative effect on the overall structural behavior for 8 and 12 story P and F frames.

3- When investigating the correlation between seismic destruction criteria for earthquake variables with IMs, MIDR has a very high correlation coefficient with GSDI for 8 and 12 stories with fix-based in sets of PLSRs and OSRs. The correlation coefficient between MIDR with GSDI was relatively strong relationship which is true in both sets of records for all models (3, 5, 8 and 12 stories) of F steel frame. In the SSI state, the selection of the PLSRs set for all of models are acceptable versus the OSRs set. When SSI is ignored for set of PLSRs all frame models with 3 and 5 story tend to closely correlate between them. When SSI is considered for set of PLSRs all frame models with 3 and 5 story tend to closely correlate between them and 8 to 12 story also correlated between them for each case of B, P and F frames. On the other hand the correlation reduces as the frames change from B to P to F frames. So it can be concluded that set PLSRs play an important role in the behavior of structure, particularly with SSI and for 8 and 12 story frames. When spearman correlation coefficient between seismic IMs and damage index is considered:

   a. It can be seen that MIDR and RDR damage indexes have very good correlation between themselves for all frame models when two sets records are used to show their correlation with parameters IMs. For all damage indexes their correlation with IM parameters are generally better with OSRs and reduce when PLSRs were used for all frame models.
   b. It should be noted that the IM parameters related to displacement, I_d and D-RMS, showed very low correlation with set of PLSRs and the

parameters PGD, SED, CAV and SMV showed increase in correlation in damaged indexes with PLSRs as the number of stories increase and frames change from bare to full infill frames. This may be due to the selected PLSR records and it may need further investigation. However, compared with all the IMs the level of correlation in general is low. So for future studies the importance of this parameter is low.

c. The correlation coefficients of the IMs of Ω with sets of OSRs improved from B to F frames for 3 story frame and reduced for 8 story frame for all damage indexes. On the other hand for 12 story frames there is considerable drop for damage index RDR from B to F frames. As for IMs of Ω with sets of PLSRs for 8 story there is improvement for all damaged indexes but for 12 story only damage indexes of MIDR and GSDI improved from B to F frames.

d. For all P and F frames the maximum decrease in the correlation coefficient was for Sa (T1), Sv (T1) and Sd (T1). The parameter Tm, Tp and Ω have the lowest correlation coefficient for P and F with OSRs.

4- The effect of PLSR on the inelastic displacement ratio, C_R, was developed from the modification coefficient of C_1 (ASCE-41-17, 2017) as a practical procedure to estimate target displacement using SSI in nonlinear static analysis.

5- In the context of building performance, the hysteresis behaviour of part of a beam on the first story, due to two sets of OSR and PLSR records, was considered. The following are the conclusions:

- For 3 story, the F frame achieved the highest displacement for both OSR and PLSR records with and without SSI. This was followed by P

and B, frames. However, consideration of SSI with OSR had considerable variation in displacement among the frames.

6- The following are the conclusions from the quantification of the impact of near-fault directivity on building seismic behaviour through nonlinear dynamic analysis of structural simulation models:

- The rate of failure of the structures with PLSR set is more visible than OSR set. In other words, the failure of structures in three state of "no damage, minor damage and moderate damage" is shown to be more due to OSR set while the failure of structures in two state of severe damage and total collapse is more due to PLSR set.

7.3 Recommendations for Future Work

1- In this study the IM parameters related to displacement, I_d and D-RMS, showed very low correlation with set of PLSRs. This needs further investigation.

2- Investigation of the effect of soil-structure interaction on inelastic behavior of embedded foundation with layered soils.

3- The effect of embedded foundation on structural damage index

4- Investigating the effect of soil-structure interaction on structure with flexible frame.

5- Investigating the effect of frequency content of near-fault earthquakes on non-elastic behavior of structures.

6- Comparison of different systems of seismic damper of high structures against near-field earthquakes.

REFERENCES

Abdollahzadeh, Gh., Sazjini, M., Shahaky, M., Tajrishi, F. Z., & Khanmohammadi, L. (2014). Considering potential seismic sources in earthquake hazard assessment for Northern Iran. Vol. 18, Issue 3, p. 357–369.

Akkar, S., & Galkan, P. (2003). A near - fault design spectrum and its drift. Fourth International conference of Earthquake Engineering and seismology, CD - Rom.p.Bs-17.

Anderson, J., & Bertero, V. (1987). Uncertainties in establishing design earthquakes. Journal of Structural Engineering, Vol.113, Issue 8, p.1709–1724.

Arias, A. (1970). A measure of earthquake intensity. In: Hansen RJ (ed) Seismic design for nuclear power plants. MIT Press, Cambridge, p. 438-483.

Arjomandi, K., Estekanchi1, H., & Vafai, A. (2009). Correlation between structural performance levels and damage indices in steel frames subjected to earthquakes. Vol.16, Issue 2, p. 147-155.

Ayala, G., Xianguo, Y. (1995). Analytical evaluation of the structural seismic damage of reinforced concrete frames. Proceedings of Seventh Canadian Conference on Earthquake Engineering, Montreal, Canada, June 3–7; 389–396.

ASCE-41-17 (2017). Seismic rehabilitation of existing buildings. American Society of Civil Engineers.

Azarhoosh, Z., & Amiri, G. R. (2010). Elastic response of soil-structure systems subjected to near-fault rupture directivity pulses, Soil Dynamics and Earthquake Engineering, Proceedings of the Geo shanghai International Conference, June 3-5, Shanghai, China - Hind: 90, 50 EUR.

Baker, J.W. (2008). Identification of near-fault velocity pulses and prediction of resulting response spectra, in Geotechnical Earthquake Engineering and Soil Dynamics IV, Sacramento, California, 10 pp.

Barkhordary, M., & Tariverdilo, S. (2011).Vulnerability of ordinary moment resistant concrete frames, Earthq Eng & Eng Vib , pp. 519-533.

Bertero, V.V., Mahin, S.A., & Herrera, R.A. (1978). Aseismic design implications of near-fault San Fernando earthquake records. Earthquake Engineering & Structural Dynamics, Vol.6, Issue 1, p. 31-42.

Bielak, J. (1975). Dynamic behavior of structure with embedded foundations. Earthquake Eng. & Structural Dyn, pp: 529 - 574.

Bozorgnia, Y., Bertero, V.V. (2001). Evaluation of damage potential of recorded earthquake ground motion. 96th Annual Meeting of Seismological Society of America, San Francisco, CA, April 17-21.

Bozorgnia, Y., Bertero, V.V. (2001). Improved shaking and damage parameters for post-earthquake applications. Proceedings, SMIP01 Seminar on Utilization of Strong-Motion Data, pp. 1-22, September 12.

Cao, V. V., & Ronagh, H. R. (2014). Correlation between seismic parameters of far-fault motions and damage indices of low-rise reinforced concrete frames. Journal of Soil Dynamics and Earthquake Engineering, Vol. 66, p. 102–112.

Chenouda, M., & Ayoub, A. (2008).Inelastic Displacement Ratios of Degrading Systems. J. Struct. Eng. Vol. 134, Issue 6.

Chopra, A. K., & Gutierres, J. A. (1973). Earthquake Analysis of Multistory Building Including Foundation Interaction. Report no. EERC 73-16. Berkeley, California: University of California.

Chung, Y.S., Meyer, C., & Shinozuka, M. (1987). Seismic damage assessment of reinforced concrete members. Report NCEER-87- 0022, National Center for Earthquake Engineering Research, State University of New York at Buffalo, Buffalo, NY.

Crisafulli, F., & Carr, A. (2007). Proposed macro-model for the analysis of infilled frame structures. Bulletin of the New Zealand Society for Earthquake Engineering, Vol.40, Issue 1, pp.69–77.

Decanini, L., & Saragoni, R. (2000). Energy and displacement demand imposed by near - source ground motions. 12WCEE, New Zealand, pp.1136.

DiPasquale, E., & Cakmak, A. S. (1988). Identification of the serviceability limit state and detection of seismic structural damage. Report NCEER-88-0022, National

Center for Earthquake Engineering Research, State University of New York at Buffalo, NY.

DiPasquale, E., & Cakmak, A. S. (1990). Seismic damage assessment using linear models. Soil Dynamics and Earthquake Engineering, 9(4), pp. 194-215.

Dolsek, M., & Fajfar, P (2008). The effect of masonry infills on the seismic response of a four storey reinforced concrete frame-a probabilistic assessment. Engineering Structures. Vol 30, Issue 11, pp: 1991–2001.

Elenas, A. (2000). Correlation between seismic acceleration parameters and overall structural damage indices of buildings. Journal of Soil Dynamics and Earthquake Engineering, Vol. 20, p. 93-100.

Elenas, A. (2011). Intensity Parameters as Damage Potential Descriptors of Earthquakes, Proceeding of the Conference on Computational Methods in Structural Dynamics and Earthquake Engineering, Greece.

Elenas, A., & Meskouris, K. (2001). Correlation study between seismic acceleration parameters and damage indices of structures. Journal of Engineering Structures, Vol. 23, Issue 6, 2001, p. 698-704.

Elms, D., Paulay, T., & Ogawa, S. (1989). Code-implied structural safety for earthquake loading. Proceedings of Fifth International Conference on Structural Safety and Reliability (ICOSSAR 89), San Francisco CA, Aug. 8–11: 2003–2010.

Fajfar, P., Vidic, T., & Fischinger, M. (1990). A measure of earthquake motion capacity to damage medium-period structures. Soil. Dyn. Earthq. Eng, Vol. 9 , Issue 5 , p.236–242.

FEMA 356 (2000). Prestandard and commentary for the seismic rehabilitation of buildings, Federal Emergency Management Agency: Washington, D.C.

FEMA 440 (2005) Improvement of nonlinear static seismic analysis procedures, Applied Technology Council (ATC-55 project). Federal Emergency Management Agency, Washington, DC.

Filippou, F. C., Popov, E. P., & Bertero, V. V. (1983). "Effects of Bond Deterioration on Hysteretic Behavior of Reinforced Concrete Joints". Report EERC 83-19, Earthquake Engineering Research Center, University of California, Berkeley.

Ghannad, M. A., & Ahmadnia, A. (2006). The Effect of Soil-Structure Interaction on Inelastic Structural Demands, European Earthquake Engineering, Vol. 20, No. 1, pp. 23-35.

Ghannad, M. A., & Jahankhah, H. (2007). Site Dependent Strength Reduction Factors for Soil-Structure Systems. Soil Dynamics and Earthquake Engineering, Vol. 27, No. 2, pp. 99-110.

Giuffrè, A., & Pinto, P. E. (1970). “II Comportamento Del Cemento Armato Per Sollecitazioni Cicliche di Forte Intensith.” Giornale del Genio Civile, Maggio.

HAZUS-MH MR5. (2003). Multi-Hazard loss Estimation Methodology. Earthquake Model. Department of Homeland security, FEMA, Washington, DC.

Hall, J. F., Heaton, T. H., Halling, M. W., & Wald, D. J., (1995). Near-source ground motions and its effects on flexible buildings, Earthquake Spectra. Vol 11 Issue 4 , pp: 569–605.

Hassania, N., Bararniaa, M., & Amiri, G. (2018) Effect of soil-structure interaction on inelastic displacement ratios of degrading structures. Soil Dynamics and Earthquake Engineering 104 .75–87.

Ibarra, L. F., Medina, R. A., & Krawinkler, H. (2005). Hysteretic models that incorporate strength and stiffness deterioration, Earthquake Engineering and Structural Dynamics 34, pp:1489- 1511.

Jafari, H. (2018).Investigation of the 20% reduction of the analytical period of the structure instead of the modeling of infill structures on the seismic performance of steel frames (in Persian).

Işık, E., & Özdemir, M. (2017). "Performance Based Assessment of Steel Frame Structures by Different Material Models" International Journal of Steel Structures 17(3): 1021-1031.

Iran National Buildings Code (INBC 2013) for Steel Design of Buildings. Third Edition Iranian codes of practice for seismic resistant design of buildings, (2014) (Standard No. 2800). Fourth Edition, BHRC publication.

Kappos, A. J., & Ellul, F. (2000). Seismic Design and Performance Assessment of Masonry Infilled R/C Frames. Proceedings of the 12th World Conference on Earthquake Engineering, 0989 on CD-ROM, New Zealand.

Karabalis, D., & Beskos, E. (1986). Dynamic response of 3-D embedded foundation by the boundary element method. Computer method in Applied Mechanics and Engineering, Vol 56, Issue 1, pp: 91-119.

Kim, S., & Roesset, J. M. (2004). Effect of nonlinear soil behavior on inelastic seismic response of structure. Int. J. Geomech, 4-2- pp: 104-114.

Ko, H., Park, Y. K. & Lee, D. G. (2008). Evaluation of seismic behavior for low-rise RC moment resisting frame with masonry infill walls", 14th World Conference on Earthquake Engineering (14WCEE), Beijing, China.

Korkmaz, K.A., Demir, F., Tekeli, H. & Karahan, A.E. (2008).Effects of infilled masonry walls on nonlinear structural behavior of precast concrete structures in Turkey", 14th World Conference on Earthquake Engineering (14WCEE), Beijing, China.

Kostinakis, K., Athanatopoulou, A., & Morfidis, K. (2015). Correlation between ground motion intensity measures and seismic damage of 3D R/C buildings Engineering Structures. Vol. 82, Issue1, p. 151–167.

Kramer, S. L., & Mitchell, R. A. (2006). Ground motion intensity measures for liquefaction hazard evaluation. Earthquake Spectra, Vol. 22, Issue 2, p.413–438.

Krishnan, S., Casarotti, E., Goltz, J., Ji, C., Komatitsch, D., Mourhatch, R., Muto, M., Shaw, J. H., Tape, C., & Tromp, J. (2012). Rapid estimation of damage to tall buildings using near real-time earthquake and archived structural simulations. Bulletin of the Seismological Society of America, Vol.102, Issue 6, p. 2646–2666.

Kunnath, S. K., Reinhorn, A. M., & Lobo, R. F. (1992). IDARC Version 3.0: A program for the inelastic damage analysis of reinforced concrete structures. Report No. NCEER-92-0022, National Center for Earthquake Engineering Research, State University of New York at Buffalo.

Li, Sh., & Xie, L. (2007). Progress and trend on near-field problems in civil engineering. CTA SeismologicaSinica, 20: pp 105-114.

Luco, N., & Bazzurro, P. (2007). Does amplitude scaling of ground motion records result in biased nonlinear structural drift responses. Seismic Reliability Analysis of Structures.Vol36, Issue13, Pages 1813-1835.

Mahsuli, M. (2006). The Effect of Soil--Structure Interaction on Inelastic Behavior of Structures with Embedded Foundation. M.Sc. Thesis. Sharif University.

Malhotra, P.K. (1999). Response of buildings to near-field pulse-like ground motions. Earthquake Engineering and Structural Dynamics, Vol28, Issue 11,pp: 1309-1326.

McCabe, S., & Hall, W. (1989). Assessment of seismic structural damage. Journal of Structural Engineering 115:9, 2166-2183.

Meek, J. W., & Veletsos, A. S. (1974). Simple models for foundations in lateral and rocking motion. Proceedings of the 5thworld Conference on Earthquake Engineering, IAEE, Rome 1974, Vol.2, pp: 2610-2613.

Menegotto, M., & Pinto, P. E. (1973). "Method of anaysis for cyclically loaded reinforced concrete plane frames including changes in geometry and non-elastic behavior of elements under combined normal force and bending." Proc., IABSE Symp. Of Resistance and Ultimate Deformability of Structures Acted on by Well-Defined Repeated Loads, International Association of Bridge and Structural Engineering, Libson, Portugal, Vol. 13: 15-22.

Moghadam, H. (2006). Earthquake engineering. Third edit, Iran. Tehran.

Mohraz, B. (1976). A study of earthquake response spectra for different geological conditions. BSSA; 66(3):915-935.

Nanos, N., Elenas, A., Ponterosso, P. (2008). Correlation of different strong motion duration parameters and damage indicators of reinforced concrete structures.

Proceeding of the Conference on Earthquake Engineering, China, Beijing, 2008, p. 12-17.

Otani, S. (1981). Hysteresis models of reinforced concrete for earthquake response analysis. Journal of the Faculty of Engineering, 36(2), pp. 125-159.

Park, Y. J., & Ang, A. H. S. (1985). Seismic damage analysis of RC buildings. Journal of Structural Engineering ASCE, 111(ST4), pp. 740-757.

Perrault, M., & Guéguen, P. (2015). Correlation between ground motion and building response using Californian earthquake records. Vol. 31, Issue. 4, 2015, p. 2027-2046.

Personeni, S., Di Pilato, M., Palermo, A. & Pampanin, S. (2008). Numerical investigations on the seismic response of masonry infilled steel frames", 14th World Conference on Earthquake Engineering (14WCEE), Beijing, China.

Riddell, R. (2007). On ground motion intensity indices, Earthq. Spectra, Vol. 23, Issue 1, p.147–173.

Roufaiel, M. S. L., & Meyer, C. (1981). Analysis of damaged concrete frame buildings. Technical Report No. NSF-CEE-81-21359-1, Columbia University, New York, NY.

Ruiz-García, J., & Miranda E (2003). Inelastic displacement ratios for evaluation of existing structures. Earthq Eng Struct Dyn; 32:1237–58.

Sattar, S., & Liel, A. (2010). Seismic Performance of Reinforced Concrete Frame Structures with and without Masonry Infill Walls. In Proceedings of the 9th US National and the 10th Canadian Conference on Earthquake Engineering—Reaching Beyond Borders, Toronto, Canada; pp: 1–10.

Sattar, S., & Abbie B. Liel. (2016) Seismic Performance of Nonductile Reinforced Concrete Frames with Masonry Infill Walls—I: Development of a Strut Model Enhanced by Finite Element Models. Earthquake Spectra. Vol 32, Issue 2, pp:795-818.

Shinozuka, M., Saxena, V., Deodatis, G., & Feng, M. (2001). Development Of Fragility Curve for Multi - Span Reinforced Concrete Bridge. Dept. of Civil and Environmental Engineering, Princeton University.

Smith, B.S. (1962). Lateral Stiffness of Infilled Frames. Journal of the Structural Division, ASCE, 88(6): 183-199.

Stephens, J. E. (1985). A damage function using structural response measurements. Structural Safety Journal 5: 22–39.

Trifunac, M.D., Stewart, J.P., & Fenves, G.L. (2000). Seismic soil - structure interaction in building. Analytical methods. Journal of Geothech and Geoenvir Eng, Vol 126, pp: 668 - 681.

Tothong, P., & Cornell, C,A. (2008). Structural performance assessment under near-source pulse-like ground motions using advanced ground motion intensity

measures", Earthquake Engineering & Structural Dynamics, Vol 37, Issue7, pp: 1013-1037.

Veletsos, A. S. (1993). Design concepts for dynamics of soil-structure interaction. Development in Dynamic Soil-Structure Interaction, Gulkan and Clough (eds), pp. 307-325.

Veletsos, A. S., & Nair, V. D. (1974). Response of torsionally excited foundations. Journal of the Geotechnical Engineering Division, ASCE; 100(3), pp: 476-482.

Veletsos, A. S., & Newmark, N. M. (1960). Proce. of the 2nd World Conf. on Earthq.Eng., Japan, 2, 895.

Veletsos, A. S., & Prasad, A. M. (1989). Seismic interaction of structure and soils: Stochastic approach. J. Struct. Eng, 115-4-, pp: 935-956.

Vrbik, Jan. (2018). "Small-Sample Corrections to Kolmogorov-Smirnov Test Statistic". Pioneer Journal of Theoretical and Applied Statistics. 15 (1–2): 15–23.

Williams, M. S., & Sexsmith, G. S. (1995). Seismic damage indexes for concrete structures: A state-of-the-art review, Earthquake Spectra, 11(2), pp. 319-349.

Wolf, J. P., & Deeks, AJ. (2004). Foundation Vibration Analysis: A Strength-of-Material Approach. London: Elsevier. 214 p.

Xiaoming, Y., Rui, S., & Meng, S. (2003). Effect of asymmetry and irregularity of seismic waves on earthquake - induced differential settlement of buildings on natural subsoil. Soil Dynamics and Earthquake Engineering, Volume 21, Issue 2, pp: 107 - 114.

Yang, D., Pan, J., & Li, G. (2009). Non-structure-specific intensity measure parameters and characteristic period of near-fault ground motions. Earthquake Engineering & Structural Dynamics, Vol. 38, Issue 11, p. 1257–1280.

Yerli, H. R., Kacin, S., & Kocak, S. (2003). A paralel finite - infinite element model for two dimensional soil - structure interaction problems. Soil Dynamics and Earthquake Engineering, Volume 23, Issue 4, pp: 249 – 253.

Žarnic, R., & Gostic, S. (1997). Masonry infilled frames as an effective structural sub-assemblage. In: Fajfar, Krawinkler, Ed. Seismic design methodologies for the next generation of codes. Rotterdam: Balkema, 335–46.

APPENDICES

Appendix A: Earthquake Records

Table A.1: List of Ordinary Seismic Records.

No.	Earthquake	Date	Station	Magnitude	Closest distance (km)	PGA (g)
1	Imperial Valley	15/10/1979	Compuertas	6.9	32.6	0.20011
2	Kocaeli,Turkey	17/8/1999	Atakoy	7.8	67.5	0.15739
3	Kocaeli,Turkey	17/8/1999	Cekmece	7.8	76.1	0.17401
4	Landers	28/6/1992	Coachella Canal	7.4	55.7	0.11111
5	Loma-Prieta	18/10/1989	Halls Valley	7.1	31.6	0.13591
6	Loma-Prieta	18/10/1989	Agnews State Hospital	7.1	28.2	0.18984
7	Loma-Prieta	18/10/1989	Gilroy Array #7	7.1	24.2	0.33231
8	Morgan-Hill	24/4/1984	Hollister City Hall	6.1	32.5	0.0732
9	Northridge	17/1/1994	Downey-Birchdale	6.7	40.7	0.16833
10	Northridge	17/1/1994	Glendale-Las Palmas	6.7	25.4	0.35952
11	Coalinga	02/05/1983	Parkfield-Cholame 5W	6.5	47.3	0.14145
12	Coalinga	02/05/1983	Parkfield-Cholame 8W	6.5	50.7	0.10129
13	Whittier-Narrows	01/10/1987	Bell Gardens-Jaboneria	5.7	9.8	0.22515
14	Whittier Narrows	01/10/1987	El Monte-Fairview Av	5.7	9.8	0.23746
15	Whittier Narrows	01/10/1987	Santa Fe Springs-E Joslin	5.7	10.8	0.46066
16	Imperial Valley	19/5/1940	El Centro Array #9	7	8.3	0.28068
17	Parkfield	28/6/1966	Cholame #5	5.3	5.3	0.44506
18	Chi-Chi,Taiwan	20/9/1999	TCU	7.6	4.5	0.23355
19	Loma Prieta	18/10/1989	Gilroy Array #3	7.1	14.4	0.57575
20	Whittier Narrows	01/10/1987	LA-Fletcher Dr	5.7	14.4	0.21743
21	Spitak	07/12/1988	Gukasian	6.7	20	0.18825
22	Manjil (Iran)	20/6/1990	Abhar	7.4	75	0.22012
23	Manjil (Iran)	20/6/1990	Rudsar	7.4	61	0.1013
24	Friuli (Italy)	11/09/1976	Buia	5.5	7	0.12025
25	Friuli (Italy)	15/9/1976	Buia	6	9	0.23052
26	Umbria Marche (Italy)	26/9/1997	Colfiorito	6	5	0.21425
27	Duzce (Turkey)	12/11/1999	LDEO Station No.C1062 FI	7.2	14	0.25388
28	Livermore	27/1/1980	San Ramon-Eastman Kodak	5.5	17.6	0.29392
29	Loma Prieta	18/10/1989	Gilroy Array #4	7.1	16.1	0.44053
30	Loma Prieta	18/10/1989	Oakland-Title & Trust	7	77.4	0.22899
31	Loma Prieta	18/10/1989	Sunnyvale-Colton Ave.	7.1	28.2	0.21918
32	Northridge	17/1/1994	Downey-Co Maint Bldg	6.7	47.6	0.23041
33	Northridge	17/1/1994	LA-Fletcher Dr	6.7	29.5	0.24641
34	Northridge	17/1/1994	LA-N Faring Rd	6.7	23.9	0.2778
35	Northridge	17/1/1994	LA-S Grand Ave	6.7	36.9	0.27523
36	Northridge	17/1/1994	La-Habra-Briarcliff	6.7	61.6	0.21246
37	Northridge	17/1/1994	Manhattan Beach-Manhattan	6.7	42	0.18117
38	Northridge	17/1/1994	Pasadena-N Sierra Madre	6.7	39.2	0.25944
39	San Fernando	09/02/1971	LA-Hollywood Stor FF	6.6	22.7	0.21051

Table A.1: List of Ordinary Seismic Records (continued)

40	Superstitn Hills	24/11/1987	Calipatria Fire Station	6.6	28.3	0.2554
41	Whittier Narrows	01/10/1987	Glendale-Las Palmas	5.9	19	0.30027
42	Whittier Narrows	01/10/1987	Lakewood-Del Amo Blvd	5.7	20.9	0.2883
43	N.Palm Springs	08/07/1986	Palm Springs Airport	6	16.6	0.19927
44	Northridge	17/1/1994	LA-Pico & Sentous	6.7	32.7	0.18116
45	Northridge	17/1/1994	Leona Valley #6	6.7	38.5	0.16606
46	Superstitn Hills	24/11/1987	Plaster City	6.6	21	0.20181
47	Livermore	24/1/1980	San Ramon-Eastman Kodak	5.5	17.6	0.29392
48	Loma Prieta	18/10/1989	APEEL 2E Hayward Muir Sch	7.1	57.4	0.17363
49	Northridge	17/1/1994	Elizabeth Lake	6.7	37.2	0.1569
50	Imperial Valley	15/10/1979	Aeropuerto Mexicali	6.9	8.5	0.34277
51	Imperial Valley	15/10/1979	Calexico Fire Station	6.6	10.6	0.27152
52	Superstitn Hills	24/11/1987	Westmorland Fire Sta	6.6	13.3	0.21166
53	Morgan Hill	24/4/1984	Gilroy Array #4	6.1	12.8	0.3627
54	Imperial Valley	15/10/1979	El Centro Array #11	6.9	12.6	0.40079
55	Morgan Hill	24/4/1984	Halls Valley	6.1	3.4	0.35035
56	Parkfield	06/28/1966	Cholame-Shandon Array#8	6.19	12.9	0.28519
57	Managua,Nicaragua-01	12/23/1972	Managua,ESSO	6.24	3.51	0.39623
58	Victoria,Mexico	06/09/1980	SAHOP Casa Flores	6.33	39.1	0.09785
59	Morgan Hill	04/24/1984	Gilroy Array#4	6.19	11.53	0.3627
60	Parkfield-02,CA	09/28/2004	Parkfield-Cholame 5W	6	6.27	0.27271
61	Parkfield-02,CA	09/28/2004	PARKFIELD-1-STORY SCHOOL BLDG	6	0.95	0.26709
62	Parkfield-02,CA	09/28/2004	Parkfield-Gold Hill 2W	6	2.13	0.26786
63	Parkfield-02,CA	09/28/2004	Parkfield-Gold Hill 6W	6	15.45	0.09684
64	Joshua Tree,CA	04/23/1992	Indio-Jackson Road	6.1	25.04	0.40316
65	Kozani_Greece-01"	05/13/1995	Larisa	6.4	74.06	0.03197
66	Dinar_Turkey"	10/01/1995	Dinar	6.4	3.36	0.36211
67	Northwest China-03"	04/11/1997	Jiashi	6.1	9.98	0.30096
68	Umbria Marche_Italy"	09/26/1997	Aquilpark-Citta	6	83.48	0.00406
69	Umbria Marche_Italy"	09/26/1997	Aquilpark-Galleria	6	83.48	0.00353
70	Umbria Marche_Italy"	09/26/1997	Aquilpark-Parcheggio	6	83.48	0.00384
71	Umbria Marche_Italy"	09/26/1997	Castelnuovo-Assisi	6	17.28	0.17522
72	L'Aquila_Italy"	04/06/2009	Avezzano	6.3	23.67	0.07096
73	L'Aquila_Italy"	04/06/2009	Cattolica	6.3	177.23	0.00413
74	L'Aquila_Italy"	04/06/2009	Forli	6.3	224.68	0.00163

Table A.2: List of Pulse-like Seismic Records.

No.	Earthquake	Date	Station	Magnitude	Closest distance (km)	PGA (g)
1	Coyote Lake	08/06/1979	Gilroy Array #2	5.74	8.47	0.29159
2	Coyote Lake	08/06/1979	Gilroy Array #3	5.74	6.75	0.26294
3	Coyote Lake	08/06/1979	Gilroy Array #4	5.74	4.79	0.26719
4	Imperial Valley-06	10/15/1979	Agrarias	6.53	0.6	0.21251
5	Imperial Valley-06	10/15/1979	Brawley Airport	6.53	8.54	0.16687
6	Imperial Valley-06	10/15/1979	EC County Center FF	6.53	7.31	0.26369
7	Imperial Valley-06	10/15/1979	El Centro Meloland Geot. Array	6.53	0.07	0.37713
8	Imperial Valley-06	10/15/1979	El Centro Array #10	6.53	8.6	0.17957
9	Imperial Valley-06	10/15/1979	El Centro Array #3	6.53	10.79	0.29553
10	Imperial Valley-06	10/15/1979	El Centro Array #4	6.53	4.9	0.39235
11	Imperial Valley-06	10/15/1979	El Centro Array #5	6.53	1.76	0.40169
12	Imperial Valley-06	10/15/1979	El Centro Array #6	6.53	0	0.44903
13	Imperial Valley-06	10/15/1979	El Centro Array #7	6.53	0.56	0.4985
14	Imperial Valley-06	10/15/1979	El Centro Differential Array	6.53	5.09	0.50411
15	Imperial	10/15/1979	Holtville Post Office	6.53	5.35	0.22905
16	Westmorland	04/26/1981	Parachute Test Site	5.9	16.54	0.24233
17	Superstition Hills-02	11/24/1987	Kornbloom Road(temp)	6.54	18.48	0.12855
18	Superstition Hills-02	11/24/1987	Parachute	6.54	0.95	0.48865
19	Loma Prieta	10/18/1989	Gilroy-Historic Bldg.	6.93	10.27	0.33309
20	Loma Prieta	10/18/1989	Gilroy Array #2	6.93	10.38	0.32532
21	Loma Prieta	10/18/1989	Gilroy Array #3	6.93	12.23	0.35368
22	Loma Prieta	10/18/1989	Saratoga-W Valley Coll.	6.93	8.48	0.38717
23	Landers	06/28/1992	Yermo Fire Station	7.28	23.62	0.22626
24	Northridge 01	01/17/1994	Newhall- Fire Station	6.69	3.16	0.68306
25	Northridge 01	01/17/1994	Newhall-W Pico Canyon Rd	6.69	2.11	0.45193
26	Northridge 01	01/17/1994	Pardee - SCE	6.69	5.54	0.55004
27	Northridge 01	01/17/1994	Rinaldi Receiving Sta	6.69	0	0.97168
28	Northridge 01	01/17/1994	Sylmar Converter Sta	6.69	0	0.63222
29	Kobe,Japan	01/16/1995	KJMA	6.9	0.94	0.57164
30	Kobe,Japan	01/16/1995	Port Island	6.9	3.31	0.32532
31	Kobe,Japan	01/16/1995	Takarazuka	6.9	0.27	0.6638
32	Kobe,Japan	01/16/1995	Takatori	6.9	1.46	0.61529
33	Kocaeli,Turkey	08/17/1999	Yarimca	7.51	1.38	0.34452
34	Chi-Chi,Taiwan	09/20/1999	CHY101	7.62	9.94	0.33801
35	Chi-Chi,Taiwan	09/20/1999	TCU038	7.62	25.42	0.1401
36	Chi-Chi,Taiwan	09/20/1999	TCU051	7.62	7.64	0.2199
37	Chi-Chi,Taiwan	09/20/1999	TCU059	7.62	17.11	0.17984
38	Chi-Chi,Taiwan	09/20/1999	TCU065	7.62	0.57	0.834
39	Duzce,Turkey	11/12/1999	Bolu	7.14	12.02	0.82755
40	Denali,Alaska	11/03/2002	TAPS Pump Station #10	7.9	0.18	0.42627
41	Tottori,Japan	10/06/2000	TTR008	6.61	6.86	0.42248
42	Parkfield-02,CA	09/28/2004	Parkfield- Cholame 1E	6	1.66	0.46225
43	Parkfield-02,CA	09/28/2004	Parkfield- Cholame 2WA	6	1.63	0.68383

Table A.2: List of Pulse-like Seismic Records (continued)

44	Parkfield-02,CA	09/28/2004	Parkfield- Cholame 3W	6	2.55	0.57884
45	Parkfield-02,CA	09/28/2004	Parkfield-Fault Zone 1	6	0.02	0.8504
46	Parkfield-02,CA	09/28/2004	Parkfield-Fault Zone 12	6	0.88	0.28342
47	Parkfield-02,CA	09/28/2004	Parkfield-Stone Corral 1E	6	2.85	0.81725
48	Montenegro,Yugoslavia	04/15/1979	Ulcinj-Hotel Olimpic	7.1	3.97	0.23859
49	Darfield, New Zealand	09/03/2010	Christchurch Botanical Gardens	7	18.05	0.15743
50	Darfield, New Zealand	09/03/2010	DSLC	7	5.28	0.26908
51	Darfield, New Zealand	09/03/2010	GDLC	7	1.22	0.87209
52	Darfield, New Zealand	09/03/2010	HORC	7	7.29	0.4364
53	Darfield, New Zealand	09/03/2010	LINC	7	5.07	0.53171
54	Darfield, New Zealand	09/03/2010	NNBS North New Brighton School	7	26.76	0.21014
55	Darfield, New Zealand	09/03/2010	Christchurch Resthaven	7	19.48	0.26653
56	Darfield, New Zealand	09/03/2010	Riccarton High School	7	13.64	0.24398
57	Darfield, New Zealand	09/03/2010	ROLC	7	1	0.31577
58	Darfield, New Zealand	09/03/2010	Shirley Library	7	22.33	0.1879
59	Darfield, New Zealand	09/03/2010	Styx Mill Transfer Station	7	20.86	0.18465
60	Darfield, New Zealand	09/03/2010	TPLC	7	6.11	0.33184
61	Christchurch, New Zealand	02/21/2011	Pages Road Pumping Statuion	6.2	1.92	0.58103
62	Christchurch, New Zealand	02/21/2011	Christchurch Resthaven	6.2	5.11	0.69143
63	El Mayor Cucapah, Mexico	04/04/2010	El-Centro Array #12	7.2	9.98	0.43863
64	El Mayor Cucapah, Mexico	04/04/2010	Westside Elementary School	7.2	10.3	0.28924

Table A.3: Assessed Features of Intensity Measures of each Earthquake.

No	Seismic parameter	Formulation
1	Peak Ground Acceleration (PGA) (g)	$PGA = max\left\|a(t)\right\|.$
2	Peak Ground Velocity (PGV) (cm/s)	$PGV = max\left\|v(t)\right\|.$
3	Peak Ground Displacement (PGD) (cm)	$PGD = max\left\|d(t)\right\|.$
4	PGV / PGA	-
5	Acceleration Root-mean-square (RMS)	$a_{rms} = \sqrt{\left(\frac{1}{t_f}\int_0^{t_f} a(t)^2 dt\right)}; t_f = total\ duration$
6	Velocity RMS	$v_{rms} = \sqrt{\left(\frac{1}{t_f}\int_0^{t_f} v(t)^2 dt\right)}$
7	Displacement RMS	$d_{rms} = \sqrt{\left(\frac{1}{t_f}\int_0^{t_f} d(t)^2 dt\right)}$
8	Arias Intensity	$AI = \frac{\pi}{2g}\int_0^{t_f} a(t)^2 dt$
9	Characteristic Intensity	$CI = \sqrt[3]{a_{rms}^2} * \sqrt{t_d}$
10	Specific Energy Density	$SED = \int_0^{t_f} v(t)^2 dt$
11	Cumulative Absolute Velocity (CAV)	$CAV = \int_0^{t_f} \left\|a(t)\right\| dt.$
12	Acceleration Spectrum Intensity (ASI)	$ASI = \int_{0.1}^{0.5} S_a(\xi = 0.05, T)dT.$
13	Velocity Spectrum Intensity (VSI)	$VSI = \int_{0.1}^{2.5} S_v(\xi = 0.05, T)dT.$
14	Housner Intensity	$HI = \int_{0.1}^{2.5} PS_v(\xi = 0.05, T)dT.$
15	Sustained Maximum Acceleration (SMA)	The 3rd_largest peak in the acceleration time history.
16	Sustained Maximum Velocity (SMV)	The third highest absolute peak in the velocity time history
17	Effective Design Acceleration (EDA)	the peak acceleration that remains after filtering out accelerations above 8 to 9 Hz
18	A95 parameter	-
19	Predominant Period (Tp)	The maximum spectral acceleration occurs in an acceleration response spectrum calculated at 5% damping
20	Significant Duration (sec)	
21	Mean Period (Tm)	$T_m = \frac{\sum_i FA_i^2 (1/f_i)}{\sum_i FA_i^2}$, $for\ 0.25Hz \le f_i \le 20Hz\ with\ \Delta f \le 0.05Hz$

Table A.3: Assessed features of Intensity Measures of each Earthquake (continued)

22	Spectral acceleration	$T_1 : S_a(T_1)$
23	Spectral velocity	$T_1 : S_v(T_1)$
24	Spectral displacement	$T_1 : S_d(T_1)$
25	Compound velocity-related intensity measure	$I_F = PGV \cdot \sqrt[4]{t_d}\ , t_d = t_2 - t_1 (5-95\% AI)$
26	Compound acceleration-related intensity measure	$I_a = PGA * \sqrt[3]{t_d}.$
27	Compound displacement-related intensity measure	$I_d = PGD \cdot \sqrt[3]{t_d}$
28	Compound velocity-related intensity measure	$I_v = \sqrt[3]{PGV^{\,2}} * \sqrt[3]{t_d}.$
29	Effective Peak Acceleration	$EPA = \dfrac{mean(S_a^{0.1-0.5}(\xi = 0.05))}{2.5}.$
30	Effective Peak Velocity	$EPV = \dfrac{mean(S_v^{0.7-2.5}(\xi = 0.05))}{2.5}.$
31	bandwidth, as a function of the spectral parameters computed for the squared velocity spectra	$\Omega = \sqrt{\left[1 - \dfrac{(\lambda_1^*)^2}{\lambda_0^* \lambda_2^*}\right]}$ $\lambda_0^* = \sum_{i=1}^{n} S_{v,i}^2 . \Delta T$ $\lambda_1^* = \sum_{i=1}^{n} T_i . S_{v,i}^2 . \Delta T$ $\lambda_2^* = \sum_{i=1}^{n} T_i^{\,2} . S_{v,i}^2 . \Delta T$
32	destructiveness potential	$P_D = \dfrac{I_A}{v_0^{\,2}}$

Appendix B: Masonry Wall

Table B.1: Equivalent Diagonal Strut (FEMA 356(2000)) in OpenSees Software.

type	Size (cm)	I (cm^4)	f_{me}	t_{inf}	h_{inf}	L_{inf}	h_{col}	L_{col}	E_m	E_{fe}	I_{col}	r_{inf}	θ-inf	L_{dig}	θ	λ_1	a (cm)
IPB180	18	3830	48	11	280	482	320	500	26400	2100000	3830	557.42623	0.5262666	593.63288	0.5693132	0.0129362	55.264135
IPB200	20	5700	48	11	280	480	320	500	26400	2100000	5700	555.69776	0.5280744	593.63288	0.5693132	0.0117182	57.315629
IPB220	22	8090	48	11	280	478	320	500	26400	2100000	8090	553.97112	0.5298936	593.63288	0.5693132	0.0107415	59.161603
IPB240	24	11260	48	11	280	476	320	500	26400	2100000	11260	552.24632	0.5317241	593.63288	0.5693132	0.0098944	60.947496
IPB260	26	14920	48	11	280	474	320	500	26400	2100000	14920	550.52339	0.533566	593.63288	0.5693132	0.0092268	62.478889
IPB280	28	19270	48	11	280	472	320	500	26400	2100000	19270	548.80233	0.5354195	593.63288	0.5693132	0.0086595	63.884638
IPB300	30	25170	48	11	280	470	320	500	26400	2100000	25170	547.08317	0.5372847	593.63288	0.5693132	0.0081043	65.395203
IPB320	32	30820	48	11	280	468	320	500	26400	2100000	30820	545.36593	0.5391616	593.63288	0.5693132	0.0077081	66.510101
IPB340	34	36660	48	11	280	466	320	500	26400	2100000	36660	543.65062	0.5410504	593.63288	0.5693132	0.0073846	67.447809
IPB360	36	43190	48	11	280	464	320	500	26400	2100000	43190	541.93727	0.5429511	593.63288	0.5693132	0.0070916	68.332713
IPB400	40	57680	48	11	280	460	320	500	26400	2100000	57680	538.51648	0.5467888	593.63288	0.5693132	0.0066034	69.86648
IPB450	45	79890	48	11	280	455	320	500	26400	2100000	79890	534.25181	0.551655	593.63288	0.5693132	0.0060946	71.572574
IPB500	50	107200	48	11	280	450	320	500	26400	2100000	107200	530	0.5565993	593.63288	0.5693132	0.0056696	73.085731
IPB550	55	136700	48	11	280	445	320	500	26400	2100000	136700	525.76135	0.5616235	593.63288	0.5693132	0.0053418	74.248993
IPB600	60	171000	48	11	280	440	320	500	26400	2100000	171000	521.53619	0.5667292	593.63288	0.5693132	0.0050572	75.283363